



UNIVERSIDAD DE LAS PALMAS DE GRAN CANARIA
Instituto Universitario de Microelectrónica Aplicada
Sistemas de información y Comunicaciones

Máster en Tecnologías de Telecomunicación



Trabajo Fin de Máster

Detección de tumores cerebrales usando imágenes hiper-espectrales mediante algoritmos semi-supervisados combinando spectral unmixing y clasificación supervisada

Autor: Miguel Ángel Tejedor Hernández
Tutor: Gustavo Iván Marrero Callicó

Fecha: Septiembre 2016



t +34 928 451 086 | iuma@iuma.ulpgc.es
f +34 928 451 083 | www.iuma.ulpgc.es

Campus Universitario de Tafira
35017 Las Palmas de Gran Canaria



UNIVERSIDAD DE LAS PALMAS DE GRAN CANARIA
Instituto Universitario de Microelectrónica Aplicada
Sistemas de información y Comunicaciones

Máster en Tecnologías de Telecomunicación



Trabajo Fin de Máster

Detección de tumores cerebrales usando imágenes hiperespectrales mediante algoritmos semi-supervisados combinando spectral unmixing y clasificación supervisada

HOJA DE FIRMAS

Alumno/a: Miguel Ángel Tejedor Hernández Fdo.:

Tutor/a: Gustavo Iván Marrero Callicó Fdo.:

Fecha: Septiembre 2016



t +34 928 451 086 iuma@iuma.ulpgc.es
f +34 928 451 083 www.iuma.ulpgc.es

Campus Universitario de Tafira
35017 Las Palmas de Gran Canaria



Máster en Tecnologías de Telecomunicación



Trabajo Fin de Máster

Detección de tumores cerebrales usando imágenes hiperespectrales mediante algoritmos semi-supervisados combinando spectral unmixing y clasificación supervisada

HOJA DE EVALUACIÓN

Calificación:

Presidente Javier García García Fdo.:

Secretario Pablo F. Hernández Morera Fdo.:

Vocal Fernando de la Puente Arrate Fdo.:

Fecha: Septiembre 2016



RESUMEN

La presente memoria resume el trabajo de investigación realizado por Miguel Ángel Tejedor Hernández con motivo de su trabajo de fin de máster (TFM). En concreto, el presente trabajo describe un estudio sobre la aplicación de un enfoque semi-supervisado para la clasificación de tumores cerebrales humanos mediante el uso de imágenes hiperespectrales. El documento sigue la estructura clásica de un trabajo de investigación en dicho campo, presentando en primer lugar las motivaciones y objetivos que han incentivado el desarrollo de un algoritmo de clasificación semi-supervisado basado en técnicas de desmezclado espectral y clasificadores supervisados, respondiendo a una necesidad claramente existente en este campo de estudio, pues actualmente no existen mecanismos fiables para delimitar el tejido tumoral con el fin de resecarlo en su totalidad y de forma precisa durante una operación de neurocirugía. A continuación, se realiza un estudio en profundidad del estado del arte en dicho campo, desde el concepto de píxel hiperespectral hasta los algoritmos existentes que fundamentan la base de este estudio. Posteriormente se detallan los módulos de desmezclado espectral y clasificación que se han combinado en forma de diferentes cadenas de procesamiento orientadas a clasificar datos hiperespectrales de forma semi-supervisada. En este sentido, el núcleo del presente trabajo viene dado por la comparativa del algoritmo de clasificación semi-supervisada desarrollado en este trabajo frente a un enfoque puramente supervisado, todo ello dentro del marco de un caso de estudio centrado en la utilización de imágenes hiperespectrales de tejido tumoral obtenidas mediante sensores hiperespectrales durante intervenciones quirúrgicas. Como resultado del estudio cuantitativo y cualitativo realizado al analizar los resultados de clasificación obtenidos utilizando diferentes estrategias en relación con información de referencia (muestras etiquetadas) disponible para dichas imágenes, se ofrecen una serie de conclusiones y recomendaciones generales acerca del mejor uso posible del algoritmo de clasificación semi-supervisada que integra las estrategias desarrolladas. Dichas recomendaciones suponen un aspecto innovador en la literatura especializada dedicada a la clasificación de datos hiperespectrales, y serán de gran utilidad para los usuarios de este tipo de datos interesados en aplicaciones relacionadas con la clasificación semi-supervisada de los mismos.

Contents

Chapter 1 Introduction	1
1.1. Objectives.....	1
1.2. Context and motivations.....	2
1.3. Petitioner.....	4
1.4. Memory organization.....	4
Chapter 2 Hyperspectral Imaging	7
2.1. Hyperspectral imaging concept.....	7
2.2. Medical hyperspectral imaging	10
2.2.1. Brain tumours.....	10
2.2.2. Hyperspectral imaging applied to tumour detection.....	11
2.2.3. Hyperspectral Imaging system	14
2.2.4. Hyperspectral imaging data sets	16
2.3. Hyperspectral analysis techniques.....	18
2.4. Hyperspectral data classification	20
2.4.1. Unsupervised classification algorithms.....	23
2.4.2. Supervised classification algorithms	24
2.4.3. Semi-supervised classification algorithms	24
2.4.4. Evaluation metrics used in classification algorithms	24
2.5. Summary	28
Chapter 3 Image processing techniques	29
3.1. Introduction	29
3.2. Data pre-processing techniques for hyperspectral images	31
3.2.1. Image Calibration	32
3.2.2. De-noising filtering.....	33
3.2.3. Dimensionality Reduction	35
3.2.4. Data Normalization	37
3.3. Ground Truth Generation	37
3.4. Feature extraction.....	39
3.4.1. Spectral unmixing Techniques	42
3.4.1.1. Number of endmember estimation.....	44
3.4.1.2. Endmember extraction algorithms.....	45
3.4.1.3. Abundance estimation algorithms.....	45

3.4.1.3.1. Linear Spectral Unmixing	45
3.4.1.4. Abundance Maps	47
3.5. Classification algorithms	47
3.5.1. Support Vector Machine Classifier (SVM)	48
3.5.1.1 Theoretical foundations of SVM classifier	48
3.5.1.2 Kernel functions available	52
3.5.2. Semi-supervised learning (SSL)	54
3.6. Summary	57
Chapter 4 Proposed process for cancer detection using hyperspectral images.....	59
4.1. Case studies.....	59
4.2. Semi-supervised algorithm.....	60
4.2.1. Critical points of the algorithm	62
4.3. Summary	63
Chapter 5 Experimental results.....	65
5.1. Introduction	65
5.2. Results of semi-supervised experiments.....	66
5.2.1. Results of support vector machine classifier used in brain cancer detection.....	66
5.2.2. Results of semi-supervised approach based on SVM used in brain cancer detection	68
5.2.3. Results of semi-supervised approach based on spectral unmixing concepts used in brain cancer detection	70
5.2.4. Results of semi-supervised approach based on Mixed techniques Unmixing-SVM used in brain cancer detection.....	73
5.2.5. Results of semi-supervised approach using different number of selected samples in each iteration	80
5.2.6. Thematic maps generated by semi-supervised approach using Unmixing-SVM techniques	81
5.3. Global discussion of results.....	93
5.4. Summary	94
Chapter 6 Conclusions and future research lines	97
6.1. Conclusions	97
6.2. Future research lines.....	98
Bibliography.....	101
Budget	111
Specifications.....	119

Figures

Figure 2.1: Electromagnetic spectrum.	8
Figure 2.2: Comparison between hypercube and RGB image. Hypercube is a three-dimensional dataset of a two-dimensional image on each wavelength. The lower left is the reflectance curve (spectral signature) of a pixel in the image. RGB color image only has three image bands on red, green, and blue wavelengths respectively. The lower right is the intensity curve of a pixel in the RGB image.....	9
Figure 2.3: Magnetic resonance of patient suffering from multiform glioblastoma.	11
Figure 2.4: The concept of spectral data cube. The data cube contains two spatial dimensions (x and y) and one spectral dimension, in which the cube face is a function of the spatial coordinates and the depth is a function of wavelength.....	13
Figure 2.5: HELICoiD demonstrator main parts.....	15
Figure 2.6: Intra-operative images with markers location the presumed position of tumours and normal brain. (a) Meningioma, (b) Lung Adenocarcinoma, (c) Renal Carcinoma, (d) Breast Carcinoma, (e) and (f) Glioblastoma, (g) Ganglioglioma, (h) Anaplastic oligodendroglioma.....	17
Figure 2.7: Hyperspectral analysis procedure.	19
Figure 2.8: Graphic illustration of the classification problem in hyperspectral imaging.	22
Figure 2.9: Example of constructing of a confusion matrix.	26
Figure 3.1: Classification system overview.	29
Figure 3.2: Data pre-processing chain flowchart.	31
Figure 3.3: Raw spectral signature of a grade IV glioblastoma tumour tissue.	32
Figure 3.4: Calibrated spectral signature of a grade IV glioblastoma tumour tissue.	33
Figure 3.5: Spectral signature with the HySIME filter applied to a grade IV glioblastoma tumour tissue.	34
Figure 3.6: Spectral signature with the noise and band reduction step and the normalization applied to a grade IV glioblastoma tumour tissue.	37
Figure 3.7: HELICoiD Labelling tool process flowchart. (a) Pre-Processed hypercube. (b) Syntetic RGB image extracted from the hypercube. (c) SAM masked over the sRGB image. (d) Final ground truth map generated.....	39
Figure 3.8: Spectral unmixing Diagram Process.....	43
Figure 3.9: classic method for analyzing hyperspectral images using linear mixed model.	44
Figure 3.10: Functional diagram of the SVM classifier.....	49
Figure 3.11: The decision boundary of a Linear SVM.	52
Figure 3.12: The decision boundary with a Polynomial kernel.....	53
Figure 3.13: The decision boundary with a Radial Basis Function (RBF) kernel.	53
Figure 3.14: The decision boundary with a Sigmoid kernel.....	54
Figure 4.1: Self-training algorithm scheme.	61
Figure 4.2: Semi-supervised approach.	62
Figure 5.1: CS1 using SVM with different kernels.....	67
Figure 5.2: CS1, CS2 and CS3 using SVM for brain cancer detection.....	68
Figure 5.3: Semi-supervised algorithm based on SVM using normal and tumour tissues.	69
Figure 5.4: Semi-supervised algorithm based on SVM using all classes defined.....	70

<i>Figure 5.5: Semi-supervised algorithm based on spectral unmixing with FCLSU using normal and tumour tissues.</i>	71
<i>Figure 5.6: Semi-supervised algorithm based on spectral unmixing with FCLSU using all classes defined.</i>	72
<i>Figure 5.7: Semi-supervised algorithm based on spectral unmixing with LSU using all classes defined.</i>	73
<i>Figure 5.8: Unmixing-SVM process 1 using FCLSU for estimating abundances.</i>	74
<i>Figure 5.9: Unmixing-SVM process 1 using LSU for estimating abundances.</i>	74
<i>Figure 5.10: Unmixing-SVM process 2 using FCLSU for estimating abundances.</i>	75
<i>Figure 5.11: Unmixing-SVM process 2 using LSU for estimating abundances.</i>	76
<i>Figure 5.12: Unmixing-SVM process 3 using FCLSU for estimating abundances.</i>	77
<i>Figure 5.13: Unmixing-SVM process 3 using LSU for estimating abundances.</i>	77
<i>Figure 5.14: Unmixing-SVM process 3 using FCLSU for moving CS3 to CS2 in a semi-supervised system.</i>	78
<i>Figure 5.15: Semi-supervised algorithm based on SVM selecting different number of samples in each iteration.</i>	80
<i>Figure 5.16: RGB image of Op8C1.</i>	82
<i>Figure 5.17: Thematic map of Op8C1 using CS3.</i>	83
<i>Figure 5.18: Thematic map of Op8C1 using semi-supervised algorithm.</i>	83
<i>Figure 5.19: RGB image of Op8C2.</i>	84
<i>Figure 5.20: thematic map of Op8C2 using CS3.</i>	85
<i>Figure 5.21: thematic map of Op8C2 using semi-supervised algorithm.</i>	85
<i>Figure 5.22: RGB image of Op12C1.</i>	86
<i>Figure 5.23: thematic map of Op12C1 using CS3.</i>	86
<i>Figure 5.24: thematic map of Op12C1 using semi-supervised algorithm.</i>	87
<i>Figure 5.25: RGB image of Op12C2.</i>	88
<i>Figure 5.26: thematic map of Op12C2 using CS3.</i>	88
<i>Figure 5.27: thematic map of Op12C2 using semi-supervised algorithm.</i>	89
<i>Figure 5.28: RGB image of Op15C1.</i>	90
<i>Figure 5.29: thematic map of Op15C1 using CS3.</i>	90
<i>Figure 5.30: thematic map of Op15C1 using semi-supervised algorithm.</i>	91
<i>Figure 5.31: RGB image of Op20C1.</i>	91
<i>Figure 5.32: thematic map of Op20C1 using CS3.</i>	92
<i>Figure 5.33: thematic map of Op20C1 using semi-supervised algorithm.</i>	92

Tables

<i>Table 1.1: List of acronyms used in this dissertation.</i>	5
<i>Table 2.1: Spectral range definitions.</i>	12
<i>Table 2.2: Camera Specifications.</i>	16
<i>Table 2.3: Spectrographic medical samples used in this set of experiments related with the different characteristics of the available.</i>	18
<i>Table 2.4: Confusion matrix.</i>	27
<i>Table 5.1: Confusion matrix of Op4C1 previous to apply semi-supervised approach.</i>	79
<i>Table 5.2: Colours assigned by class.</i>	82

MEMORIA

Chapter 1

Introduction

1.1. Objectives

The main objective of this Master dissertation is to design a classification process based on a semi-supervised approach, combining supervised classification and spectral unmixing techniques for hyperspectral imaging in order to obtain accurate and efficient results for this type of data, improving the advantages of each technique applied while minimizing the disadvantages associated with the separate application of each technique. For this purpose, the next overall objective is proposed: **to study, to evaluate and to compare the different existing techniques for hyperspectral classification processes and to draw some conclusions with regard to the efficient approaches for human brain cancer detection.** In order to achieve this general objective, several specific objectives have also been accomplished:

- O1. To develop a state of the art study on hyperspectral imaging in the medical field (data format and representation), acquiring the necessary knowledge of the hyperspectral analysis.
- O2. To gain knowledge of tools and programs management to work with this type of processing data.

- O3. To analyze the images used to better understand their behavior in certain applications (source, characteristics, special properties, types of tissue...).
- O4. To compare the most important data processing techniques currently in the literature for hyperspectral imaging and to establish those that provide better results or more accurately.
- O5. To perform a comprehensive study regarding spectral unmixing and the supervised algorithm SVM, one of the main techniques used for supervised classification.
- O6. To study thoroughly the main techniques for semi-supervised classification.
- O7. To implement and evaluate a set of experiments focusing on the influence of using semi-supervised classification process.
- O8. To design and develop a final system for hyperspectral image classification based on semi-supervised approaches in order to detect brain tumor samples.
- O9. To validate a final classification system using real hyperspectral images of human brain tumors.
- O10. To draw conclusions from the performed quantitative and qualitative studies, and propose possible future work.

1.2. Context and motivations

The work developed in this dissertation is the analysis and study of different automatic processing techniques for hyperspectral classification focused on human brain tumour samples using semi-supervised methods. This work is included in the actual research lines funded by the European Commission through the FP7 FET Open programme ICT-2011.9.2, the European Project HELICoiD “HypErspectral Imaging Cancer Detection” under Grant Agreement 618080.

Hyperspectral images are an extension of the concept of digital image, in the sense that each pixel in a hyperspectral image is not only formed by a single discrete value, but by a wide range of values for different spectral measurements recorded by a sensor or

measuring instrument in different wavelength values. The collection of all the wavelength values (one per spectral band) which are associated to a given pixel is called a *spectral signature*. As a result, we can understand a hyperspectral image as a collection of spectroscopic measurements that provide very detailed of information on the properties of the materials appearing on the scene.

This fact involves the provision of a large amount of information with a high level of detail. The scientific community dedicated to the analysis of hyperspectral data has identified the need to interpret such data properly and obtain relevant information for different fields with little effort [1]. Therefore, the basis for defining and testing a flexible chain of collection and processing of hyperspectral data to produce efficient results should be set.

In the literature, there are a variety of methodologies and techniques applicable, which may be considered as combinable functional blocks within the entire processing chain. Considering the main purpose of processing as the classification and characterization of hyperspectral pixels to produce a thematic map that identifies different classes or regions of interest in the image, the steps which are executed a priori and a posteriori are known as pre-processing and post-processing techniques respectively. This work has taken into account large part of the research for this discipline and is intended to increase or deepen the understanding of how to implement a classification system based on semi-supervised approach, combining different techniques in the process to obtain high levels of accuracy and make an approach to the most appropriate sequence of applications to define a general standard processing chain or a processing chain applicable to a given case.

The number and variety of processing tasks in hyperspectral imaging is enormous [2]. However, this dissertation is mainly focused on the integration of two of those techniques:

- **Classification**, which consists of assigning a label (class) to each pixel of a hyperspectral data cube [2].
- **Spectral unmixing**, which consists of estimating the fraction of the pixel area covered by each material present in the scene [3].

In the present work, these techniques will be applied to a set of samples in which it is intended to classify different types of tissues using a semi-supervised architecture based on spectral unmixing and Support Vector Machine (SVM) classifier. Finally, it should be noted that the experiments performed represent a part of the whole process suffered by a hyperspectral imaging since it is collected by the sensor until the user takes advantage of the interpretation made. Therefore, the accuracy that can be obtained will always be conditioned by the transformations carried out on the data previously pre-processed and on effectiveness in the definition of the parameters which apply.

1.3. Petitioner

The development of this Master Thesis is carried out as a request from the Research Institute for Applied Microelectronics (IUMA) of the University of Las Palmas de Gran Canaria (ULPGC) as an official requirement for obtaining the title of Master in Telecommunication technologies, once the student has passed all the credits that comprise this Master.

1.4. Memory organization

This dissertation is organized into six chapters as follows.

- Chapter 2 provides an introduction and review of the state of the art in the context of hyperspectral imaging in the medical field, paying particular attention to the supervised classification techniques in this field and different preprocessing methods, which are described in more detail in chapter 3.
- Chapter 4 presents the different processes considered in this research.
- Chapter 5 performs a comprehensive experimental validation of the results obtained after applying the different processing chains considered to the hyperspectral data of tumour tissues. This chapter also includes a general discussion of the results obtained by the different processing chains in different study cases, extrapolating conclusions about the performance of each processing chain in terms of the accuracy obtained in the classification.

- Chapter 6 provides the conclusions about the studies conducted and proposes some future research lines.
- The paper concludes with the bibliographic references taken into account in the drafting of the report and other references enabling the extension of the concepts presented in this work.

To conclude this chapter, Table 1.1 provides a list of the acronyms used throughout the dissertation document. Hereinafter, these acronyms will be used instead of the full terms for simplicity.

Acronyms	
ANC	Abundance Non-negativity Constraint
ASC	Abundance Sum-to-one Constraint
CS	Case Studies
FCLSU	Fully Constrained Linear Spectral Unmixing
GBM	Glioblastoma
GUI	Graphical User Interface
HELiCoID	HypErspectraL Imaging Cancer Detection
HSI	Hyperspectral imaging
HySime	Hyperspectral Subspace Identification by Minimum Error
K	Kappa coefficient
LIBSVM	Library of SVM [Online: https://www.csie.ntu.edu.tw/~cjlin/libsvm/]
LSU	Linear Spectral Unmixing
MIMD	Multiple Instruction Multiple Data
MIR	Mid-infrared
ML	Machine Learning
NIR	Near-infrared
OA	Overall Accuracy
QTH	Quartz Tungsten-Halogen system
RBF	Gaussian Radial Basis function
SA	Spectral Angles
SAM	Spectral Angle Mapper
SSL	Semi-supervised learning
SVM	Support Vector Machine
UV	Ultraviolet
VIS	Visible
WHO	World Health Organization

Table 1.1: List of acronyms used in this dissertation.

Chapter 2

Hyperspectral Imaging

2.1. Hyperspectral imaging concept

The observation of a particular object is based on the capture of electromagnetic radiation from the interaction between the object and the radiation source by a measuring instrument or sensor. Electromagnetic radiation received several names depending on the wavelength that characterizes it, as shown in Figure 2.1. For measuring the emitted or reflected radiation by a given surface is necessary to quantify the amount of energy flux that proceeds from the surface. For this, the radiance measure is used, which depends on factors such as the perceived brightness, reflectance and viewing angles, among others [4].

Spectral detection techniques are based on the fact that all materials in the real world reflect, absorb and emit electromagnetic energy differently in different wavelengths [5].

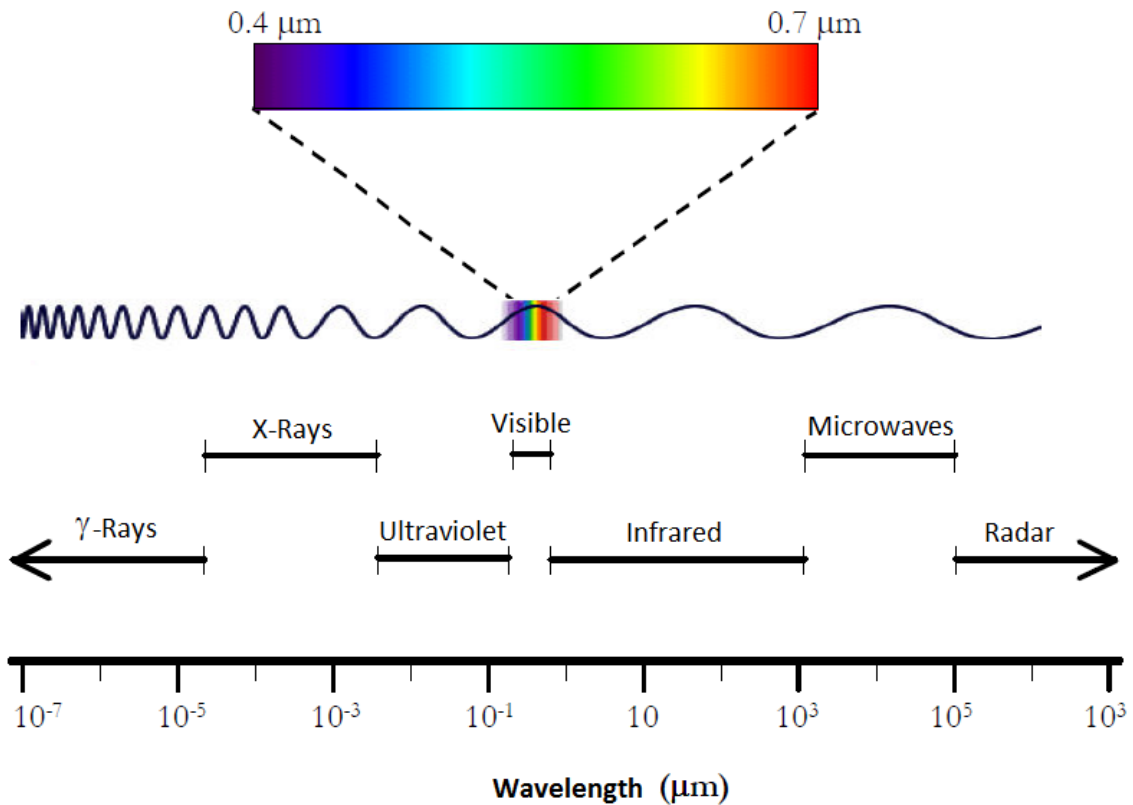


Figure 2.1: Electromagnetic spectrum.

Currently, there is a wide range of instruments or sensors capable of measuring spectral singularities in different wavelengths [6]. The availability of these instruments has provided a redefinition of the digital image concept through the extension of the idea of pixel.

It is important to remember that the associated value with each pixel is defined by a numerical value called digital level. This is a numeric value, not visual, but can easily be translated into a visual intensity or grey level by any digital-analog converter. Thus, in a purely spatial schema one pixel is constituted by a single discrete value, while in a spectral schema one pixel consists of a set of values. These values may be understood as N-dimensional vectors [7], where N is the number of spectral bands in which the sensor measures information.

Extending the concept of pixel results in what is known as multidimensional image. The order of magnitude of N allows a distinction when talking about multidimensional images. Thus, when the value of N is small, typically a few spectral bands [8], one speaks of multispectral images, whereas when the order of N is hundreds of bands [9], there is talk of hyperspectral imaging, which are also known as hypercubes.

Hyperspectral imaging (HSI), like other spectral imaging, collects and processes information from across the electromagnetic spectrum. The goal of hyperspectral imaging is to obtain the spectrum for each pixel in the image of a scene, with the purpose of finding objects, identifying materials, or detecting processes [10][11].

Much as the human eye sees visible light in three bands (red, green, and blue), spectral imaging divides the spectrum into many more bands. This technique of dividing images into bands can be extended beyond the visible as shown in Figure 2.2 [12]. In hyperspectral imaging, the recorded spectra have fine wavelength resolution and cover a wide range of wavelengths.

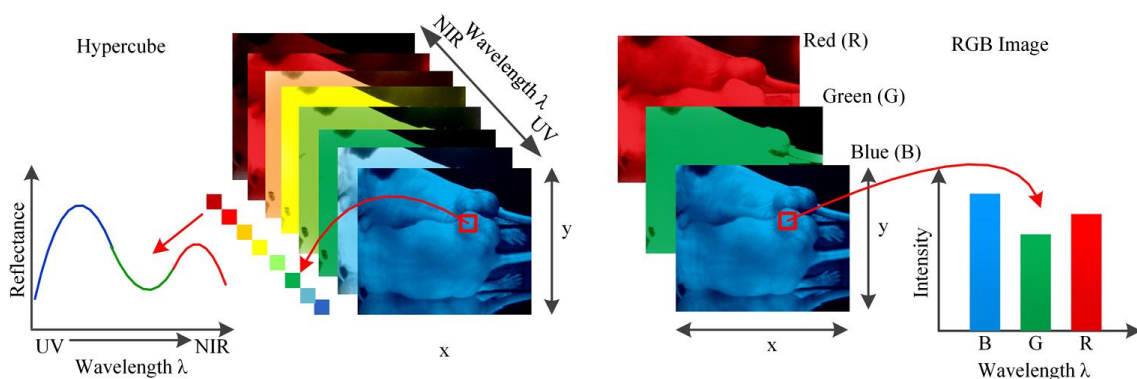


Figure 2.2: Comparison between hypercube and RGB image. Hypercube is a three-dimensional dataset of a two-dimensional image on each wavelength. The lower left is the reflectance curve (spectral signature) of a pixel in the image. RGB color image only has three image bands on red, green, and blue wavelengths respectively. The lower right is the intensity curve of a pixel in the RGB image.

Hyperspectral sensors look at objects using a vast portion of the electromagnetic spectrum. Certain objects leave unique *fingerprints* in the electromagnetic spectrum. If the difference between each of these wavelengths is a few nanometers, it can be obtained for each pixel an “almost continuous” spectral response of the photographed material at that pixel. This response is called spectral signature which is unique to each material. Known as spectral signatures, these *fingerprints* enable identification of the materials that make up a scanned object and it can be used to identify specific substances in an image. For example, a spectral signature for tumour tissue helps surgeons find tumour areas.

Most hyperspectral image pixels are mixed pixels. This is because the spatial resolution of the sensor cannot separate different materials in a pixel. The denotation of mixed pixel is given by the presence of pixels composed by the combination of several pure spectral signatures. In the process of spectral unmixing we find an efficient possibility

to express the composition of each mixed pixel in proportion to the pure pixels present in the material [13][14].

With the advantage of acquiring two-dimensional images across a wide range of electromagnetic spectrum, HSI has been applied to numerous areas, engineers have built hyperspectral sensors and processing systems for applications in astronomy, agriculture, biomedical imaging, geosciences, physics, and surveillance [12].

The primary disadvantages of these techniques are cost and complexity. Fast computers, sensitive detectors, and large data storage capacities are needed for analysing hyperspectral data. Significant data storage capacity is necessary since hyperspectral cubes are large, multidimensional datasets, potentially exceeding hundreds of megabytes. All of these factors greatly increase the cost of acquiring and processing hyperspectral data.

2.2. Medical hyperspectral imaging

2.2.1. Brain tumours

Due to the increase in the incidence and mortality from brain tumours in world population in recent decades, the number of research papers related to its diagnosis has grown exponentially. An early diagnosis of such diseases can be vital to prevent a benign tumour evolves into a more aggressive cancer.

Brain tumours are due to abnormal growth of cells derived from brain components in the case of primary tumours or tumour cells localized elsewhere in the organism in the case of metastases. According to their evolution, size and dimension, World Health Organization (WHO) classifies them into four degrees of danger. This classification is ranging from grade I tumours (benign tumours of slow growth) to grade IV tumours (malignant cancers with very rapid growth) [15].

The 77% of malignant brain cancers belongs to the group of tumours called gliomas. These tumours affect glial cells responsible for supporting neurons and information brain processing. Depending on the type of glial cells affected (astrocytes, oligodendrocytes, ependymal cells, etc.) are different types of gliomas, being multiform glioblastoma (astrocytoma grade IV) the most aggressive and less likely to survive [16][17].

Figure 2.3 shows magnetic resonance imaging of a patient afflicted with a multiform glioblastoma.

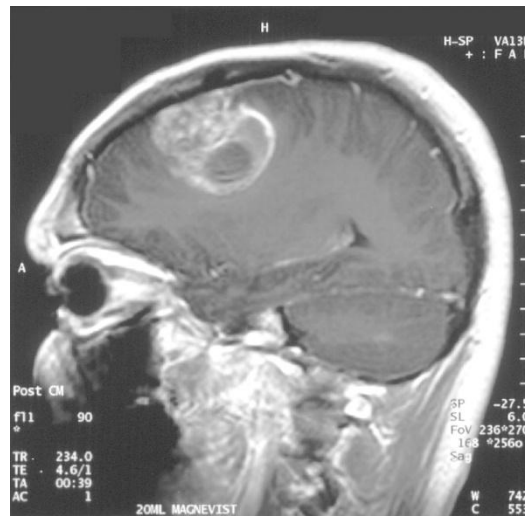


Figure 2.3: Magnetic resonance of patient suffering from multiform glioblastoma.

Symptoms and treatment of these tumours depend largely on the patient's age, the type of tumour and its location in the brain. However, these tumours tend to infiltrate into healthy brain tissue, so that surgery is complex and sometimes impossible. That is why it is vitally important research and study of non-invasive techniques that provide the most accurate diagnosis possible.

Proper removal (resection) of brain tumour eliminates malignant tissue and prevents the tumour to be reproduced. Increase resection area with an additional safety margin maximizes the chances of patient survival, but in the case of brain tumours, excessive resection can lead to significant damage of all kinds (motor, cognitive, visual, etc.). For this reason, a technique to determine accurately and minimally invasive glioma limits is necessary.

2.2.2. Hyperspectral imaging applied to tumour detection

Spectral imaging is a technology that integrates conventional imaging and spectroscopy methods to obtain both spatial and spectral information from an object. Although this technology was originally developed for remote sensing, it has been extended to the biomedical engineering field as a powerful analytical tool for biological and biomedical research [18].

Hyperspectral imaging field is an emerging imaging modality for medical applications. It offers great potential for non-invasive disease diagnosis and surgical guidance. Light delivered to biological tissue undergoes multiple scattering from inhomogeneity of biological structures and absorption primarily in haemoglobin, melanin, and water as it propagates through the tissue [19][20]. One of the most important advantages of this technique is that it can acquire reflectance, absorption, or fluorescence spectrum for each pixel in the image. It is assumed that the absorption, fluorescence, and scattering characteristics of tissues change during the progression of disease [21], which can be used to detect the biochemical changes of objects that cannot be identified with traditional grey or colour imaging methods [18]. Therefore, the reflected, fluorescent, and transmitted light from tissues captured by HSI carries quantitative diagnostic information about tissue pathology [22-25].

In recent years, advances in hyperspectral cameras, image analysis methods, and computational power make it possible for many exciting applications in the medical field. These applications mainly cover the ultraviolet (UV), visible (VIS), and near-infrared (near-IR or NIR) regions. Table 2.1 defines the spectral range from UV to mid-IR (200 to 25,000 nm) [24].

Short name	Full name	Spectral range (nm)
UV	Ultraviolet	200 to 400
VIS	Visible	400 to 780
NIR/near-IR	Near-infrared	780 to 2500
MIR/mid-IR	Mid-infrared	2500 to 25,000

Table 2.1: Spectral range definitions.

Visible light penetrates only 1 to 2 mm below the skin and thus obtains information from the sub-papillary [25], while light in the NIR region penetrates deeper into the tissue than VIS or mid-IR radiation [26]. NIR light is preferred for surgical guidance due to its deep penetration into the tissue, which can help the surgeon see through connective tissue for visualizing critical anatomical structures of interest that are not visible and detecting molecules with detectible spectra [12]. By expanding light beyond the visual spectrum, additional information can be obtained to further characterize the cells of interest [27].

HSI acquires a three-dimensional dataset called hypercube, with two spatial dimensions and one spectral dimension. Figure 2.4 [18] shows the concept of the hypercube data captured by a spectral imaging system. These dates can be visualized as a three-dimensional (3-D) cube or a stack of multiple two-dimensional (2-D) images because of its intrinsic structure, in which the cube face is a function of the spatial coordinates and the depth is a function of wavelength [18]. Spatially resolved spectral imaging obtained by HSI provides diagnostic information about the tissue physiology, morphology, and composition [12].

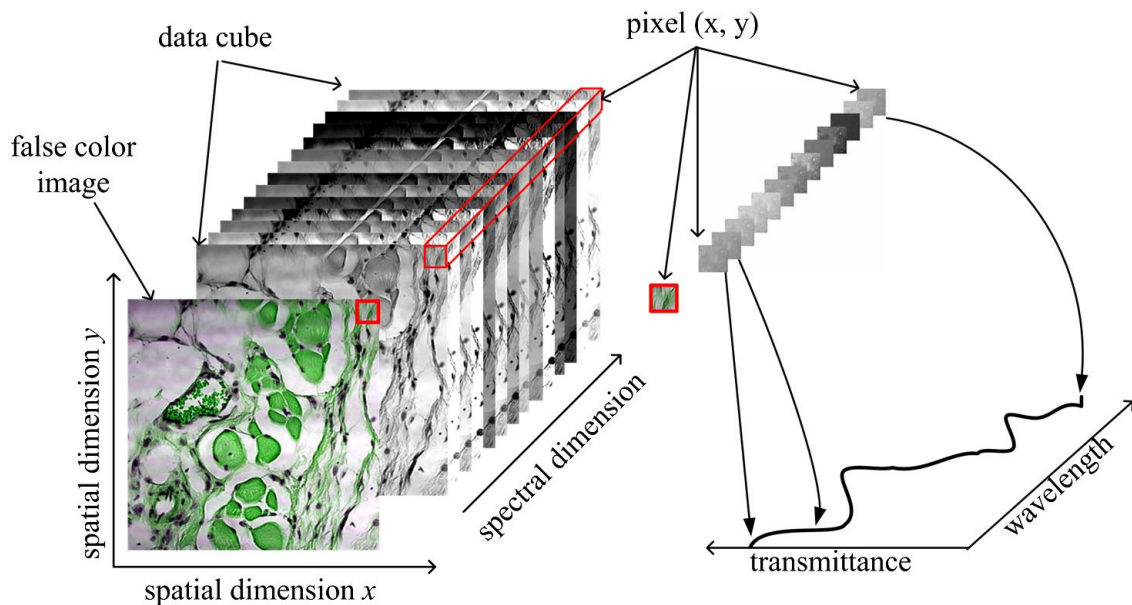


Figure 2.4: The concept of spectral data cube. The data cube contains two spatial dimensions (x and y) and one spectral dimension, in which the cube face is a function of the spatial coordinates and the depth is a function of wavelength.

According to the electromagnetic theory, different biochemical constituents commonly have different spectral signatures [28]. These signatures are usually generated by the interactions between materials and electromagnetic waves, such as electron transition, atomic and molecular vibration or rotation. The biological and pathological changes in tissues and organs also have a close relationship with the spectra. Spectral characteristics in different wavelength regions yield a distinguishable spectral signature, making pathological changes distinguishable. Therefore, the spectral imaging technology also can be extended to the biomedical engineering field to estimate the physiological status of biological tissues, since it can take advantage of the spatial relationships among the different spectra in a neighbourhood. This technology opens new prospects for life science by which scientists can identify and quantify the relationships among biologically

active molecules, observe living organisms noninvasively, perform histopathological and fluorescent analyses, and enhance biological understanding of diseases [18].

Image analysis enables the extraction of diagnostically useful information from a large medical hyperspectral dataset at the tissue, cellular, and molecular levels and is, therefore, critical for disease screening, diagnosis, and treatment. Hypercube with high spatial and spectral resolution may potentially contain more diagnostic information. However, high spatial and spectral dimensions also make it difficult to perform automatic analysis of hyperspectral data. In particular, it is complex in many aspects: (1) high data redundancy due to high correlation in the adjacent bands, (2) variability of hyperspectral signatures, and (3) curse of dimensionality [6]. With abundant spatial and spectral information available, advanced image classification methods for hyperspectral datasets are required to extract, unmix, and classify relevant spectral information. The goal is not only to discriminate between different tissues (such as healthy and malignant tissue) and provide diagnostic maps, but also to decompose mixtures into the spectra of pure molecular constituents and correlate these molecular fingerprints (biomarkers) with disease states. Although hyperspectral image analysis methods have been intensively investigated in the remote sensing area, their development and application in medical domain lag far behind. The relationships between spectral features and underlying biomedical mechanisms are not well understood. The basic steps for hyperspectral image analysis generally involve pre-processing, feature extraction and feature selection, and unmixing and/or classification [12].

2.2.3. Hyperspectral Imaging system

In order to obtain the hyperspectral images of the in-vivo human brain surface during the neurosurgical operations, the HELICoID project has built a demonstrator capable of simultaneously obtaining two hyperspectral cubes. The two hyperspectral cameras selected are the Hyperspec[®] VNIR A-Series and the Hyperspec[®] NIR X-Series, manufactured by HeadWall Photonics, Massachusetts, USA. The VNIR (visible and near infrared) camera ranges between 400 nm to 1000 nm. The NIR (near infrared) camera ranges between 900 nm to 1700 nm.

Figure 2.5 shows the main parts of the demonstrator. The most important elements of the system are located in the acquisition scanning platform. Table 2.2

presents the specifications of the two push-broom hyperspectral cameras. These cameras are fixed in a scanning unit composed by a stepper motor and a screw with a maximum path of 230 mm and a step resolution of 6.17 μm . Furthermore, a cold light emitter is located together with the cameras. The cold light emitter is connected to a 150 W Quartz Tungsten-Halogen system (QTH), which offers broadband emission in the VIS (visible) and NIR spectral ranges (400 nm to 2200 nm), through an optical fibre. This system isolates the high temperatures produced by the halogen lamp, avoiding a direct emission to the brain surface.

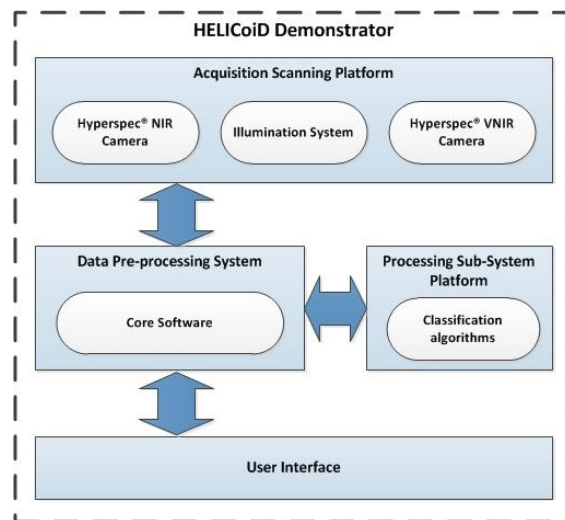


Figure 2.5: HELICoID demonstrator main parts.

	Hyperspec® VNIR	Hyperspec® NIR
Spectral range (nm)	400 – 1000	900 – 1700
Spectral resolution (nm)	2 – 3	5
Slit (μm)	25	25
Spatial bands	1004	320
Spectral bands	826	172
Frame Height (FOV) (mm)	129.21	153.6
Pixel Dimensions (IFOV) (mm)	0.1287	0.4800

Max Pixels per Frame	1004	320
Max Frames per Capture	1825	489
Dispersion per pixel (nm)	0.74	4.8
Detector array	Silicon CCD	InGaAs
Frame rate (fps)	90	100

Table 2.2: Camera Specifications.

Data pre-processing system is composed by a high performance computer which manages the entire system, especially the acquisition scanning platform and the interaction with the user through the graphical user interface (GUI).

Finally, the processing sub-system platform has the goal of performing the hyperspectral classification in order to achieve the results in real-time. The platform selected for this issue is the Kalray many-core processor that features MIMD (Multiple Instruction Multiple Data) architecture [29]. This platform is focused on intensive computing, low power and embedded applications [30].

2.2.4. Hyperspectral imaging data sets

Using the HELICoiD demonstrator, an in-vivo human brain hyperspectral image database has been created. The hyperspectral cubes have been obtained from 13 different patients at the University Hospital Doctor Negrín. The disease of the tissues captured during this study involves both primary brain tumours and secondary tumours (metastasis).

Hyperspectral images were obtained intra-operatively after craniotomy and resection of the dura. Before images were captured, the operating surgeon would initially identify the location of normal brain and tumour. Rubber ring markers were then placed on these locations and images taken with markers in situ. Tissue samples were at that point obtained from the marked areas and sent to pathology for tissue diagnosis. Depending on the location of the tumour, images were acquired at various stages of the operation. In cases with superficial tumours, some images were obtained immediately after the dura was removed while in cases with deep laying tumours images were obtained during the actual tumour resection.

Figure 2.6 presents a set of different hyperspectral brain tumour images obtained during the course of the project. Figure 2.6.a presents a meningioma tumour located in the dura while Figure 2.6.b, c and d are secondary tumours, lung carcinoma, renal carcinoma and breast carcinoma respectively. Figure 2.6.e, f, g and h show primary tumours of grade IV (glioblastoma), grade III (anaplastic oligodendroglioma) and grade I (ganglioglioma).

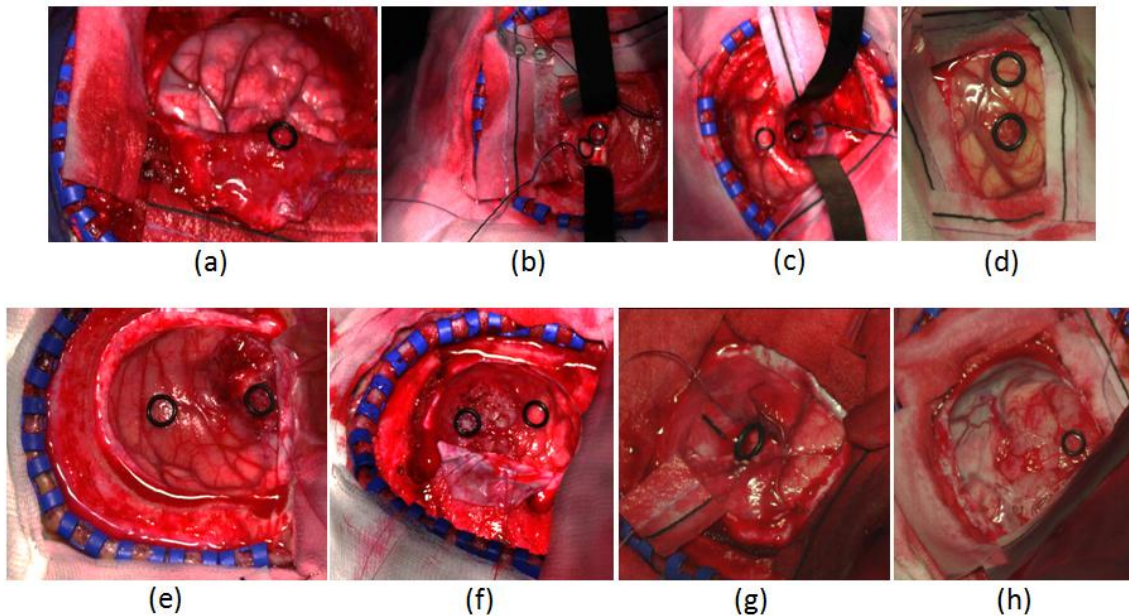


Figure 2.6: Intra-operative images with markers location the presumed position of tumours and normal brain. (a) Meningioma, (b) Lung Adenocarcinoma, (c) Renal Carcinoma, (d) Breast Carcinoma, (e) and (f) Glioblastoma, (g) Ganglioglioma, (h) Anaplastic oligodendroglioma.

In order to perform an automatic classification of the brain hyperspectral images, some pixels have been extracted and labelled from some hypercubes using a Labelling Tool which will be explained in the section 3.2. As a preliminary study, some significant patients have been taken into account. The selection of the patients has been carried out by selecting patients whose tumours share the same diagnosis: primary glioblastoma (GBM) grade IV as they are the most frequent brain cancer. This fact is because of the biological variability between the different types of tumours and also because the whole database has not enough amounts of other type of tumours that allows generalizing a model for these tumours. Furthermore, the work presented in this dissertation is only focused in the VNIR hyperspectral cubes as they have provided better results. Table 2.3 summarizes the information about the database used in this study, including four patients

and four different classes: normal tissue, blood vessels, tumour tissue and background elements.

Medical Samples					
Patient ID	Captures	Normal Tissue	Tumour Tissue	Blood Vessels	Background
Op1	C1	2295	1221	1331	630
	C2	2187	138	1000	7444
Op2	C1	4516	855	8697	1685
	C2	6553	3139	6041	8731
Op3	C1	1251	2046	4089	696
Op4	C1	1842	3655	1513	2625
Total		18644	11054	22671	21811

Table 2.3: Spectrographic medical samples used in this set of experiments related with the different characteristics of the available.

2.3. Hyperspectral analysis techniques

The hyperspectral analysis is based on the ability of hyperspectral sensors to acquire digital images in a large number of spectral channels very close to each other, obtaining for each pixel a characteristic spectral signature of each material that will be used in the analysis process [6]. These images can be represented as a data cube, with two dimensions to represent the spatial location of a pixel, and a third dimension representing the spectral singularity of each pixel at different wavelengths. This process facilitates the identification and quantification of the materials present in the scene [31][32]. Figure 2.7 illustrates the process of hyperspectral analysis using a simple diagram.

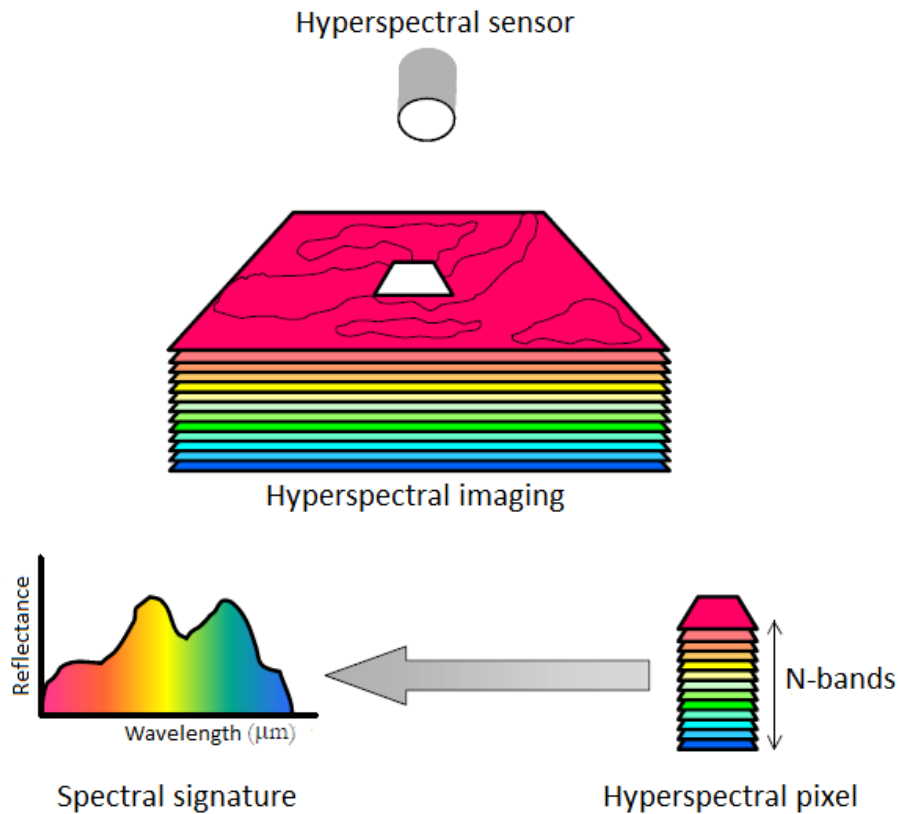


Figure 2.7: Hyperspectral analysis procedure.

It is known that the potential of these images is the large amount of information and that allows distinguishing classes and objectives in more detail. But this advantage also becomes a disadvantage when it does not have computing power enough to process and store these hundreds of bands. Then, we are faced with problems of high dimensionality of the data and data redundancy. The high dimensionality can be appreciated if we get an idea of the total size of an image like these, multiplying the pixel size in bits per the size of an image or single band per the total number of bands. The redundancy of information means the repetition of many spectral patterns and it can become quite significant, resulting in many cases inconvenient when statistical classification methods are wanted to use. For this reason, approximations or geometric and non-parametric techniques are most appropriate in many cases.

Therefore, it is necessary to perform a set of activities and processing techniques both hardware and software capable of handling effectively the inherent complexity of the hyperspectral data (high dimensionality) [33]. Although the processing chain for hyperspectral data is not an easy procedure to define consistently, within the framework

of this dissertation a set of recommendations for the definition of an appropriate processing chain for hyperspectral data have been introduced [34].

The first part of this processing chain is a specific process to obtain the data hypercube and provide noise-free samples, giving the data ready for its processing and target identification. It is in turn divided into the following steps:

- Data hypercube is formed from the image obtained by the hyperspectral camera.
- Image calibration.
- De-noising filtering.
- Band averaging.
- Pixel normalization.
- Samples extraction from data hypercube using the Labelling Tool.

Once the data of interest have been obtained and pre-processed to be used correctly, there is the need to extract relevant information from the collected data sets. Then, the second part of the data processing chain is further divided into the following additional steps:

- Feature extraction in order to reduce the high dimensionality and study the nature of each tissue.
- Classification.

It is important to emphasize that any data processing chain in any scientific field has to be flexible enough and adapted not only to its application on different scenarios, but also to the various types of resolutions that provide different spectral and spatial variations of the instruments.

The next section explains what the main goal in this processing is: the hyperspectral data classification. The processing chains used before will be described in detail in the next chapter.

2.4. Hyperspectral data classification

The simplest way to address the problem of pixels classification in a hyperspectral image is to consider that the pixels of interest are composed of a single material, using

conventional pattern classification techniques [35] but more accurately, because of the high number of spectral bands available.

In practice, the use of hyperspectral sensors allow a better determination of the internal composition of each pixel, which rarely will consist of a single material, since the phenomenon of the mixture is very common in the real world, regardless of the spatial scale considered [36].

There exists a set of pattern classification techniques that perform the interpretation of a scene on the basis of assigning a label or individual classification for each of the pixels of the scene. These techniques offer interesting results in certain applications, particularly those highlighted below.

- **Thematic classification:** Classification techniques have been used successfully in applications that aim to obtaining a thematic map in which each pixel in the hyperspectral image is properly labelled as belonging to a particular class [37]. There may be an additional class called “background” or “others” representing the pixels that are not classified in any of the previous classes. The ideal result is achieved when all classes are mutually exclusive of each other, including the class “background”. The key task in this type of application is usually determining the number of classes and its characterization in terms of training data or ground-truth information.
- **Targets detection:** Classification techniques have also been used very extensively in targets detection applications in hyperspectral imaging [38]. In these applications, the main objective is the identification of a specific material or object (called target in the literature) between all pixels of the image.

Conceptually, the two problems mentioned can be considered as binary classification problems:

- In the thematic classification, there are several possible classes associated with different objects. The goal is to ultimately determine the presence or absence of each of the objects considered in each pixel, situation that can be expressed as a binary classification problem [39].

- In the targets detection, the pixels are classified into two classes called “target” and “background”, depending on whether they contain the target sought or not.

The binary classification problem can be formulated mathematically as follows. Let R be the N -dimensional space formed by all pixels in the hyperspectral image. Given a N -dimensional array $\mathbf{u} = (u_1, u_2, \dots, u_N)^T$ associated with a specific pixel. The binary classification consists of dividing the space R into two regions, R_o and R_f , such that \mathbf{u} is classified as “target” if $\mathbf{u} \in R_o$ and “background” if $\mathbf{u} \in R_f$. This problem can be illustrated graphically using a scatterplot between two bit correlated bands of hyperspectral imaging, as shown in Figure 2.8.

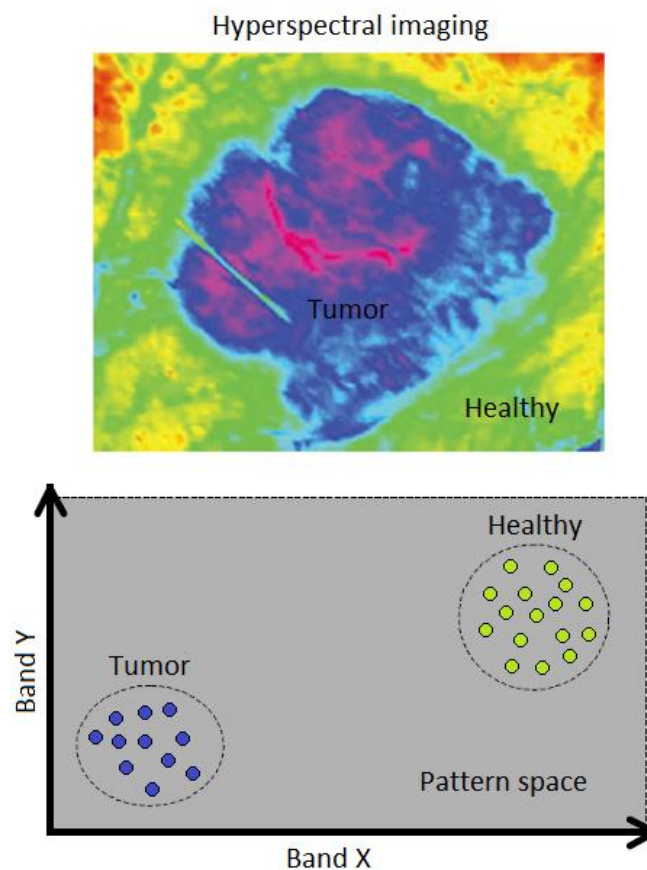


Figure 2.8: Graphic illustration of the classification problem in hyperspectral imaging.

As shown in Figure 2.8, the ideal situation in a classification problem occurs when the separation between target and background is clearly defined in clearly distinguishable clusters.

The hyperspectral image classification algorithms can be divided into three broad categories [40]: unsupervised algorithms, supervised algorithms and semi-supervised algorithms:

- **Unsupervised algorithms:** These algorithms assume that there is no a priori knowledge about existing classes. The aim of these techniques is to identify automatically classes or groups of pixels using a similarity metric.
- **Supervised algorithms:** It start with some knowledge about existing classes, from which it can be derived some classification criteria. This approach tends to be given by a preliminary step in which spectral signatures of the existing classes are selected.
- **Semi-supervised algorithms:** It is halfway between supervised and unsupervised learning. In addition to unlabelled data, the algorithm is provided with some supervision information – but not necessarily for all examples. Often, this information will be the targets associated with some of the examples.

2.4.1. Unsupervised classification algorithms

The pixels classification techniques in an unsupervised way for hyperspectral imaging are in full development phase [6]. Among the existing techniques highlights the *K-Means* method [41], which supposes the existence of K classes (parameter to be determined a priori) and performs a grouping of the pixels of the image in such classes, using purely statistical methods of vector quantization based on the average spectra of these classes.

Moreover, the *ISODATA* method [42] also requires initialization of a K parameter relating to the number of desired classes, prior to the execution of the algorithm. In addition, this method requires information on the minimum number of signatures belonging to one class. If the initial value of K is low, the dispersion between classes can be very high. Conversely, if the initial value of K is high, the distance between classes can be very small, causing the partitioning of the same class in several classes similar to each other.

Overall, the recent literature shows that the results obtained by these two techniques have not been very satisfactory, except in very specific applications [43].

2.4.2. Supervised classification algorithms

In supervised classification techniques highlights the *matched filters* and *Spectral Angle Mapper (SAM)* method, both based on first-order statistics [44]. Within this category may also be other classifiers as the *nearest neighbour*, *minimum distance*, *parallelepiped* or *maximum likelihood* techniques. However, this dissertation is focused on the *Support Vector Machine (SVM)* technique, which has demonstrated excellent performance when working with high-dimensional data such as hyperspectral data.

2.4.3. Semi-supervised classification algorithms

Regarding semi-supervised learning methods, most algorithms can be organized into four classes: generative models, low-density separation, graph-based methods and change of representation [40]. Nevertheless, this dissertation is focus on a semi-supervised algorithm based on the heuristic approach of self-training.

Once presented the most common techniques of hyperspectral image classification, this section is concluded highlighting some techniques used to evaluate the performance of these algorithms.

2.4.4. Evaluation metrics used in classification algorithms

The large number of existing techniques as well as the continued proliferation of new methodologies makes clear the need for comparative schemes or metrics to qualitatively analyse the performance of new methodologies arose, contrasting its results with those provided by the existing ones. Most of the evaluation techniques of digital image analysis algorithms are based on the concept of ground-truth [45]. Ideally, it is possible to define the concept of ground-truth as the optimal classification or interpretation result which should get an algorithm [46][47].

The ground-truth usually comes characterized by relevant information about the properties in the real world of a set of targets that are desired to identify or characterize. This information is usually obtained by measurements made directly in the study area covered by the image [48], although it is also possible to obtain ground-truth information

by applying algorithmic techniques [5]. In any case, the first alternative is the more reliable, but it can be expensive due to the need to label all the samples obtained [49].

Assuming the existence of ground-truth information, there are several methodologies to compare that information with the results provided by an image analysis algorithm. This section provides a brief description of the different metrics that can be applied to assess the ability of a computer algorithm in terms of classification and identification of targets of interest in a digital image. In particular, it will highlight one of the most widely used approaches called the confusion matrix, that will serve for the subsequent comparative study of this dissertation and from which other metrics are derived as the percentage of success in the classification.

The confusion matrix [50] is a technique to assess the accuracy of classification algorithms of digital images. This technique assumes that the ground-truth information is expressed as a thematic map [51][52] characterized by the following properties:

1. Each pixel is labelled as belonging to a particular class, so as to have N classes or reference regions $\{R_i\}_{i=1}^N$.
2. The reference regions are mutually exclusive of each other, i.e., two different regions have no pixel in common: $R_i \cap R_j = \emptyset, \forall i \neq j$.

Assuming that each pixel i of the image to evaluate I is assigned by the algorithm as belonging to a certain class C_i , so as to have N classes. C_i sets are a partition of the image to be evaluated, that is, the union of all sets resulting in the image and two different sets have no element in common:

$$\bigcup_{i=1}^N C_i = I \text{ and } C_i \cap C_j = \emptyset, \forall i \neq j \quad (2.1)$$

Given the above considerations, Figure 2.9 shows an example of the process of constructing a confusion matrix. In the figure, the thematic map of ground-truth classification associated with the image to classify, the classification result provided by a given algorithm to that image, and the confusion matrix that quantifies the accuracy of the algorithm in the classification task are shown. As shown, the matrix entries are expressed in the form of a_{jk} where $a_{jk} = \text{cardinal}\{C_j \cap R_k\}$, that is, the number of pixels of the

resulting region when performing the intersection between a C_j class obtained by the algorithm and a ground-truth class R_k [50].

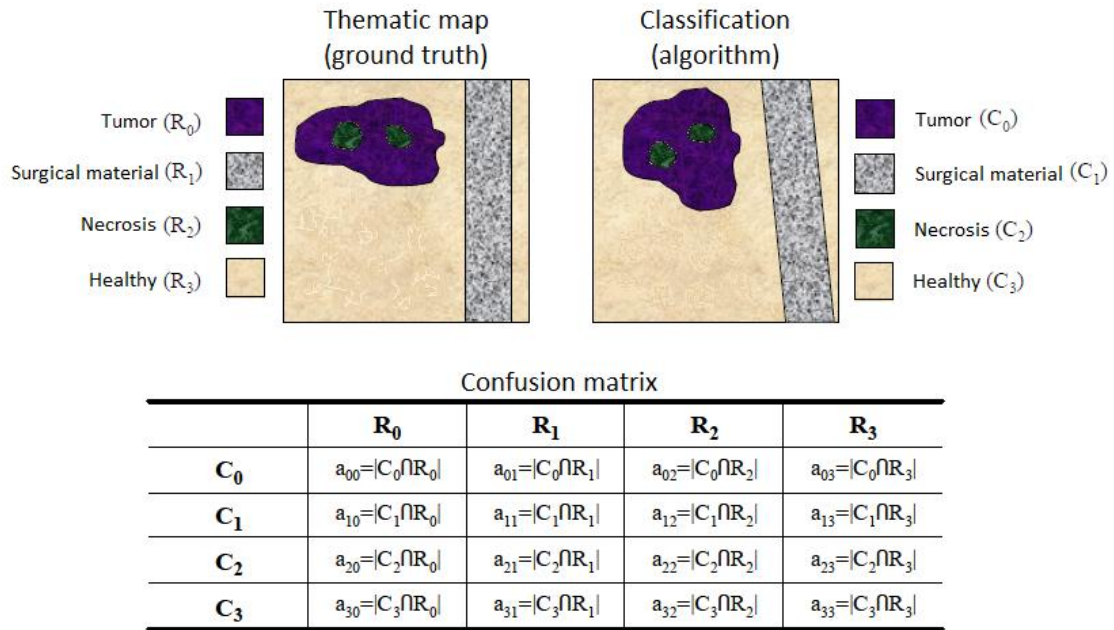


Figure 2.9: Example of constructing of a confusion matrix.

From the confusion matrix can be derived some generic accuracy measures [53] as:

- **Overall accuracy (OA):** Percentage of pixels correctly classified in all classes:

$$OA = \frac{\sum_i^N a_{ii}}{\sum_{ij}^N a_{ij}} \times 100 \quad (2.2)$$

OA is a percentage should approach 100%, which would be the ideal classification; however, theoretically any predictor will possess a minimum error bound known as the Bayes error rate. When the reference set is not well defined, the OA will not be representative regarding the true performance of the classifier. For example, if a class has very few pixels of reference, its influence on the computation of OA will be very low.

Moreover, in order to deepen the metrics an alternative representation of the confusion matrix is presented.

Let us imagine a study evaluating a new test that screens healthy and tumour samples. Each sample taking the test either has or does not have the disease. The test outcome can be positive (predicting that the sample is a tumour sample) or negative

(predicting that the sample is not a tumour sample and therefore it is healthy sample). The test results for each sample may or may not match the sample's actual status. In that setting:

- True positive: Tumour sample correctly diagnosed as tumour.
- False positive: Healthy sample incorrectly identified as tumour.
- True negative: Healthy sample correctly identified as healthy.
- False negative: Tumour sample incorrectly identified as healthy.

In general, Positive = identified and negative = rejected. Therefore:

- True positive = correctly identified.
- False positive = incorrectly identified.
- True negative = correctly rejected.
- False negative = incorrectly rejected.

The four outcomes can be formulated in a confusion matrix as follows:

	Condition (ground-truth)	
Total population	Condition positive	Condition negative
Test outcome positive	True positive	False positive (Type I error)
Test outcome negative	False negative (Type II error)	True negative

Table 2.4: Confusion matrix.

There are other metrics such as average accuracy, sensitivity and specificity, which are really important in the medical field, Kappa coefficient, the commission errors and omission errors that are not considered in this study [54].

2.5. Summary

Hyperspectral imaging is a very powerful tool that can be used to provide a solution in many different fields. In this dissertation, it is intended to apply hyperspectral imaging in the medical field, particularly in the brain cancer detection.

For this purpose, a study of main existing techniques for hyperspectral imaging processing is performed because it is necessary to properly process hyperspectral data with the ultimate goal of obtaining the best possible classification. In order to evaluate the classification process, a set of standard evaluation metrics will be used to subsequently draw conclusions with regard to the efficiency approaches for brain cancer detection.

On the other hand, an overview of the instrumentation and the methodology used to collect the in-vivo hyperspectral data of human brain samples was provided in this section.

Chapter 3

Image processing techniques

3.1. Introduction

Image processing is the processing of images using mathematical operations in any form of signal processing for which the input is an image, such as a photograph, video frame or hyperspectral imaging; the output of image processing may be either an image or a set of characteristics or parameters related to the image [55]. Namely, image processing is the set of techniques applied to images in order to improve quality or facilitate the search for information.

For performing a spectral classification using the hyperspectral images captured, a classification system based on a Support Vector Machine (SVM) classifier has been defined. The processing chain in this project can be divided into four different stages as we can observe in Figure 3.1, which shows an overview of this classification system:

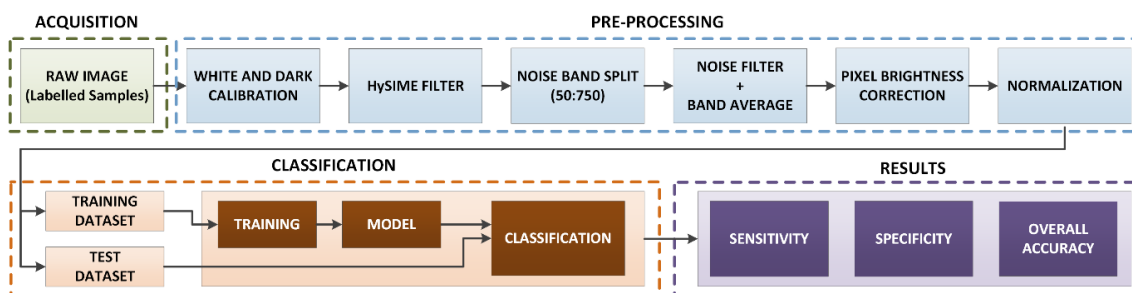


Figure 3.1: Classification system overview.

The first stage of the proposed classification system is the acquisition step, where the labelled dataset of the normal tissue, blood vessels, tumour tissue and background elements samples are collected. The procedure followed to collect these data will be described later in section 3.2.

After the acquisition stage, a pre-processing chain is applied to the labelled dataset. In this pre-processing stage an image calibration is done in order to address the problem of the spectral non-uniformity of the illumination device and the dark current. Furthermore, a set of steps with the goal of removing the noise of the spectral signatures and to reduce the number of bands of the samples without lose the main spectral information are applied.

In addition, so as to homogenize the spectral signatures in terms of reflectance level, a pixel bright correction step and a normalization step are performed.

In the classification stage, a feature extraction step is performed. Features are functions of the original measurement variables that are useful for classification and/or pattern recognition, and feature extraction is the process of defining a set of features, or image characteristics, which will most efficiently or meaningfully represent the information that is important for analysis and classification. In this regard, there are several applicable methodologies, of which will be applied in this dissertation, mainly spectral unmixing techniques. Once the data have been processed, and with some analyses already performed, they will be classified. For this purpose, the labelled dataset is partitioned into two different datasets. Training dataset is used to generate the classifier model while test dataset is used to validate this model, obtaining the results of the classification.

As noted in the previous chapter, classification is generally a process in which the individual elements or items are differentiated into groups, based on quantitative information of one or more inherent characteristics of the elements, usually by items previously labelled using sets or training patterns. At last, and as an option, the resulting data from the classification may be post-processed (for example using spatial techniques) to improve the coherence of them.

Finally, overall accuracy is the evaluation metrics chosen in order to know the goodness of the classifier model. Overall accuracy measures the ability of the model to

correctly predict the class label of new or previously unseen data, given the rate of the samples that has been correctly classified. This evaluation metrics has been previously described in section 2.4.4.

3.2. Data pre-processing techniques for hyperspectral images

This section describes the pre-processing methods discussed previously. The hyperspectral data obtained in the data acquisition campaign have been pre-processed following the processing chain presented in Figure 3.1. This chain is composed mainly by four steps presented in Figure 3.2, namely: image calibration, noise filtering, band averaging and pixel normalization, which have been developed by the department in order to homogenize the spectral signatures of the labelled samples obtained from the in-vivo hyperspectral data-cubes [30].



Figure 3.2: Data pre-processing chain flowchart.

After the image acquisition, the hyperspectral raw data are calibrated using a white reference image (captured from a white reference tile in the same illumination conditions that the images were captured) and a dark reference image (obtained by keeping the camera shutter closed) so as to avoid the problem of the spectral non-uniformity of the illumination device and the dark currents of the camera sensor. Next, due to the high spectral noise generated by the camera sensor, a set of steps with the goal of removing this noise from the spectral signatures and to reduce the number of bands of the samples without lose the main spectral information are applied. The noise filter which conforms the first step of the HySIME algorithm is employed for the noise removal [56][57]. Finally, a normalization step is performed in order to homogenize the spectral signatures in terms of reflectance level.

The following sections describe the steps performed in this pre-processing chain.

3.2.1. Image Calibration

The first step in the pre-processing chain is the image calibration, where the significant signal variations caused by the non-uniform illumination over the surface of the captured scene are corrected. The acquired raw image is calibrated using the white and dark reference images.

White and dark reference images are acquired by the demonstrator inside the operating theatre under the same illumination conditions used to acquire the in-vivo brain surface images. The white reference image is obtained from a standard white reference tile and the dark reference image is obtained by keeping the camera shutter closed. The hyperspectral calibrated image is calculated using the equation (3.1), where CI is the calibrated image, RI is the raw image and WR and DR are the white and dark reference images respectively. Figure 3.3 shows the spectral signature of a grade IV glioblastoma tumour tissue before the calibration step (raw pixel) and Figure 3.4 after the applied calibration.

$$CI = 100 \cdot \frac{RI - DR}{WR - DR} \quad (3.1)$$

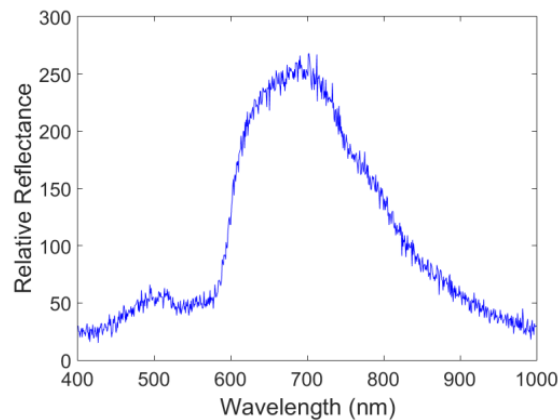


Figure 3.3: Raw spectral signature of a grade IV glioblastoma tumour tissue.

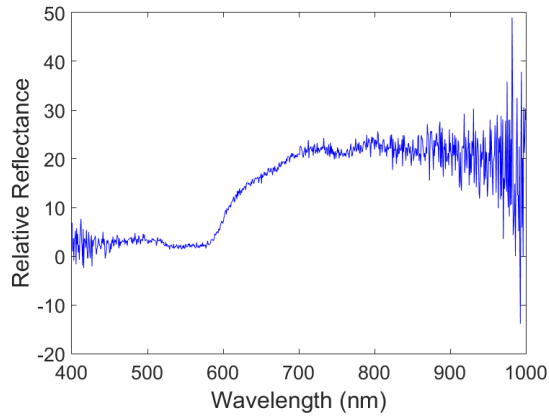


Figure 3.4: Calibrated spectral signature of a grade IV glioblastoma tumour tissue.

3.2.2. De-noising filtering

Noise reduction is the process of removing noise from a signal. All recording devices, both analogic and digital, have traits which make them susceptible to noise. Noise can be random or white noise with no coherence, or coherent noise introduced by the device's mechanism or processing algorithms.

The second step in the pre-processing chain is to apply a series of filters in order to remove the noise existing in the spectral signatures, mainly due to the CCD sensor of the VNIR camera.

First of all, the noise filter which conforms the first step of the HySIME algorithm is applied, reducing a large amount of noise from the spectral signatures. Hyperspectral subspace identification by minimum error (HySime) is an eigen-decomposition based technique and does not depend on any tuneable parameters. HySime initializes by determining the signal and noise correlation matrices and then representing the subspace by minimizing the mean square error between the signal projection and the noise projection, estimating the number of spectrally distinct signal sources in hyperspectral dataset. The result is an estimate of the number of spectrally distinct signal sources or the inherent dimensionality of the dataset [58][59][60]. This method was proposed in [56] and it is eigen-decomposition based i.e. it decomposes or reduces the original signal into subsets of eigen-vectors. The subspace obtained by HySime optimally represents the original signal with minimum error. HySime uses multiple regressions for the estimation of the noise and signal covariance matrices and is adaptive, i.e. it does not require any tuning parameters. Also it makes no assumptions about the noise being independent and identically distributed (i.i.d.) and the subspace dimensions.

The difficulty in getting reliable noise estimation from these eigenvalues is that these eigenvalues are still representing the mixtures of the signal sources and the noise present in the data. When the signal sources are too weak, their contribution towards the computation of eigenvalues is very low, which can be observed if there is no sudden drop in eigenvalues distribution [61]. HySime instead finds the subset of eigenvectors and the corresponding eigenvalues by minimizing the mean square error between the original signal and the noisy projection of it.

HySime [56] starts with the noise estimation step in which the noise correlation matrix of the data is computed. Then it calculates the signal correlation matrix and computes the eigenvectors by performing the eigen-decomposition of the signal correlation matrix. The signal subspace is then derived by minimizing the sum of projection error power and noise power, which are decreasing and increasing functions of the subspace dimensions respectively.

This function, which is named Hyperspectral Noise Estimation, infers the noise in a hyperspectral data set, by assuming that the reflectance at a given band is well modelled by a linear regression on the remaining bands [56][57]. Figure 3.5 shows the same spectral signature after having applied this noise filter.

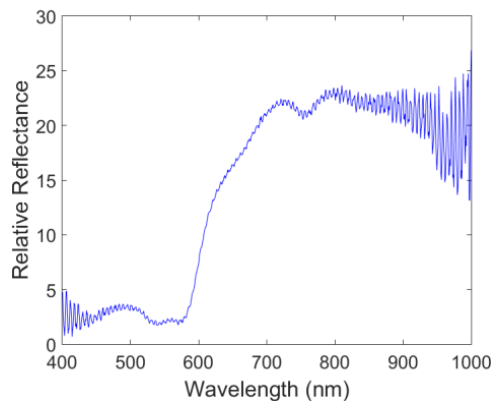


Figure 3.5: Spectral signature with the HySIME filter applied to a grade IV glioblastoma tumour tissue.

After this step, the bands from 0 to 50 and the bands from 750 to 826 are removed since these bands contain too much noise due to the limited performance of the CCD sensor, the grate and the light scattering in the extreme bands. This fact can be seen in Figure 3.5. Additionally, this step reduces the number of bands in the spectral signatures from 826 to 700 bands.

3.2.3. Dimensionality Reduction

In machine learning, dimensionality reduction is the process of reducing the number of random variables under consideration [62].

It is important to distinguish the dimension reduction techniques from compression techniques for hyperspectral imaging [63]. Contrary to the compression methods objective, the dimensional simplification process usually does not allow reconstructing the original image. By contrast, dimensional reduction aim is to obtain a minimum representation of the image that contains the necessary information to perform the analysis on a reduced subset of original image. Thus, dimensional reduction algorithms are usually designed so that minimizes errors when working with this subset, unconcerned about the possibility of recovering the original image [64].

Regarding the hyperspectral image processing, reducing the information is very important. The best results are achieved when an expert constructs a set of application-dependent features. Nevertheless, if no such expert knowledge is available, general dimensionality reduction techniques may help. Thus in literature have been investigated various methods to solve the problem of the original repetitive information and perform more efficient characterization. In this pre-processing chain, a dimensionality reduction based on a smooth filter is performed.

In many experiments in physical science, the true signal amplitudes (y -axis values) change rather smoothly as a function of the x -axis values, whereas many kinds of noise are seen as rapid, random changes in amplitude from point to point within the signal. In the latter situation it may be useful in some cases to attempt to reduce the noise by a process called smoothing. In smoothing, the data points of a signal are modified so that individual points that are higher than the immediately adjacent points (presumably because of noise) are reduced, and points that are lower than the adjacent points are increased, thus is achieved that the signal is more homogeneous. This naturally leads to a smoother signal. As long as the true underlying signal is actually smooth, then the true signal will not be much distorted by smoothing, but the noise will be reduced [65].

When processing a signal by the Smooth filter, the goal is to create an approximate function that attempts to capture important signal patterns, leaving out the noise. The Smooth filter smooths the signal by using a moving average filter.

In the moving average filters each output value is obtained as the average of a subset of the original data. Its purpose is to highlight the significant pattern i.e. it reduce the noise smoothing the fluctuations in short periods, thus highlighting trends or long periods cycles [65].

Moving average filters [66] are the most common filters used in signal processing, mostly because it is the easiest to understand and use digital filter. Despite its simplicity, it is optimal for the task of reducing random noise. This makes them the best filters to signals in the time domain. Instead, moving average filters are the worst for signals encoded in the frequency domain, as they have little ability to separate frequency bands from each other [67].

Most smoothing algorithms are based on the "*shift and multiply*" technique, in which a group of adjacent points in the original data are multiplied point-by-point by a set of numbers (coefficients) that defines the smooth shape, the products are added up to become one point of smoothed data, then the set of coefficients is shifted one point down the original data and the process is repeated. The simplest smoothing algorithm is the *rectangular* or *unweighted sliding-average smooth*; it simply replaces each point in the signal with the average of m adjacent points, where m is a positive integer called the *smooth width*.

Therefore, a smoothing technique is independently applied to each pixel of the image. This technique modified each pixel y_k of the spectral signature of the pixel under analysis, $Y = (y_1, y_2, \dots, y_{N_B})$, where k is the selected pixel and N_B is the original number of bands. The new value of the "smoothed point" $(y_k)_s$ is the average of the values corresponding to predefined number of its surrounding points, as shown in equation (3.2), where n is number of bands to be combined.

$$(y_k)_s = \sum_{i=-n}^{i=n} y_{k+i} / (2 \cdot n + 1) \quad (3.2)$$

Due to the extremely high spectral resolution of the images, it has been observed that consecutive bands are correlated, providing redundant information. In order to avoid this redundancy and speed up the hyperspectral analysis of the data set, a few bands have been removed. Moreover, it is not needed to perform the smooth filter for those bands that are going to be removed, which eases the filtering process in terms of computational

burden. In particular 129 spectral bands, from the 700 spectral bands previously processed, have been totally filtered, uniformly covering the spectral range from 400 to 1000 nm as shown in Figure 3.6.

3.2.4. Data Normalization

Due to the surgery procedure, the pixels are captured at different height, and hence, at different radiation intensity. This fact typically causes that pixels labelled as tumour and normal tissue have very different radiation intensities. If these pixels are introduced without any pre-processing in a classifier, the pixels could be classified according to its brightness, without really taking into account their spectral signatures. In order to avoid this fact, a pre-processing step which normalizes the brightness of the pixels in the image needs to be included. This process calculates the brightness of each pixel of the hyperspectral image and divides each pixel by its brightness, as shown in equation (3.3). In this equation Y_{BC} is the pixel with the brightness correction, Y is the pixel to be corrected and y_i is the i -th component of this pixel. With this pre-processing step, the brightness of each pixel is homogenized without modifying its spectral signature. Figure 3.6 illustrates the final spectral signature with the full pre-processing chain applied.

$$Y_{BC} = \frac{Y}{\sqrt{\sum_{i=1}^{129} y_i^2}} \quad (3.3)$$

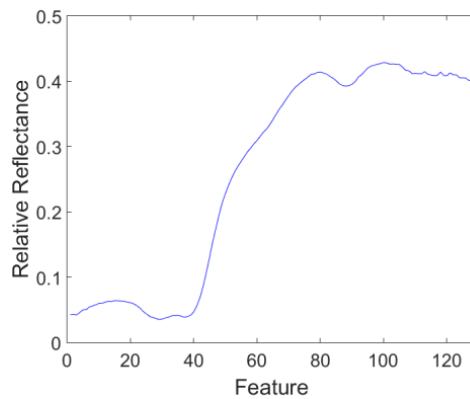


Figure 3.6: Spectral signature with the noise and band reduction step and the normalization applied to a grade IV glioblastoma tumour tissue.

3.3. Ground Truth Generation

Any supervised classifier relies on the quality of the labelled data used for training. Therefore, to allow the classifier finding the correct solution, the training samples should

be fully representative of the surface-type statistics. Manual training set definition is usually done by visual inspection of the scene and the successive labelling of each sample. This labelling methodology carries the risk of adding redundant information to the training set, due to the fact that neighbouring pixels usually carry the same information. In addition, pixels that have not the same spectral information can be labelled with a wrong label due to this manual labelling process. Therefore, in order to make the model as robust as possible, the training set should be kept as small as possible and focused on the pixels that really help to improve the performance of the model [68].

In this section, a methodology based on Spectral Angle Mapper (SAM), which have been developed by the department, is used to generate a robust and efficient ground truth [69]. First of all, an interactive graphical user interface (GUI), that allows the specialist to perform the labelling of the pixels in an easy and convenient way, was designed using Matlab® GUIDE. In the first step of the labelling process, the specialist (a neurosurgeon from the HELICoiD project) selects a pixel from a synthetic RGB image extracted from the hypercube to be labelled based on its visual appearance. Once the reference pixel has been selected, due to the difficulty of assigning a pixel to a certain class with certain degree of assurance, the Spectral Angles (SA) between the selected pixel and the other pixels in the hypercube are calculated. Applying a threshold, visually configured by the specialist to match the physiological features of the tissue, a binary mask is obtained. Adjusting this threshold dynamically, a synthetic RGB image is generated, containing only the pixels that meets the condition that its spectral angle respects to the reference pixel are lower than the threshold. Then, the specialist selects the region of interest and assigns a label to the pixels inside this region.

This framework for labelling provides two main advantages. On the one hand, when the neurosurgeon selects a reference pixel, it is possible to ensure that the pixels belong to a certain class by looking at the pixels with lower SAs with respect to the reference pixel. On the other hand, the process of manually selecting multiple pixels from a hypercube for each class is a time-consuming task, so this method allows collecting several pixels from a given class with less effort.

Nevertheless, this method has a drawback: by selecting similar pixels it is possible to include redundant information to the training set. To avoid this situation and to generate a dataset as representative and small as possible, after neurosurgeons generate

the ground truth of a hypercube, this ground truth data must be refined. This dataset refinement will be performed in future works.

Figure 3.7 presents the block diagram of this procedure and the resulting image at each stage of the labelling process. Figure 3.7.a represents the pre-processed hypercube that is the input to the labelling chain and Figure 3.7.b shows the synthetic RGB representation of the hypercube, where the reference pixels are selected.

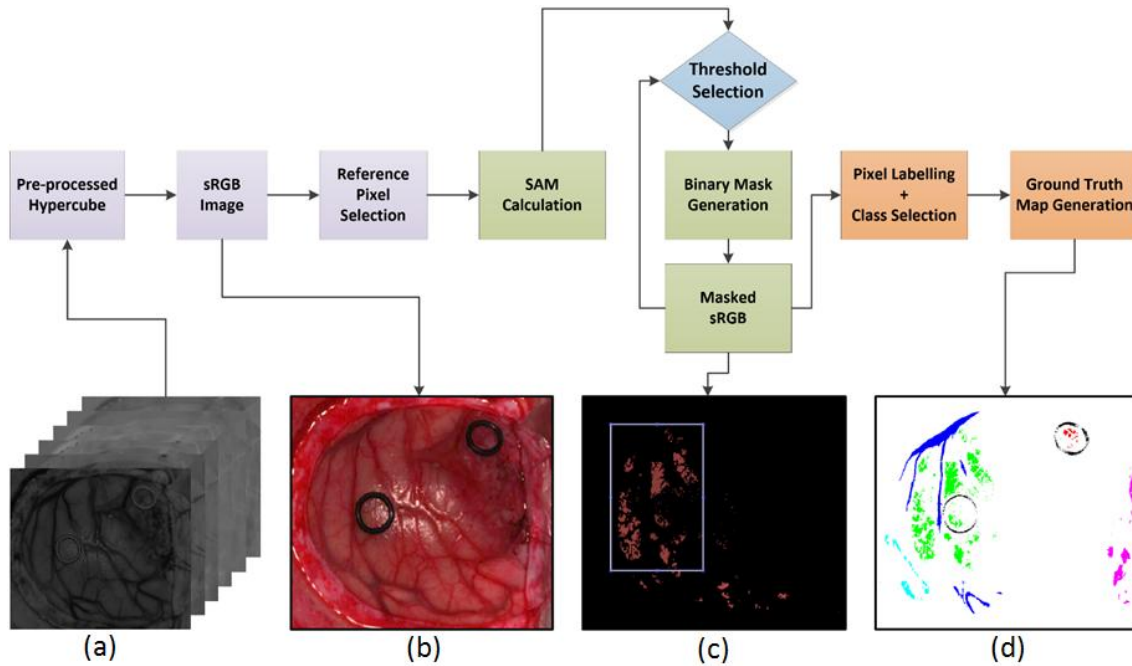


Figure 3.7: HELICoID Labelling tool process flowchart. (a) Pre-Processed hypercube. (b) Synthetic RGB image extracted from the hypercube. (c) SAM masked over the sRGB image. (d) Final ground truth map generated.

Figure 3.7.c illustrates the SAM between the reference pixel and the others pixels of the hypercube once the threshold has been set up and the area to be labelled has been selected by the specialist. Finally, Figure 3.7.d shows the final ground truth map generated after the labelling process performed by the specialist. All the ground truth maps generated using this application conform the labelled database that will be used to train the supervised algorithms.

3.4. Feature extraction

Feature extraction transforms the data in a high-dimensional space to a space of fewer dimensions. It starts from an initial set of measured data and builds derived values (features) intended to be informative, non-redundant, facilitating the subsequent learning

and generalization steps, in some cases leading to better human interpretations. The data transformation may be linear or nonlinear [70][71].

This process happens when the input data to an algorithm are too large to be processed and it is suspected to be redundant (e.g. the repetitiveness of images presented as pixels), then it can be transformed into a reduced set of features. The extracted features are expected to contain the relevant information from the input data, so that the desired task can be performed by using this reduced representation instead of the complete initial data.

Feature extraction involves reducing the amount of resources required to describe a large set of data. When performing analysis of complex data one of the major problems stems from the number of variables involved. Analysis with a large number of variables generally requires a large amount of memory and computation power or a classification algorithm which overfits the training sample and generalizes poorly to new samples. Feature extraction is a general term for methods of constructing combinations of the variables to get around these problems while still describing the data with sufficient accuracy.

The spectral transformations data acting on the vectors to get new sets or components bands in the image are processing techniques for feature extraction. These new components represent an alternative description of the data, in which a pixel vector is related to its previous brightness value of the original image by a linear transformation of the spectral bands. These techniques seek to preserve the essential information of the original image by reducing the number of transformed dimensions and are used before the classification process in order to increase accuracy.

Some applicable methodologies for feature extraction are endmembers extraction and unmixing algorithm, which there are investigations for hyperspectral image analysis. The hyperspectral unmixing is a source separation problem (scene materials) which is statistically dependent and must be combined in a nonlinear function. There are different strategies (spectral versus hybrid techniques) being compared looking for an efficient solution taking into account the high dimensionality of the data. Other feature extraction techniques based on dimensionality reduction and spectral unmixing are developed in [54].

There are also other methods for feature extraction such as spatial contexts, which takes into account the neighbourhood or space environment of the pixel considered, because they contain much more information than the pixel itself.

The fact of using pre-processing techniques of hyperspectral imaging aimed at reducing the dimensionality of the input data is given, among other reasons, by the known as Hughes phenomenon [72], described below. In a typical classification problem, the goal is to assign a class label to the input data. The minimum expected error that can be achieved by performing classification is known as the Bayes error [73]. The Bayes error is a function which decreases with the data dimensionality. A new feature adds information about the instance and then, one would expect that the classification would be as good as when this information had not been entered. However, in practice this is not thus, when adding a new feature to the data the Bayes error is decreased, but also the deviations of classification error increases. This increase is due to the fact that more parameters need be calculated based on the same number of examples. If the increase of the deviations in the classification error is greater than the decrease Bayes error, then the use of the additional characteristic degrades the decision rule. And this phenomenon is what is known as the Hughes effect [72]. Furthermore, when the data dimensionality and the complexity of the decision rule increase, the Hughes effect may become more serious [6].

In summary, the supervised classifier performance decreases with the data dimensionality unless the number of samples is infinite [72]. This dimensional reduction that arises is a step used to reduce the computational load of successive steps by removing noise and redundant information in the image. In spectral data, much of the information is repeated from image to image. This redundancy complicates analysis and classification unnecessarily. These methods perform a decrease in the number of bands. The goal is to obtain a minimum representation of the image that contains the necessary information to perform the analysis on a small subset of the original image [74]. Moreover, dimensional reduction techniques usually bring as a result an improvement in the SNR of data through the removing noise [75], which makes it attractive to use previous to classification step. The disadvantage of this alternative is the difficulty in interpreting the spectral data after the reduction step.

3.4.1. Spectral unmixing Techniques

In many studies, hyperspectral analysis techniques are divided into full-pixel and mixed-pixel classification techniques [76][77][78], where each pixel vector defines a spectral signature or fingerprint that uniquely characterizes the underlying materials at each site in a scene. Full-pixel classification techniques assume that each spectral signature comprises the response of one single underlying material. Often, this is not a realistic assumption, because the spatial resolution of the sensor is not fine enough to separate different pure signature classes at a macroscopic level. In consequence, these can jointly occupy a single pixel, and the resulting spectral signature will be a composite of the individual pure spectral, often called endmembers in hyperspectral imaging terminology [79].

In this chapter, we explore the use of spectral unmixing for feature extraction prior to supervised classification of hyperspectral data using SVM. Moreover, differently from most feature extraction techniques available in literature, the features obtained using linear spectral unmixing are potentially easier to interpret due to their physical meaning [80].

Hyperspectral data are often used to determine what materials are present in a scene. In our case, materials of interest could include some tissues as tumor, healthy, necrosis in addition to blood, veins and surgical elements, etc. In fact, each pixel of a hyperspectral image could be compared to a material database to determine the type of material making up the pixel.

Spectral unmixing aims at the decomposition of the mixed pixel spectrum into its constituent spectra, also called endmembers [81]. Each pixel in the hyperspectral image can be considered as being composed of linear combination of ground spectra or endmembers with each endmember contributing to the pixel spectra. Thus the spectral signature at each pixel in a L -dimensional hyperspectral image, $Y \in R^L$, when p is the number of endmembers, can be expressed as,

$$y = x + n \quad (3.4)$$

where, y - L -dimensional pixel vector.

x and n - L -dimensional signal and noise vectors respectively.

Since the signal vectors lie in an unknown p -dimensional subspace, each signal vector is given as,

$$x = M \cdot s = \sum_{i=1}^p m_i s_i \quad (3.5)$$

where, M is a $L \times p$ matrix, whose columns are $L \times 1$ endmembers.

s is the abundance fraction of each endmember in a pixel.

In essence, spectral unmixing can be defined as the process of determination of the number of image endmembers and their pure signatures and the amount in which they appear in the given mixes pixel [60]. Namely, Spectral unmixing consists of estimating the fraction of the pixel area covered by each material present in the scene [3].

Pixel unmixing algorithms can be separate into two main areas: Endmember Determination and Abundance Estimation algorithms as shown in Figure 3.8.

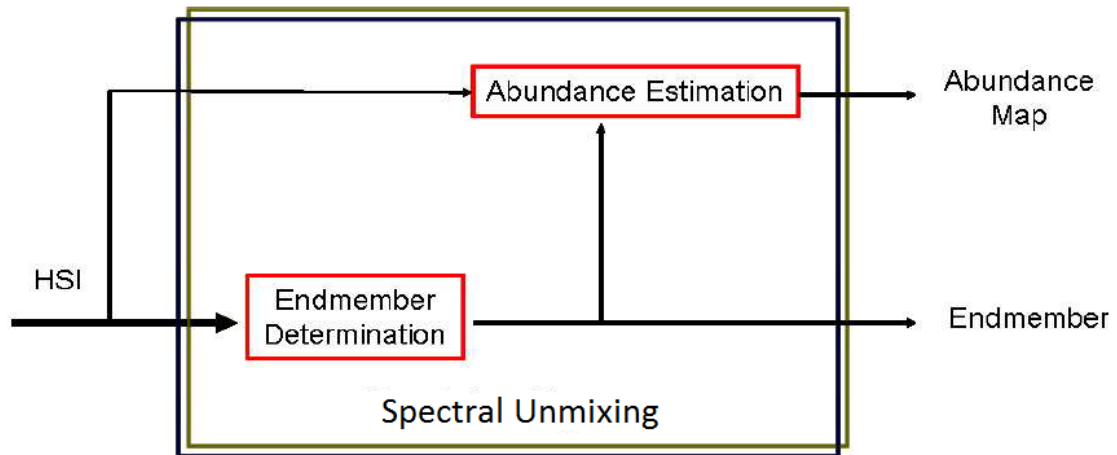


Figure 3.8: Spectral unmixing Diagram Process.

Before describing the algorithms considered, it should emphasize the context in which these algorithms will be applied. In this regard, Figure 3.9 [82] describes the classic method for analysing hyperspectral images using linear mixed model. As shown in Figure 3.9 [82], the methodology starts from a hyperspectral image and performs the following steps:

1. **Dimensionality reduction:** This step is optionally used by certain algorithms to reduce the computational load of successive steps by removing noise and redundant information in the image.
2. **Endmembers extraction:** In this step the pure spectral signatures that combine to result in mixed pixel in the image are identified.
3. **Abundances estimation:** The abundance of pure spectral signatures or endmembers is estimated at each pixel of the image.

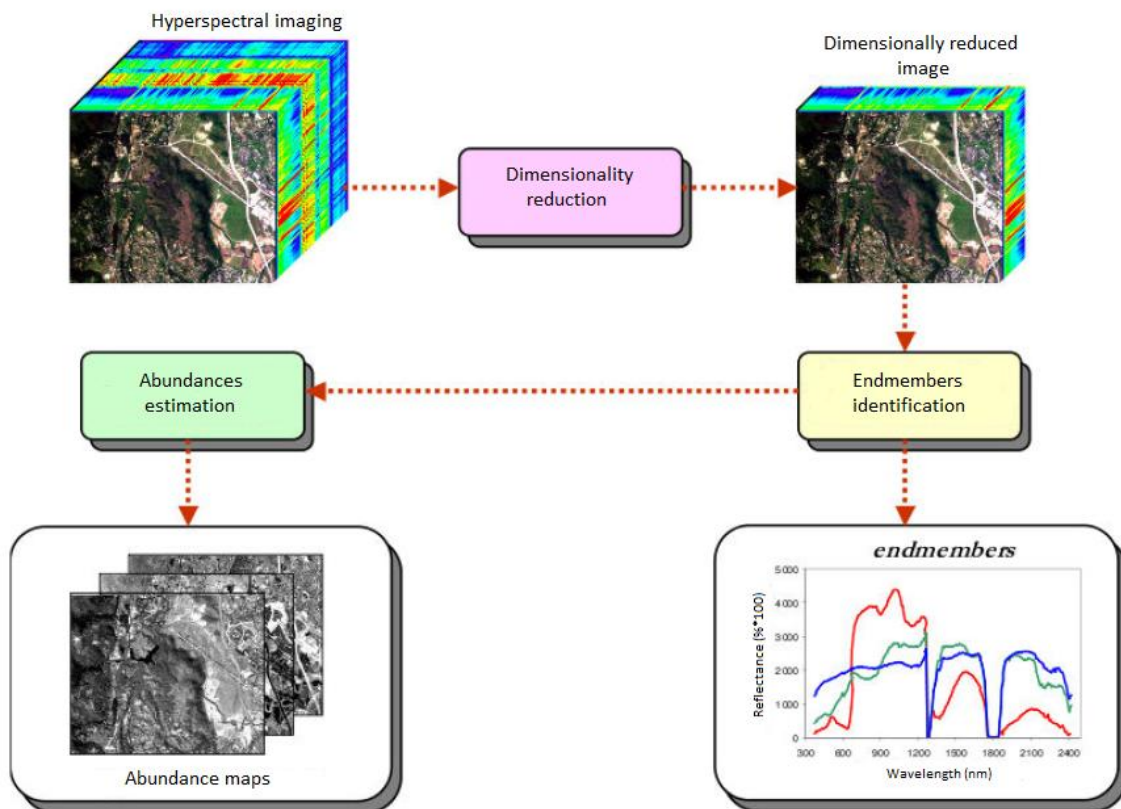


Figure 3.9: classic method for analyzing hyperspectral images using linear mixed model.

The spectral unmixing chain can be divided in three steps: number of endmember estimation, endmember extraction and abundances estimation.

3.4.1.1. Number of endmember estimation

First, the number of endmembers p is estimated directly from the original n -dimensional hyperspectral image. For this purpose, two standard techniques widely used in the literature such as the HySime method [56] and the VD concept [83] are recommended. These techniques are described in [54].

In our case, the estimation of number of endmembers is not necessary because this number is known to us a priori and associated with the number of classes.

3.4.1.2. Endmember extraction algorithms

Once the number of endmembers p has been estimated, an automatic algorithm to extract a set of endmembers from the original hyperspectral image is applied [84]. There are many algorithms to unmix hyperspectral data each with their own strengths and weaknesses. Many algorithms assume that pure pixels (pixels which contain only one material) are present in a scene.

Endmember extraction algorithms can be divided into two groups: first those based only in image spectral information and secondly those that uses both spectral and spatial information. The endmember extraction algorithms based on spectral information depends on the ability to discriminate the pixels based solely on its spectral features. These techniques are studied in [54].

In this dissertation endmembers extraction is not implemented. Instead, each endmember is calculated as the average of all pixels in its class, because this approach offers better results for this kind of applications [54].

3.4.1.3. Abundance estimation algorithms

Finally, linear spectral unmixing (either unconstrained or constrained) can be used to estimate the abundance of each endmember in each pixel of the scene, providing a set of p abundance maps [80].

3.4.1.3.1. Linear Spectral Unmixing

In hyperspectral images, spectral mixing is the result of mixing of two or more spectrally distinct substances. Spectral unmixing is the process by which we can identify the constituents of the mixed pixel and their proportions. Generally, two models of mixing are assumed: linear and nonlinear [60]. As opposed to nonlinear unmixing, which generally require detailed information about physical properties that may not be always available, linear spectral unmixing consists of identifying the pure spectral components or endmembers. When the pure spectral signatures are identified, the proportion of each material in each pixel can be estimated. Abundances provide additional information about

the composition of each pixel; if this information is used in a correct way, it may complement the results provided by traditional “hard” classification techniques. Moreover, non-linear mixing results from multiple scattering often due to non-flat surface [80].

The simplest and the most commonly assumed model for a mixed spectrum is a linear model [76]. A single pixel can be portrayed as a checkerboard mixture, assuming that there is no multiple scattering between components, then the spectral response of the pixel is a linear combination of the fractional abundances (area covered by each endmember in the pixel) of the individual substances [81], hence the term Linear Mixture Model (LMM). If there are p endmembers, then the linear mixture model can be expressed as

$$x = \sum_{i=1}^p m_i s_{ij} + w_j = M \cdot s + w \quad (3.6)$$

$$j = 1, 2, \dots, N$$

where, x is the $L \times 1$ received pixel spectra.

M is a $L \times p$ matrix, whose columns are $L \times 1$ endmembers.

s is the abundance fraction of each endmember in a pixel.

w is the $L \times 1$ additive noise.

N is the number of pixels in the image.

In linear mixing models each pixel is modelled as a linear sum of all the radiated energy curves of materials making up the pixel. Therefore, each material contributes to the sensor's observation in a linear fashion.

Additionally, a conservation of energy constraint is often observed thereby forcing the weights of the linear mixture to sum to one in addition to being positive. Namely, to be physically meaningful, the linear mixture model can be subjected to following two constraints; the first is the Abundance Non-negativity Constraint (ANC) [85],

$$s_{ij} \geq 0 \quad (3.7)$$

and the second is the full additivity Abundance Sum-to-one Constraint (ASC) [85],

$$\sum_{i=1}^p s_{ij} = 1 \quad (3.8)$$

3.4.1.4. Abundance Maps

Abundance estimation is the problem of estimating the set of corresponding fractions that indicate the proportion of each endmember present in the pixel of a hyperspectral image [86][87].

Once the fundamental materials of a scene are determined, it is often useful to construct an abundance map of each material which displays the fractional amount of material present at each pixel.

3.5. Classification algorithms

These sections are based in the classification process, particularly in support vector machine classifier.

For our set of experiments, we use the library LIBSVM [Online: <https://www.csie.ntu.edu.tw/~cjlin/libsvm/>].

The purpose of a supervised classifier is to use a set of observations called training set to find a decision function. This function classifies every new object in a pre-defined class. This is achieved by a learning process while the training objects are classified. With recent technological advances and the large amount of hyperspectral data, there are the necessary means for efficient classification to discriminate classes according to the spectral resolution for each pixel of an image obtained. However, the large number of bands is the feature that produces greatest complexity in analysis techniques [4].

In this regard, conventional methods of classification as the machine learning (ML) algorithm can be applied to hyperspectral data, but require complex processing due to the high dimensionality. The difficulty which gets many methods based on conventional statistical approaches is that these employ a specified covariance matrix of each class [88]. Another disadvantage of this type of functions which works with covariance matrices is that the classifications made with little or limited number of training sets when working

with high dimensionality data is that result in poor generalization processes (classification) [72].

3.5.1. Support Vector Machine Classifier (SVM)

At the beginning of XXI century it was tested the great effectiveness of methods based on statistical learning theory to work with both problems: high dimensional and sparse training set. The training of the classifiers, both statistical and neural networks make use of the principle of Empirical Risk Minimization (ERM), which consists of allowing the minimization of the error rate for a given training set. The problem arises when it is necessary to extend or to generalize that classification to the rest of objects, then a good performance is not achieved, i.e., the resulting error rate is higher than for the training set.

The Support Vector Machine (SVM) is a pattern recognition supervised method recently introduced in the framework of statistical learning theory of Vapnik Vladimir and his work team at AT&T Labs [89]. It combines following ideas: the optimal hyperplanes search technique as a solution, the idea of convolution scalar product, the extension of the linear functions to nonlinear and the notion of soft margin to allow for errors in the training patterns. An important advantage is that it works on the principle of Structural Risk Minimization (SRM), it is better than ERM which use others many techniques. SVM then enables better generalization rather than a better classification of the training set (at the level of errors).

There are two other reasons that have increased the interest in this newfangled classifier. SVM can be reduced to a problem of convex quadratic programming (QP), which is easier to solve compared to traditional methods and that seem to have a better performance (more robust) with high amounts of data. SVM has been used hitherto in many fields, such as: Text categorization, recognition of hand-written texts, image classification, bioinformatics, remote sensing, and now also in medical hyperspectral imaging, where it seems to have a higher performance than other classical techniques used [90].

3.5.1.1 Theoretical foundations of SVM classifier

This classifier belongs to the family of linear classifiers that induce linear separators or hyperplanes in spaces of high dimensionality characteristics, though may be easily

adapted to act as non-linear classifiers by applying a function or not linear kernel in the input data. Its main objective is to get one surface (or hyperplane) capable of separating the different classes that can be grouped in a data distribution of a N-dimensional space, using an optimization process based on obtaining vectors which defining the class boundaries. These vectors are usually referred support vectors [91]. If we see the input data as two sets of vectors in a N-dimensional space, the SVM algorithm objective is simply to build a separating hyperplane in that space, which maximizes the margin of distance to the two data sets [92].

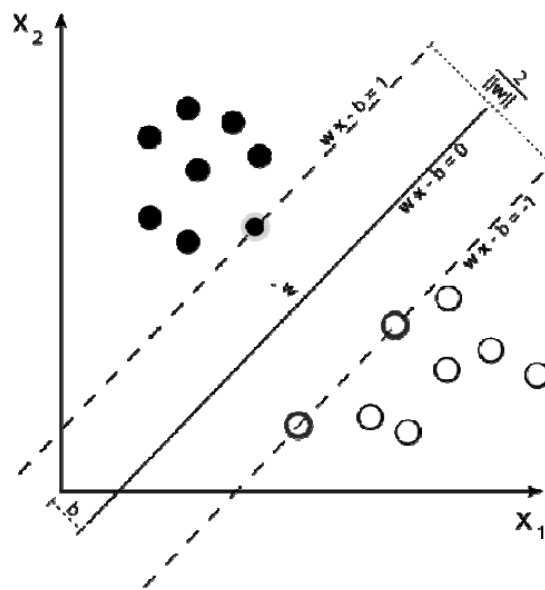


Figure 3.10: Functional diagram of the SVM classifier.

In Figure 3.10 [4] we can see how to calculate this separating hyperplane, constructing two parallel hyperplanes, one on each side of the first. The two parallel hyperplanes are pushed or widened to as close as possible to the datasets. Intuitively, a good separation is achieved when the separating hyperplane is farthest from both classes. The greater the separation distance, the lower will generally be the classifier error [91]. In mathematical terms, given a training set of the equation:

$$D = \{(x_i, c_i) | x_i \in R^p, c_i \in \{-1, 1\}\}_{i=1}^n \quad (3.9)$$

Where c_i is 1 or -1, indicating the class to which x_i belongs. Each x_i is a real vector p-dimensional, we want to obtain a maximum distance hyperplane to the training sets which divide those belonging to $c_i = 1$ of those with the value $c_i = -1$. Any hyperplane can be written as a set of points x that satisfies the equation:

$$w \cdot x - b = 0 \quad (3.10)$$

The w vector is a normal vector perpendicular to the hyperplane. The $\frac{b}{\|w\|}$ parameter determines the displacement of the hyperplane over the origin. We want to choose the w and the b which maximize the distance between the two parallel hyperplanes, which are as far apart as possible depending on the data. These hyperplanes can be described with the formulas described below:

$$w \cdot x - b = 1 \quad (3.11)$$

and,

$$w \cdot x - b = -1 \quad (3.12)$$

Note that if the training set is linearly separable, we can choose two hyperplanes on the edge of the sets such that there are no points between them and then try to maximize their distance. Using geometry, we find that the distance between them is $\frac{2}{\|w\|}$, so it is intended to minimize $\|w\|$. As we have to prevent the points are located in the boundary area, we add the constraint of equation

$$w \cdot x_i - b \geq 1 \quad (3.13)$$

for x_i belonging to the first class and the restriction of equation

$$w \cdot x_i - b \leq -1 \quad (3.14)$$

for x_i in the second class.

This can be written as:

$$c_i(w \cdot x_i - b) \geq 1, \forall 1 \leq i \leq n \quad (3.15)$$

We can compact the expression to reach the optimization problem: Choose w, b to minimize $\|w\|$:

$$\text{Subject to} \quad c_i(w \cdot x_i - b) \geq 1, \forall 1 \leq i \leq n \quad (3.16)$$

The optimization problem presented above is difficult because only depends on a value $\|w\|$. The reason is that it is a non-convex optimization problem, which is known to be

much more difficult to solve than the convex optimization problem. Fortunately, is possible to replace $\|w\|$ by $\frac{1}{2}\|w\|^2$ without changing the solution. This is an optimization problem of quadratic programming. More clearly, the optimization problem can be reformulated as follows:

$$\text{Minimize } \frac{1}{2}\|w\|^2, \quad \text{subject to } c_i(w \cdot x_i - b) \geq 1, \forall 1 \leq i \leq n \quad (3.17)$$

The $1/2$ factor is used as a mathematical convenience. Now, the problem presented to us can be resolved through programs and standard quadratic programming techniques. Writing the classification rule dual in its extended form, this reveals that the maximum distance to the hyperplane, and therefore the task of classification, it is only a function of support vectors, ie, data that are on the borderline. The second form of SVM can be derived as the following expression:

$$\max \sum_{i=1}^n \alpha_i - \frac{1}{2} \sum_{i,j} \alpha_i \alpha_j c_i c_j x_i^T x_j \quad (3.18)$$

$$\text{Subject to } \alpha_i \geq 0, \text{ and } \sum_{i=1}^n \alpha_i c_i = 0 \quad (3.19)$$

Where α terms are another representation of the weight vector in terms of the training set:

$$w = \sum_i \alpha_i c_i x_i \quad (3.20)$$

The original algorithm specifies a linear classifier, however, it may be modified to solve nonlinear classification problems, replacing the scalar product by a nonlinear kernel function. This allows the algorithm to determine the maximum distance to the hyperplane in a transformed features space. The transformation could be a nonlinear transformation and the transformed space could be a high dimensional space; this way, even though the classifier is a hyperplane in the space of high-dimensional features, it may not be linear in the original input space [93]. If the kernel used is Gaussian radial basis function type, the characteristics space is a Hilbert space of infinite dimension. The maximum distance is regulated, so the infinite dimension will not spoil the results [94]. Some of the commonly used kernels in SVM classifiers are listed below:

- Polynomial (homogeneous): $k(x, x') = (x \cdot x')^d$
- Polynomial (heterogeneous): $k(x, x') = (x \cdot x' + 1)^d$
- Radial Basis Function: $k(x, x') = \exp(-\gamma \|x - x'\|^2)$, for $\gamma > 0$
- Gaussian Radial Basis Function: $k(x, x') = \exp\left(-\frac{\|x - x'\|^2}{2\sigma^2}\right)$
- Sigmoide: $k(x, x') = \tan(kx \cdot x' + c)$, for some $k > 0$ and $c < 0$

In literature, we can find examples of kernels based on spectral metrics commonly used in hyperspectral analysis [95]. As stated at the beginning, processing used by the SVM does not require a large number of training patterns, as long as the chosen patterns are truly representative [96].

3.5.1.2 Kernel functions available

Our classifier has the following kernel functions that allow us to project information to a higher dimensional space which increases the computational capacity of the classifier:

- **Linear:**

$$u' * v \quad (3.21)$$

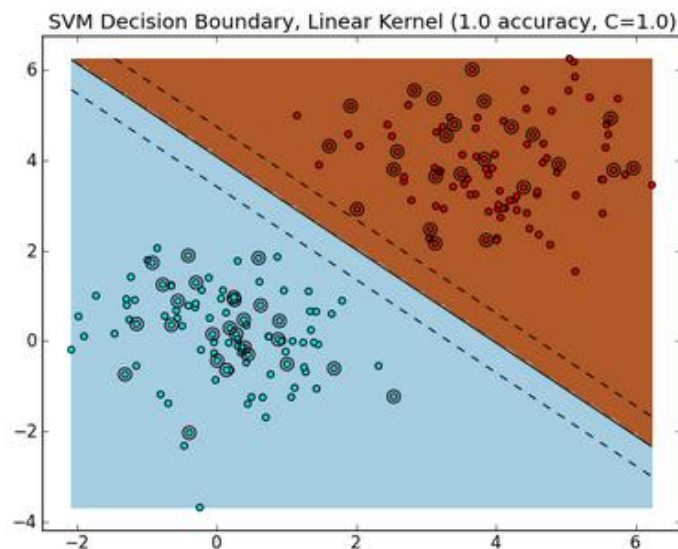


Figure 3.11: The decision boundary of a Linear SVM.

- **Polynomial:**

$$(\gamma * u' * v + coef0)^n \quad (3.22)$$

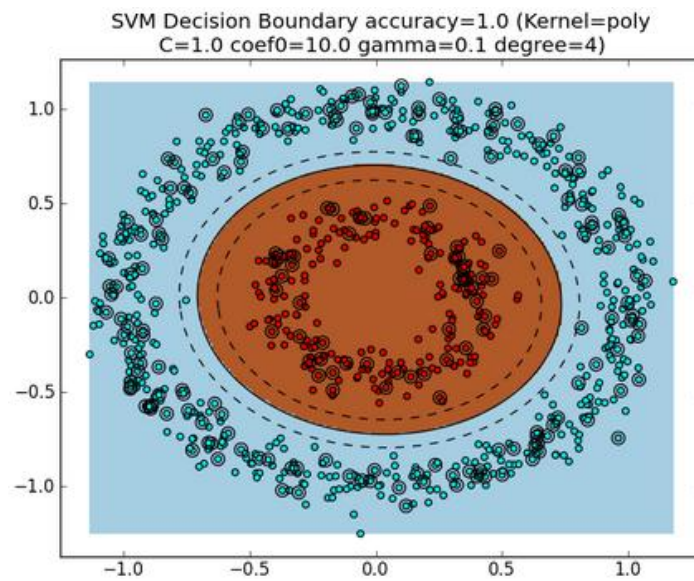


Figure 3.12: The decision boundary with a Polynomial kernel.

- **Radial basis function:**

$$e^{-\gamma * |u-v|^2} \quad (3.23)$$

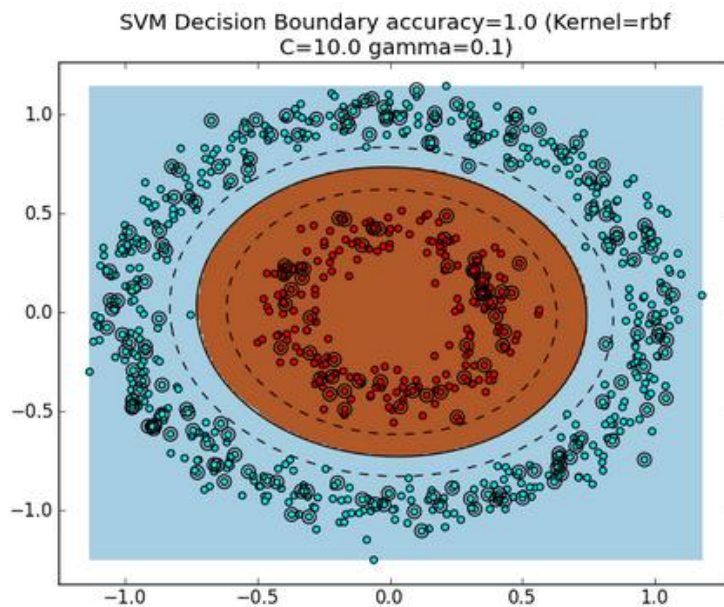


Figure 3.13: The decision boundary with a Radial Basis Function (RBF) kernel.

- **Sigmoid:**

$$\tanh(\gamma * u' * v + coef0) \quad (3.24)$$

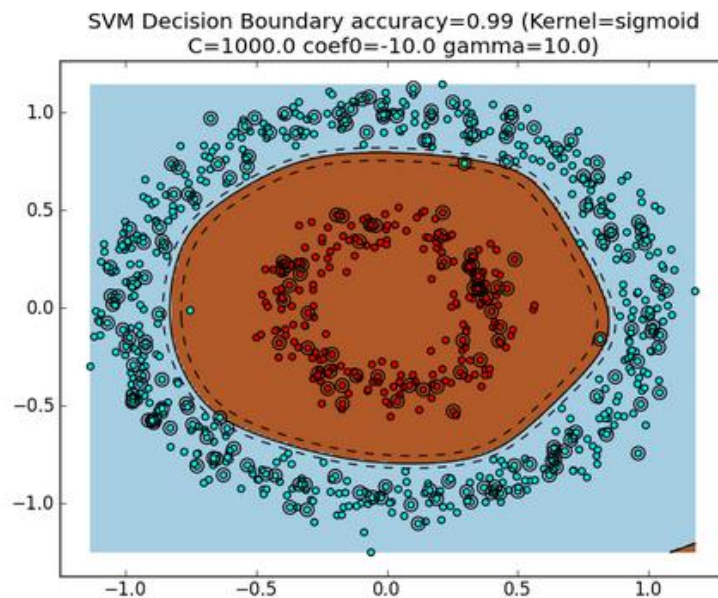


Figure 3.14: The decision boundary with a Sigmoid kernel.

- **Precomputed kernel:** Allows us to introduce our own kernel using a matrix.

By default, the classifier works with the radial basis function kernel.

It can be found in the literature that there are not important improvement regarding accuracy of results using linear kernel and RBF kernel in this kind of applications. However, there is a tremendous improvement in reducing the computation time when linear kernel is used [54]. Therefore, a study on the best kernel for this kind of applications is not performed in this work. Instead, this project is performed using linear kernel.

3.5.2. Semi-supervised learning (SSL)

Probably the earliest idea about using unlabelled data in classification is self-learning, which is also known as self-training, self-labelling, or decision-directed learning. This is a wrapper-algorithm that repeatedly uses a supervised learning method. It starts by training on the labelled data only. In each step a part of the unlabelled points is labelled according to the current decision function; then the supervised method is retrained using its own predictions as additional labelled points [97].

An unsatisfactory aspect of self-learning is that the effect of the wrapper depends on the supervised method used inside it. If self-learning is used with empirical risk

minimization, the unlabelled data will have no effect on the solution at all. If instead a margin maximizing method is used, as a result the decision boundary is pushed away from the unlabelled points. In other cases, it seems to be unclear what the self-learning is really doing, and which assumption it corresponds to.

Semi-supervised learning is a class of supervised learning tasks and techniques that also make use of unlabelled data for training – typically a small amount of labelled data with a large amount of unlabelled data. Semi-supervised learning falls between unsupervised learning (without any labelled training data) and supervised learning (with completely labelled training data). Many machine-learning researchers have found that unlabelled data, when used in conjunction with a small amount of labelled data, can produce considerable improvement in learning accuracy. The acquisition of labelled data for a learning problem often requires a skilled human agent (e.g. to transcribe an audio segment) or a physical experiment (e.g. determining the 3D structure of a protein or determining whether there is oil at a particular location). The cost associated with the labelling process thus may render a fully labelled training set infeasible, whereas acquisition of unlabelled data is relatively inexpensive. In such situations, semi-supervised learning can be of great practical value. Semi-supervised learning is also of theoretical interest in machine learning and as a model for human learning.

The semi-supervised learning problem has recently drawn large attention in the machine learning community, mainly due to its significant importance in practical applications.

In statistical machine learning, it can be distinguished between unsupervised and supervised learning. In the former scenario it is given a sample $\{x_i\}$ of patterns in \mathcal{X} drawn independently and identically distributed (i.i.d.) from some unknown data distribution with density $P(x)$. The goal is to estimate the density or a (known) functional thereof. Supervised learning consists of estimating a functional relationship $x \rightarrow y$ between a covariate $x \in \mathcal{X}$ and a class variable $y \in \{1, \dots, M\}$, with the goal of minimizing a functional of the joint data distribution $P(x, y)$ such as the probability of classification error. The marginal data distribution $P(x)$ is referred to as input distribution. Classification can be treated as a special case of estimating the joint density $P(x, y)$, but this is wasteful since x will always be given at prediction time, so there is no need to estimate the input distribution.

The term density estimation is usually preferred to denominate unsupervised learning. Traditionally, many techniques for density estimation propose a latent (unobserved) class variable y and estimate $P(x)$ as mixture distribution $\sum_{y=1}^M P(x|y)P(y)$. Note that y has a fundamentally different role than in classification, in that its existence and range c is a modeling choice rather than observable reality. However, in other density estimation techniques, such as nonlinear dimensionality reduction, the term “unsupervised” does not make sense.

The semi-supervised learning problem belongs to the supervised category, since the goal is to minimize the classification error, and an estimate of $P(x)$ is not sought after. The difference from a standard classification setting is that along with a labelled sample $D_l = \{(x_i, y_i) | i = 1, \dots, n\}$ drawn i.i.d. from $P(x, y)$ we also have access to an additional unlabelled sample $D_u = \{x_{n+j} | j = 1, \dots, m\}$ from the marginal $P(x)$. This is especially interesting in cases where $m \gg n$ which may arise in situations where obtaining an unlabelled sample is cheap and easy, while labelling the sample is expensive or difficult. It is denoted $X_l = (x_1, \dots, x_n), Y_l = (y_1, \dots, y_n)$ and $X_u = (x_{n+1}, \dots, x_{n+m})$. The unobserved labels are denoted $Y_u = (y_{n+1}, \dots, y_{n+m})$. In a straightforward generalization of SSL (not discussed here) uncertain information about Y_u is available.

There are two obvious baseline methods for SSL. It can be treated as a supervised classification problem by ignoring D_u , or it can be treated y as a latent class variable in a mixture estimate of $P(x)$ which is fitted using an unsupervised method, then associate latent groups with observed classes using D_l . One would agree that any valid SSL technique should outperform both baseline methods significantly in a range of practically relevant situations. If this sounds rather vague, note that in general for a fixed SSL method it should be easy to construct data distributions for which either of the baseline methods does better.

SSL is much more a practical than a theoretical problem. A useful SSL technique should be configurable to the specifics of the task in a similar way as Bayesian learning, through the choice of prior and model. While some theoretical work has been done for SSL, the bulk of relevant work so far has tackled real-world applications [40][97][98].

3.6. Summary

To take advantage of the large amount of information offered by hyperspectral imaging is necessary to design a robust pre-processing chain. This is because the high dimensionality that provides hyperspectral data leads to the presence of noise and redundant information which complicate its direct processing.

In addition, feature extraction is responsible for extracting the main features of the hyperspectral data using transformations theory. The result is an alternative representation of the original data set but with lower dimensionality and therefore much easier to process.

The ultimate goal of this process is to classify the data in the most efficient way possible. For this purpose, a Support Vector Machine (SVM) from a semi-supervised learning (SSL) approach will be used. SVM is a very robust classifier that provides very good results working with this type of data.

Chapter 4

Proposed process for cancer detection using hyperspectral images

4.1. Case studies

First of all, in order to validate classification algorithms for discriminating between normal tissue, blood vessels, tumour tissue and background elements, three different case studies (CSs) have been proposed. This approaches differs in which patients are included as subject of study. These proposed scenarios are described below:

- **Case study 1 (CS1):** The goal of this CS is to check if the discrimination between normal tissue, blood vessels, tumour tissue and background elements can be performed using the available labelled data, and avoiding the inter-patient variability of data. It means that the datasets explored in this CS include hypercubes from surgical operations where all type of classes, normal tissue, blood vessels, tumour tissue and background elements, are present. In order to avoid the inter-patient variability of data, each surgical procedure is used independently for training and testing the classification system.

- **Case study 2 (CS2):** In CS2 all the available labelled data are merged in a unified dataset. It means that a unique database is created by joining all single patient data, so the inter-patient variability is taken into account.
- **Case study 3 (CS3):** This case study is the most realistic one. In this approach, each surgical procedure data is used as test set of a classification algorithm, and that classifier model is built using the information from the whole rest of hyperspectral labelled data (belonging to different patients). This case study represents the real case of a new operation, where the classification must be performed with a classifier trained with previous operations hyperspectral data.

The most general processing chain can be described with a small group of elaborate block chains. In this regard, the classification system used by HELICoID in order to perform spectral classification of brain tumour has been described in Chapter 3 and shown in Figure 3.1. This system is formed by a pre-processing chain followed by a classification stage based on SVM and it showed good performance in terms of accuracy percentage in classification with respect to CS1 and CS2. However, the real case CS3 usually offers very poor results due to the inter-patient variability.

In this dissertation, a semi-supervised approach is proposed in order to turn CS3 into CS1 and obtain good performance from CS3.

4.2. Semi-supervised algorithm

In the CS1 it is possible to obtain competitive results because all samples are obtained from the same operation and as a consequence these samples are similar to each other. However, in the case of CS3, an operation is classified using training samples from the other operations, which is a challenging task because of the great variability among different patients resulting from biological human variability.

In order to address this issue, a semi-supervised algorithm based on the heuristic approach of self-training is proposed [40]. Self-training is a wrapper method for semi-supervised learning [97] in which first, a supervised learning algorithm is trained based only on the labelled data (L_{int}). This classifier is then applied to the unlabelled data to generate more labelled samples as inputs for the supervised learning algorithm. Generally, only the samples with the most confident predictions (L_{self}) are added at each step,

removing these samples from the unlabelled pool [98]. In this way, the learning algorithm is able to interactively query some information source to obtain the desired outputs at new data points and thus to make use of unlabelled data for training. Figure 4.1 shows the scheme of this self-training algorithm.

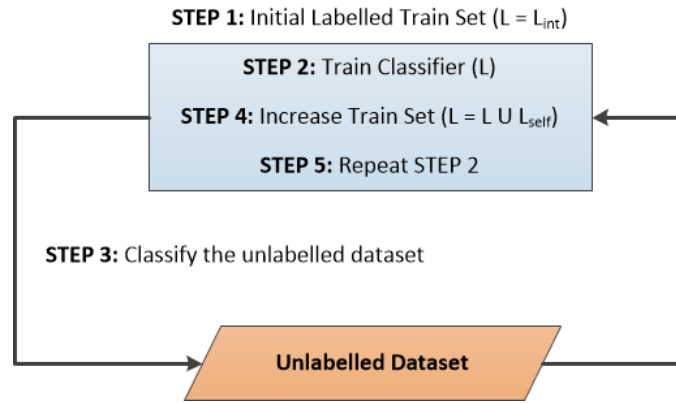


Figure 4.1: Self-training algorithm scheme.

Specifically, the developed algorithm classifies a new patient training from the rest of the operations which generally provides poor results. Nevertheless, the classification process generates a set of scores such that each pixel has an associated confidence score. These scores are calculated by the classifier and represent the probability of each pixel belonging to a particular class. Then, the scores are used to determine the best pixels from each class, so that a small set of pixels with highest scores in a particular class are chosen as a training samples for that class. The labels of the chosen pixels are given as a solution, while the pixels that were not chosen are classified again but training the classifier with the new training set formed by the chosen pixels. It is noteworthy that this new training set is formed by pixels from the new patient and there are not pixels in the training from other patients. Next, this process is repeated, and a new classification is performed using training samples with the highest score pixels. Once again the scores results are used to select a new set of pixels which are joined to the training set formed by the previous iterations. Note that during the process, the sample set from a new patient is divided into two datasets: a test set for classifying and a training set for training. As more iterations are performed, the test set is reduced while the training set is increased, until there are no samples to classify. This is a way that tries to move from CS3, which usually offers poor results, to CS1, which is proved to offers competitive results. The process followed is shown in Figure 4.2.

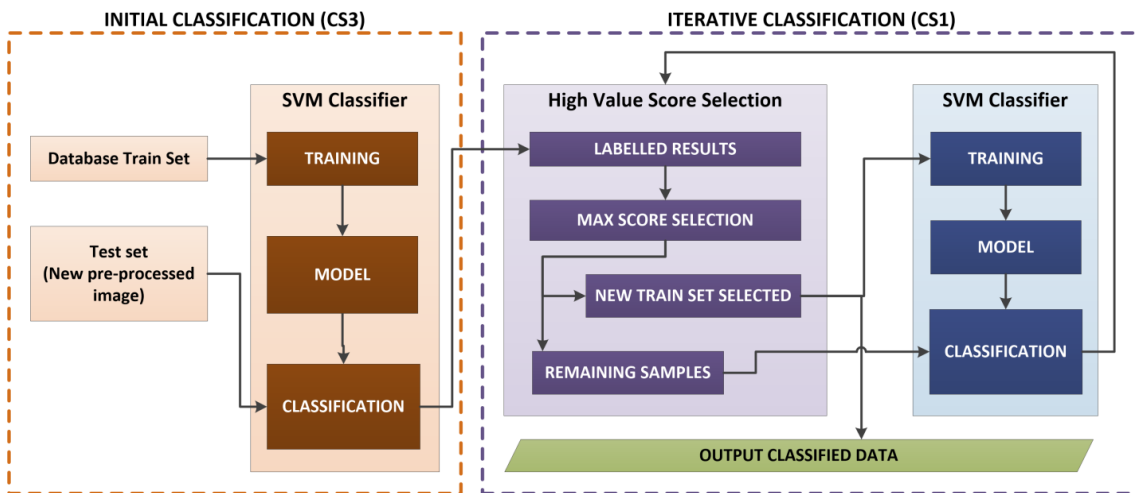


Figure 4.2: Semi-supervised approach.

4.2.1. Critical points of the algorithm

At this time, the algorithm is under development and it is apparent that this approach presents very delicate points in which it is necessary to make serious decisions. These issues are:

- High value score selection:** the good performance of this algorithm depend on the samples selected in each iteration. If these samples are wrong selected, the errors increases in the iterative process. Therefore, it is necessary to establish very accurate criteria to select the best samples possible. At first, SVM classifier is used in order to obtain the scores and the classification results. However, it is intended to improve the algorithm including others classifier working together, in order to make the decision on the labels of the samples and a combination of new selection criteria such as the scores generates by other classifiers, abundances obtained by spectral unmixing and some spatial information. In this dissertation, a spectral unmixing stage has been included for this purpose.
- Number of selected samples:** it is necessary to decide the number of samples which will be included in the training samples set in each iteration. This number could be a fixed cut-off value or a percentage depending on the number of samples labelled in each class. Some experiments have been performed in order to establish this value.
- Stopping criteria:** in a first approach, there is not stopping criteria and all samples were classified until the test set was empty. However, according to the size of the dataset increasing, the computing time was infeasible. Therefore, since it is an

iterative process with a high computing load, it needs a stopping criterion. A fixed number of iteration could be established. Nevertheless, the iterative algorithm finalize when the training samples set is formed by the 60% of the total samples to classify, because it is typical value used in the literature to divide the samples set [54], so that when the algorithm ends, the samples set to classify has been divided into two samples set: 60% for training and 40% for classifying.

4.3. Summary

In this section the algorithm developed in this dissertation has been presented. This processing chain is exhaustively tested using the dataset described in section 2.2.4.

In summary, based on the results we should make the following decisions:

1. To decide whether a semi-supervised approach is feasible to address our brain tumour detection problem.
2. To decide whether it is possible to improve the results obtained in CS3 moving this scenario to CS1.
3. To decide whether to combine SVM and spectral unmixing is a good choice to select the best samples in the iteration process.
4. To decide the best way to select the samples during de process and how many samples are selected in each iteration.

Once the best options are set, the resulting chains are used to generate the thematic maps.

Chapter 5

Experimental results

5.1. Introduction

In this chapter we conducted an experimental evaluation of the proposed semi-supervised process of hyperspectral data described in the previous sections. This algorithm is evaluated according to accuracy criteria in the classification results obtained.

The main difficulty associated with thematic classification techniques is that usually there are several possible classes associated with different targets. The goal is ultimately to determine the presence or absence of each of the targets considered in each pixel, situation that can be expressed as a binary classification problem which can subsequently be extended to any number of classes. Semi-supervised system is developed in order to evaluate the classification process in hyperspectral images. The general process is illustrated by a simple diagram in Figure 4.2. As shown in this figure, the training process consists in using a subset of the classified samples in CS3 to train again the supervised classifier (training patterns) in CS1 and evaluate performance of the classifier with the rest of patterns labelled (test patterns), then the process is repeated.

Although the distinction between training patterns and test patterns is generally performed randomly, in this project it is performed using a semi-supervised approach, trying to minimize the maximum number of training patterns necessary to achieve a

satisfactory result of classification with the rest of samples, mainly because it is often difficult to obtain training patterns in this kind of applications. Due to the presence of mixed pixels in the hyperspectral imaging is attempted to solve the problem by applying unmixing techniques which it is intended to help in the process of selecting the most appropriate samples in the iterative algorithm. Therefore, throughout this chapter is intended to validate the semi-supervised system combining unmixing techniques with a supervised classifier SVM.

As for the set of hyperspectral imaging selected to perform the experiments, these have been fully described in the corresponding section 2.2.4.

5.2. Results of semi-supervised experiments

In this section we describe the results obtained by applying the semi-supervised process presented in the previous chapter on the different hyperspectral imaging considered, using ground-truth (this term refers to the accuracy of the training set's classification for supervised learning techniques) information to statistically validate the classification results obtained by applying the analysis methodology and evaluation metrics described above. Once the results obtained are presented separately for each experiment, we proceed to discuss the results globally previously to the end of this chapter.

The classification is done by assigning a specific class label to each pixel once the learning phase of SVM classifier is completed, in which involves a number of training patterns selected from labelled pixels in the image from ground-truth information.

Followed we present a detailed quantitative and comparative study analysing the results obtained by different experiments of hyperspectral imaging used.

5.2.1. Results of support vector machine classifier used in brain cancer detection

In this experiment, it is intended to evaluate the goodness of SVM using for brain cancer detection and defining the classes mentioned in section 2.2.4: normal tissue, blood vessels, tumour tissue and background elements.

First of all, a test using the most common kernels for this kind of application is performed. As we discussed above in section 3.5.1.2, RBF kernel does not provide a significant improvement in comparison with linear kernel in the accuracy of the results. Instead, linear kernel supplies a significant improvement regarding computing time. The results obtained using these kernels in CS1 are shown in Figure 5.1.

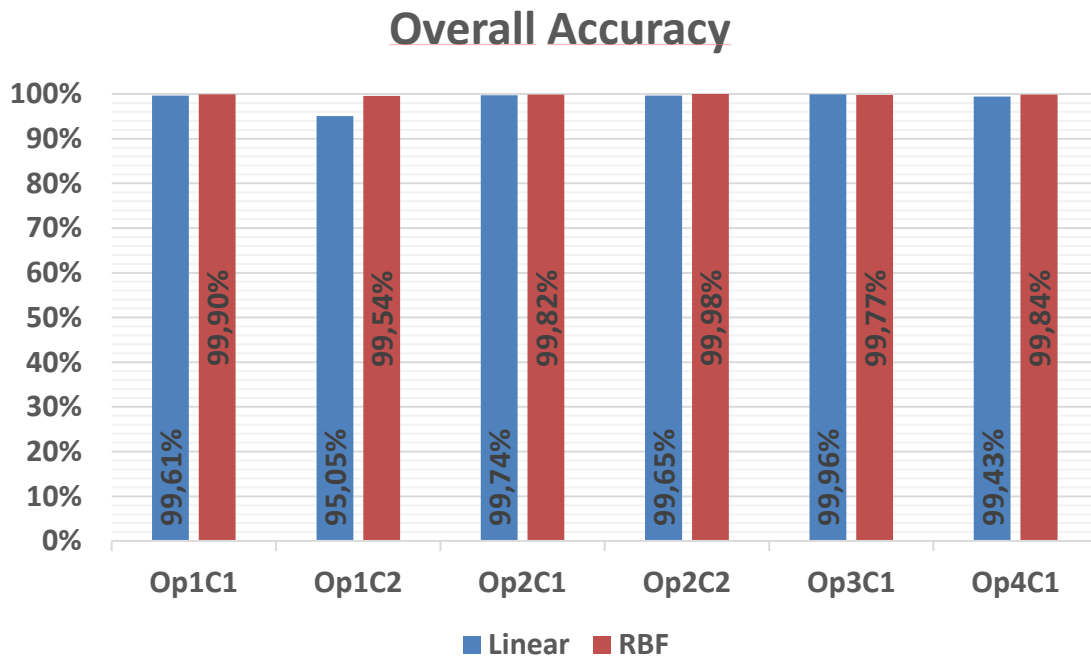


Figure 5.1: CS1 using SVM with different kernels.

This experiment was performed using 60% of samples to train the algorithm and 40% of samples to test in each patient samples set, this same procedure is carried out in the following experiments. As we can see in the previous figure, the results obtained with RBF kernel are slightly better than those obtained with linear kernel. Therefore, in a final approach, it might be interesting to use RBF kernel in order to maximize the results obtained. However, we work using always linear kernel from now on, because the main purpose of this work is to test the goodness of the semi-supervised system proposed and use RBF kernel involve a huge computational load.

Subsequently, SVM is used to perform the cases of study presented in section 4.1, in which it is worth recalling that CS2 and CS3 include biological human variability while CS1 does not. The results obtained in these CSs are shown in Figure 5.2.

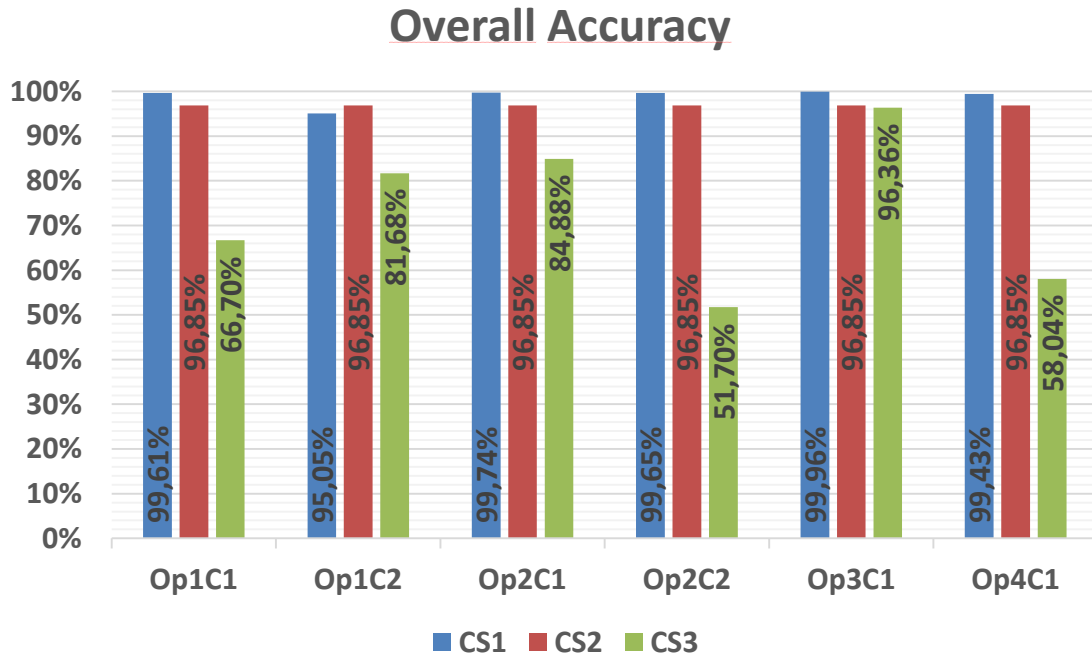


Figure 5.2: CS1, CS2 and CS3 using SVM for brain cancer detection.

As we can see in Figure 5.2, the results are as expected. While CS1 and CS2 offers good results, the performance decreases dramatically in CS3 excepting Op3C1 that even in this case offers competitive results. These results highlight the problems related to this real case study.

The good generalization ability exhibited by SVM is demonstrated by the classification results reported for CS1 and CS2, showing a high capacity to discriminate the proposed classes. For this reason, an improvement of the results offered by CS3 is intended in this work by using semi-supervised approach in order to remove the biological human variability included in this CS.

5.2.2. Results of semi-supervised approach based on SVM used in brain cancer detection

A first semi-supervised approach is performed in this section. For this algorithm, a SVM is used to select the samples based on the scores assigned by this classifier, which has demonstrated a good performance in this kind of application. These samples will form the training set in each iteration.

Firstly, all experiments were performed selected always 20% of samples of each class with highest scores in each iteration. This value was selected randomly to carry out all experiments in the same conditions and in the following sections an exhaustive study of how affects this value in the semi-supervised approach is conducted.

As a preliminary experiment, only normal and tumour tissues are selected in order to evaluate the capability of distinguish brain cancer from the semi-supervised algorithm based on SVM. The results are shown below:

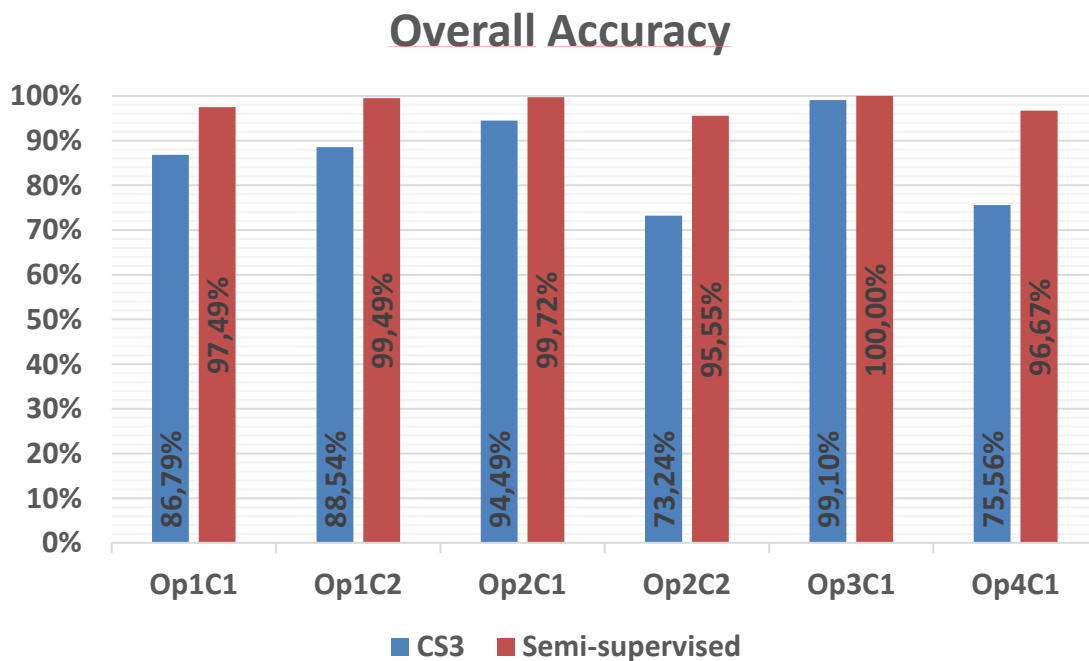


Figure 5.3: Semi-supervised algorithm based on SVM using normal and tumour tissues.

As it is shown in Figure 5.3, the semi-supervised algorithm offers very competitive results distinguishing between normal and tumour tissues, solving the issues related to CS3 and its biological human variability and demonstrating that a semi-supervised approach based on SVM can be used for this application.

The next step in this set of experiments is to include the remaining classes in the dataset in order to test a real situation. Therefore, the experiment is repeated using all classes defined: normal tissue, blood vessels, tumour tissue and background elements.

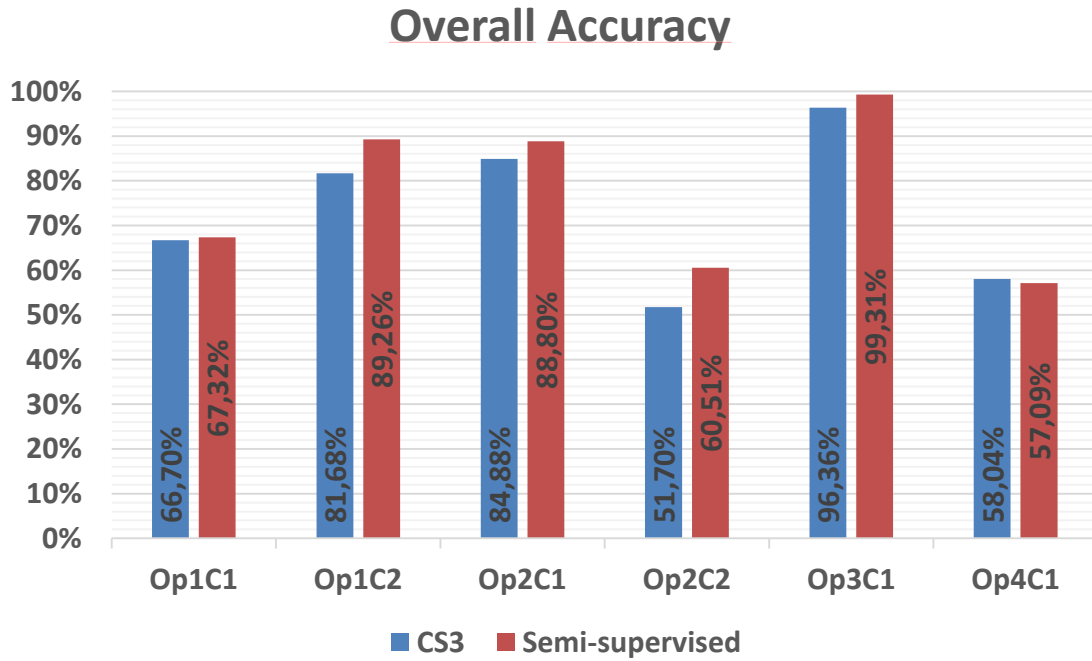


Figure 5.4: Semi-supervised algorithm based on SVM using all classes defined.

In the results shown in Figure 5.4 it can be seen how although the results generally improve slightly except in the case of patient Op4C1, the performance of semi-supervised system proposed decreases after using all available classes. In order to improve these results, semi-supervised algorithm combining SVM and spectral unmixing is proposed.

5.2.3. Results of semi-supervised approach based on spectral unmixing concepts used in brain cancer detection

In this section it is intended to test the goodness of spectral unmixing techniques using in a semi-supervised approach for brain cancer detection.

In this process, unmixing techniques are applied independently. It means that this process has not classification stage. In this case, to measure the accuracy of success in this algorithm, the results are obtained from to label each pixel with its greatest abundance.

Several unmixing techniques were tested in which we used the different techniques described in its theoretical section 3.4.1.3. It is important to remember that in this work, endmembers extraction is not implemented. Instead, each endmember is calculated as the average of all pixels in its class and then the abundances estimation is

performed. Moreover, the estimation of number of endmembers is not necessary because these are associated with the number of classes defined by us. Note that when spectral unmixing is used, the abundances estimated are equivalent to the scores calculated by SVM.

Firstly, as in the previous section, a preliminary experiment using only normal and tumour tissues is performed in order to evaluate the capability of distinguish brain cancer from the semi-supervised algorithm based on spectral unmixing. In this case, FCLSU approach was used to estimate the abundances. The results are shown in Figure 5.5.

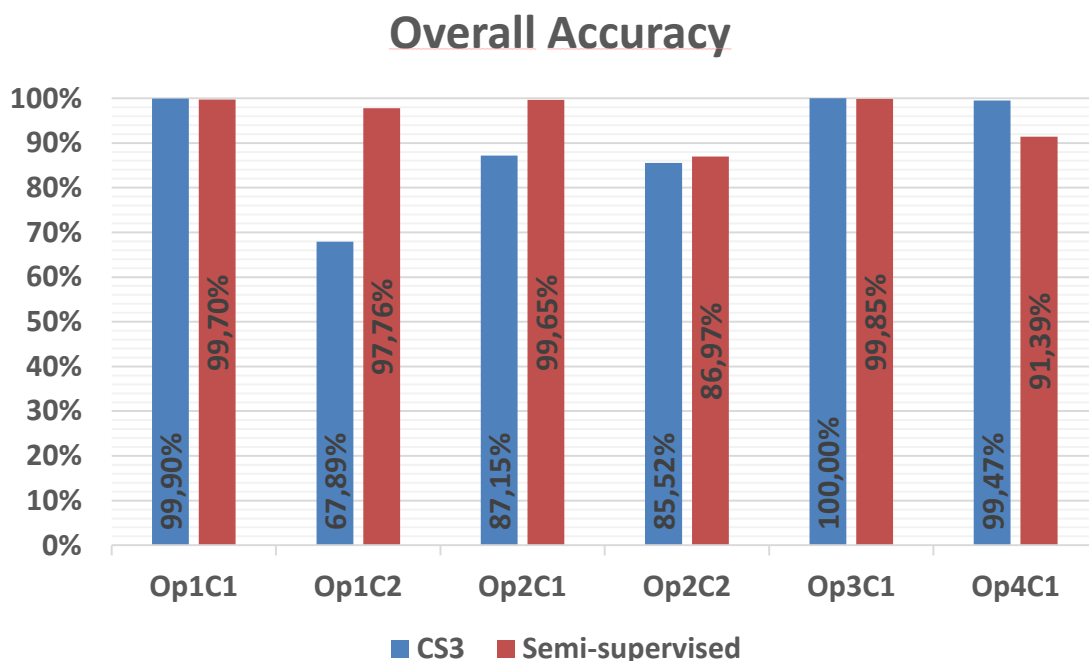


Figure 5.5: Semi-supervised algorithm based on spectral unmixing with FCLSU using normal and tumour tissues.

In the results we can see that in the cases of Op1C1 and Op3C1 the accuracy decreases slightly while in Op1C2, Op2C1 and Op2C2 the accuracy increases, especially in Op1C2 and Op2C1. Only in the case on Op4C1 the accuracy decreases significantly. From these results it can be concluded that spectral unmixing has certain capacity to distinguish between normal and tumour tissues and combining these techniques with SVM in the semi-supervised system might provide some extra information improving the results obtained.

Then, the all classes were included in this experiment using different techniques in the abundances estimation process in order to evaluate the performance of this semi-supervised algorithm based on spectral unmixing. In the following figures the results obtained for this set f experiments are shown.

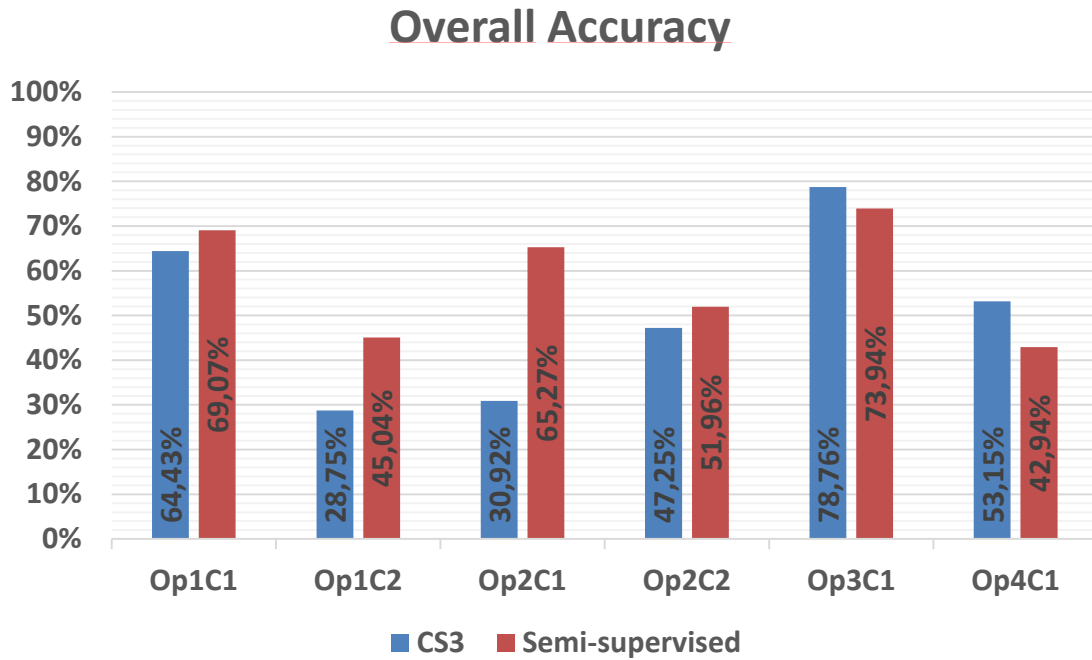


Figure 5.6: Semi-supervised algorithm based on spectral unmixing with FCLSU using all classes defined.

Once again we can see how in the case of including all classes the results worsen drastically. Although the semi-supervised approach improves the results in all cases except in Op3C1 and Op4C1, overall results are quite poor.

The results obtained using LSU algorithm for estimating the abundances are shown in Figure 5.7.

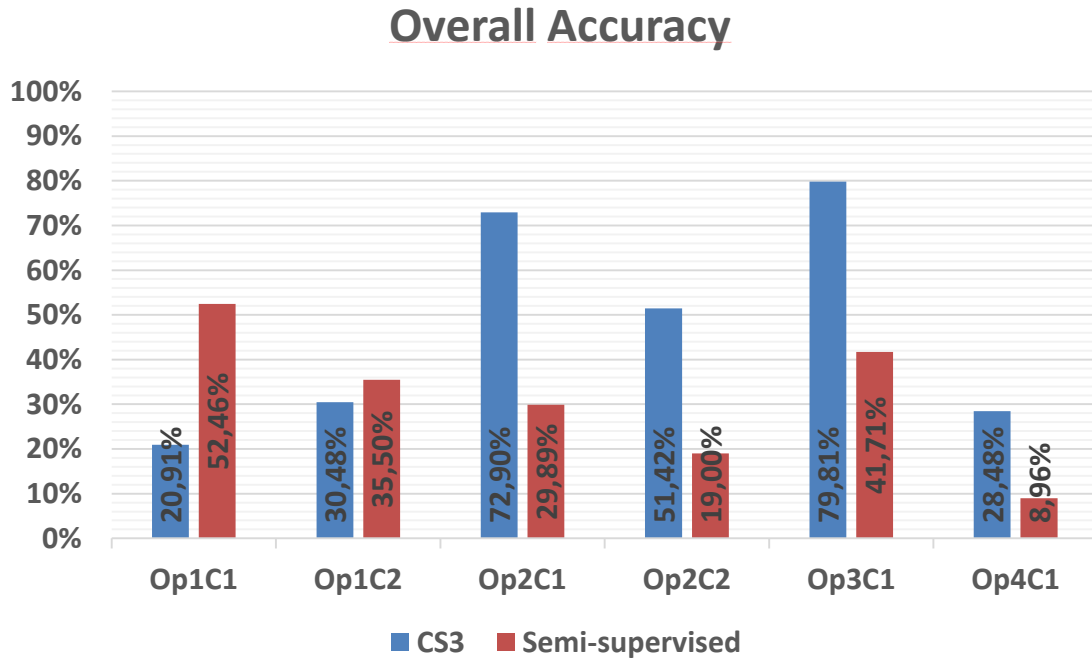


Figure 5.7: Semi-supervised algorithm based on spectral unmixing with LSU using all classes defined.

In this case, the overall results are really poor and only in Op1C1 and Op1C2 the semi-supervised approach improve the results obtained, therefore in this experiment the abundances estimation using FCLSU offers better results than using LSU from a semi-supervised process.

5.2.4. Results of semi-supervised approach based on Mixed techniques Unmixing-SVM used in brain cancer detection

In this section we apply mixed techniques Unmixing-SVM in order to improve the results obtained in the previous sections in which both techniques were applied separately. For this purpose, a semi-supervised algorithm based on the combination of these techniques has been developed.

Several combinations of these techniques were tested in order to find the best procedure in which these techniques maximize the results obtained, some of these processes proposed are the following:

1. **Unmixing-SVM process 1:** the classification step is performed by the SVM classifier, which has as input data the estimated abundances.

Overall Accuracy

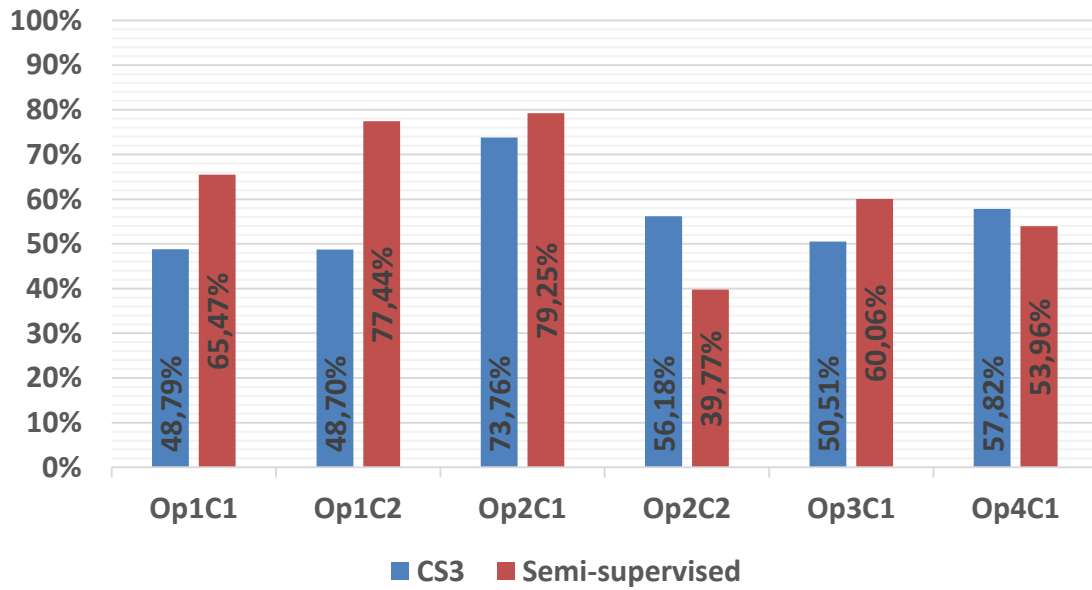


Figure 5.8: Unmixing-SVM process 1 using FCLSU for estimating abundances.

In Figure 5.8 we can see that in most patients semi-supervised algorithm proposed improves the results obtained by CS3, excepting Op2C2 and Op4C1. However, these results are really poor in comparison with the results obtained using only SVM classifier.

Overall Accuracy

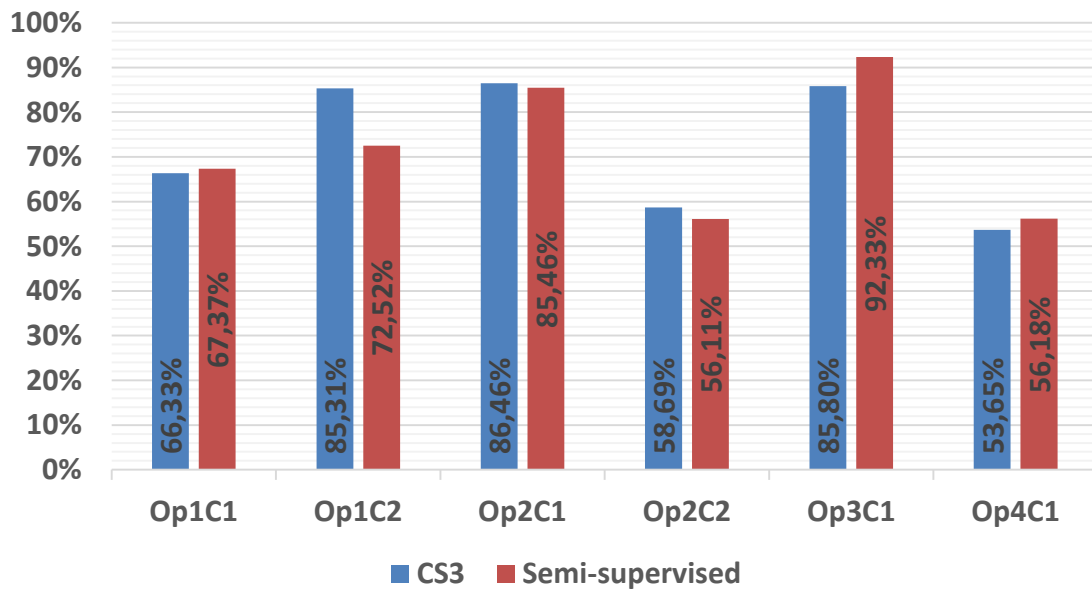


Figure 5.9: Unmixing-SVM process 1 using LSU for estimating abundances.

Once again, Figure 5.9 shows that this semi-supervised process offers worse results than use only SVM. Furthermore, in this set of experiments our algorithm only improves the results in half of the patients.

In general, the LSU algorithm offers better results than FCLSU algorithm, which means that in this set of experiments, the SVM classifier interpret better the information provided by LSU abundances estimation. However, in this process the use of unmixing techniques combined with SVM worse results compared to using only SVM. Furthermore, there are some patients in which the semi-supervised approach does not work properly and using it decreases the accuracy.

- 2. Unmixing-SVM process 2:** the abundances estimated are appended to spectral signatures adding some extra features and information in each sample.

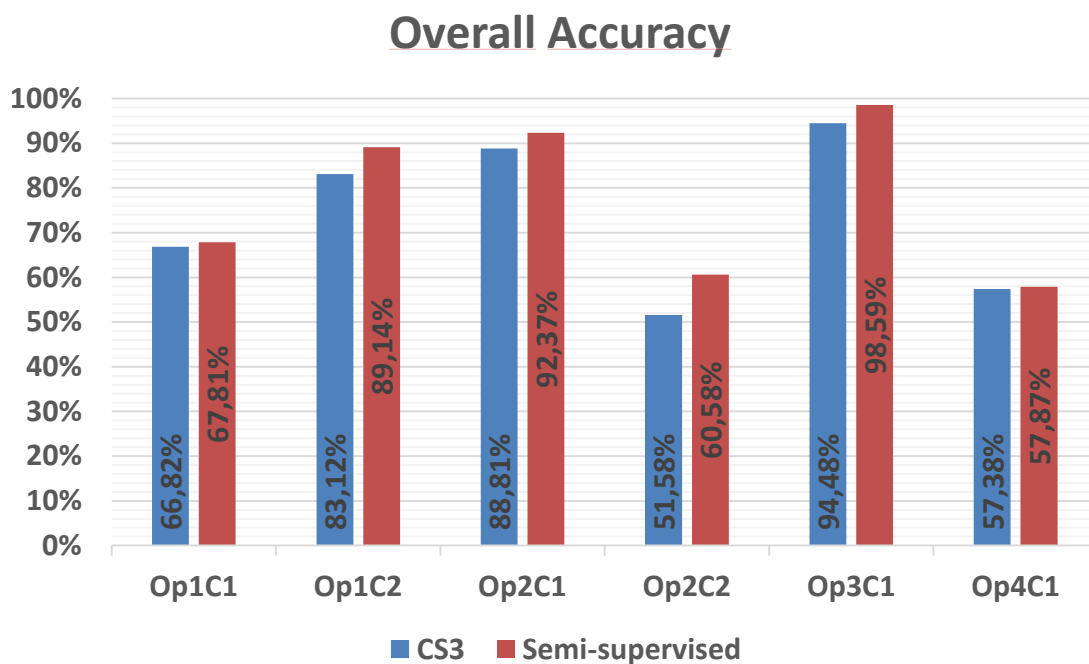


Figure 5.10: Unmixing-SVM process 2 using FCLSU for estimating abundances.

For Unmixing-SVM process 2 using FCLSU, Figure 5.10 shows that in this case the semi-supervised algorithm improves the results obtained with all patients of this study. However, the results are still lower than using SVM without spectral unmixing.

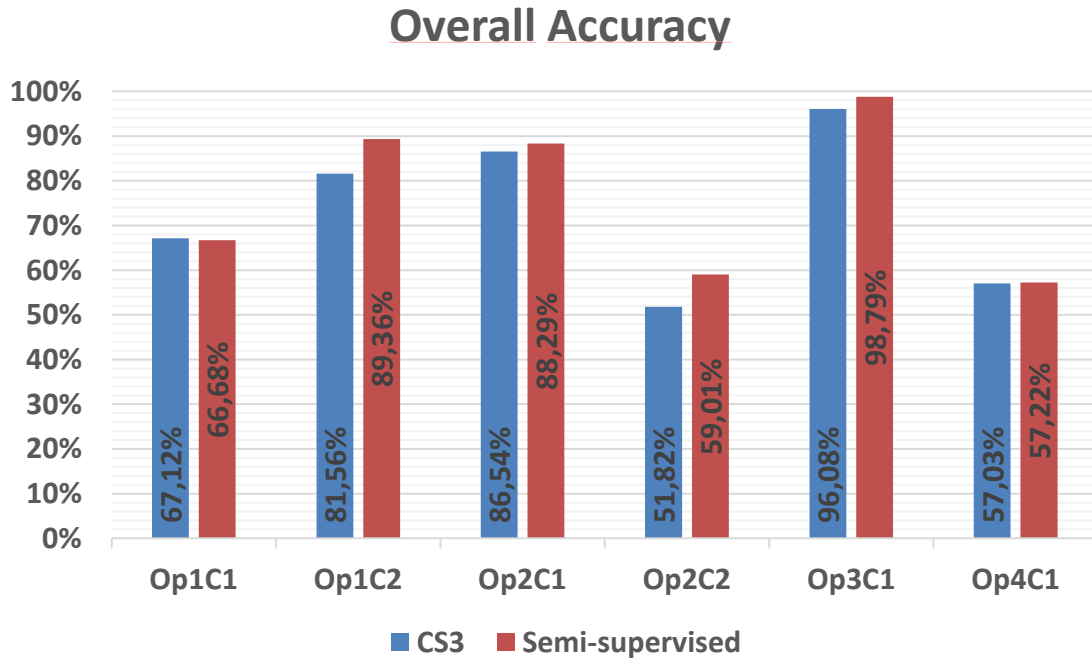


Figure 5.11: Unmixing-SVM process 2 using LSU for estimating abundances.

For this process, applying spectral unmixing using FCLSU offers better results than using LSU, as shown in Figure 5.11. Even so, the accuracy was improved in all patients excepting Op1C1.

For this set of experiments, the results obtained by Unmixing-SVM process 1 were improved. However, no improvement was seen regarding use SVM without spectral unmixing for selecting the samples in the iterative process, the accuracy increases only in Op2C1 using FCLSU.

- 3. Unmixing-SVM process 3:** the abundances and scores are calculated independently and then are added in order to select the best samples in each iteration. Thereby, the samples are selected taking into account that unmixing and SVM techniques agree on the class assigned to each sample.

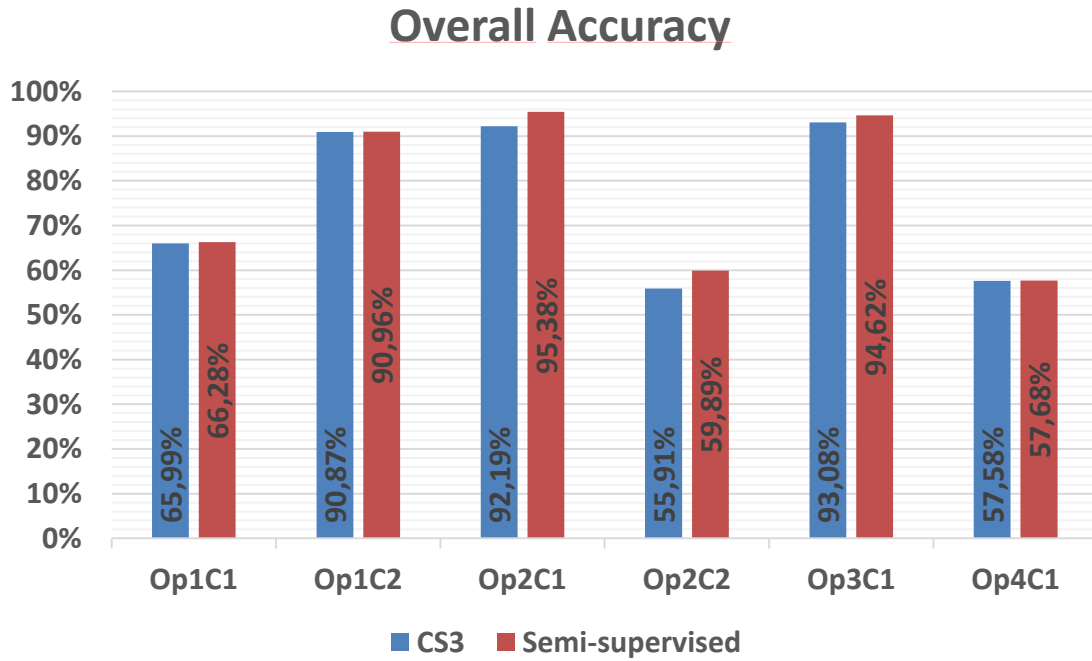


Figure 5.12: Unmixing-SVM process 3 using FCLSU for estimating abundances.

As we can see in Figure 5.12, using this Unmixing-SVM process offers very competitive results, in which this semi-supervised approach is more accurate than CS3 in all patients.

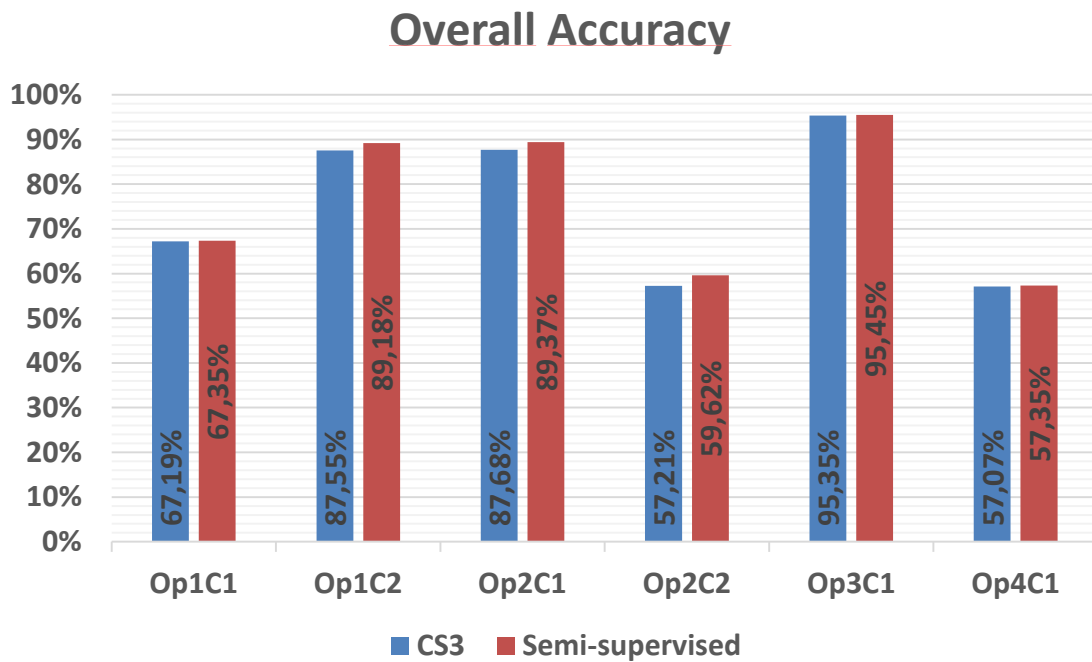


Figure 5.13: Unmixing-SVM process 3 using LSU for estimating abundances.

When LSU is used in the spectral unmixing stage, once again all results are improved using semi-supervised classifier in comparison with CS3, as we can see in Figure 5.13.

In this set of experiments, FCLSU offers more accurate results than LSU, which does not show a significant improvement over using only SVM classifier. However, a combination Unmixing-SVM techniques using FCLSU in a semi-supervised approach improves the results obtained in Op1C2 and Op2C1 and is emerging as the best way to apply a semi-supervised algorithm, although there is a decrease in accuracy obtained in Op3C1.

It is noteworthy that results obtained in Op1C1, Op2C2 and Op4C1 have remained almost unchanged throughout all experiments. For this reason, this last Unmixing-SVM process 3 using FCLSU is used in a new semi-supervised approach in which CS3 is moved to CS2 instead to obtain more accurate results.

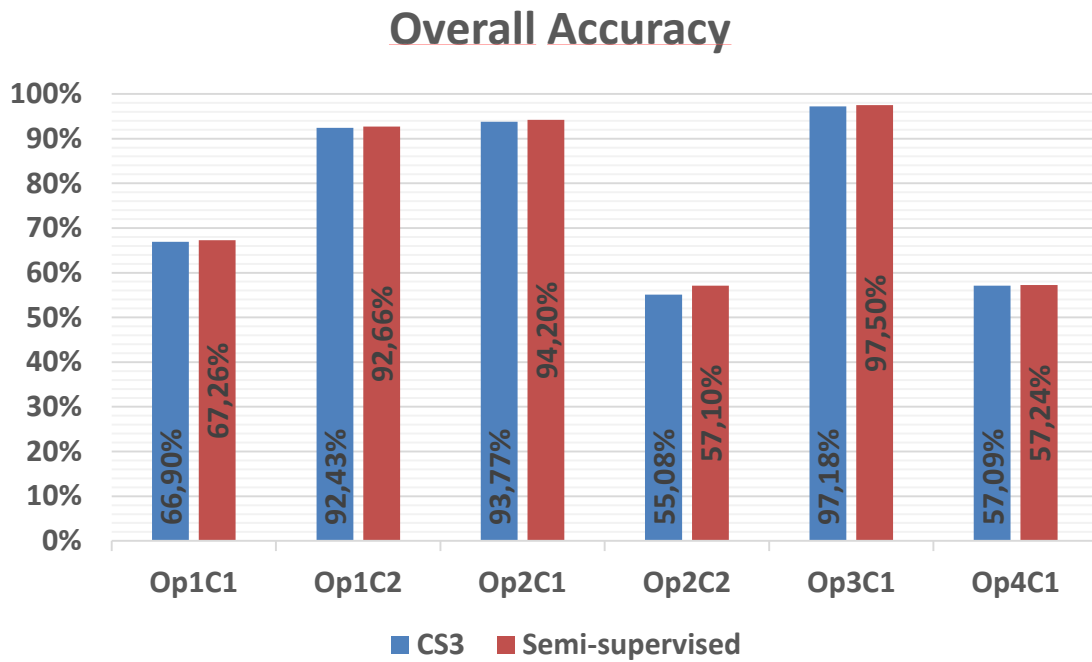


Figure 5.14: Unmixing-SVM process 3 using FCLSU for moving CS3 to CS2 in a semi-supervised system.

As is shown in the results in Figure 5.14, this approach improves the accuracy obtained in Op1C2 and Op3C1 while worsens slightly the results obtained in Op2C1, which means that it is an interesting alternative to the first approach. However, significant changes in Op1C1, Op2C2 and Op4C1 have not been seen. In order to go deeper into this

fact, a study of the confusion matrix was performed. For instance, the confusion matrix of Op4C1 previous to apply semi-supervised approach is shown in Table 5.1.

	Normal Tissue	Tumour Tissue	Blood Vessels	Background
Normal Tissue	1688	0	142	12
Tumour Tissue	3625	0	0	30
Blood Vessels	265	0	1248	0
Background	3	1	0	2621

Table 5.1: Confusion matrix of Op4C1 previous to apply semi-supervised approach.

As we can see in the previous confusion matrix, while the classes normal tissue, blood vessels and background are well classified, in the class tumour tissues it is not classified nor a sample well. For this reason, it is impossible that semi-supervised algorithm works well since there are no samples to select in the tumour class. Similar behaviours in which there are difficulties to distinguish tumour tissue are also present in Op1C1 and Op2C2. This fact is due to the database is really small since it is formed so far only by 4 patients therefore there is no enough variability in the samples. In addition, there might be some patients in whom the tumour tissues could be covered by other elements in the image, such as normal tissues or blood vessels. In order to solve this issue, it would be necessary to increment the database and the variability of the samples including new patients in it. Moreover, it would be interesting to include other additional techniques in the samples process selection of the semi-supervised algorithm since this will help the algorithm to decide which class each sample belongs, developing this way a meta-classifier.

5.2.5. Results of semi-supervised approach using different number of selected samples in each iteration

In this set of experiment, it is intended to decide the appropriate number of samples selected in each iteration of the semi-supervised algorithm. For that end, different percentages of samples are proposed to select the subset of samples in each class which will form part of the training set. Furthermore, because it is thought that the samples process selection should be more accurate in the first steps of the iterative algorithm, a method in which the percentage of samples selected in each class is increasing progressively in each iteration is proposed. The results obtained using semi-supervised approach based on SVM are shown in Figure 5.15.

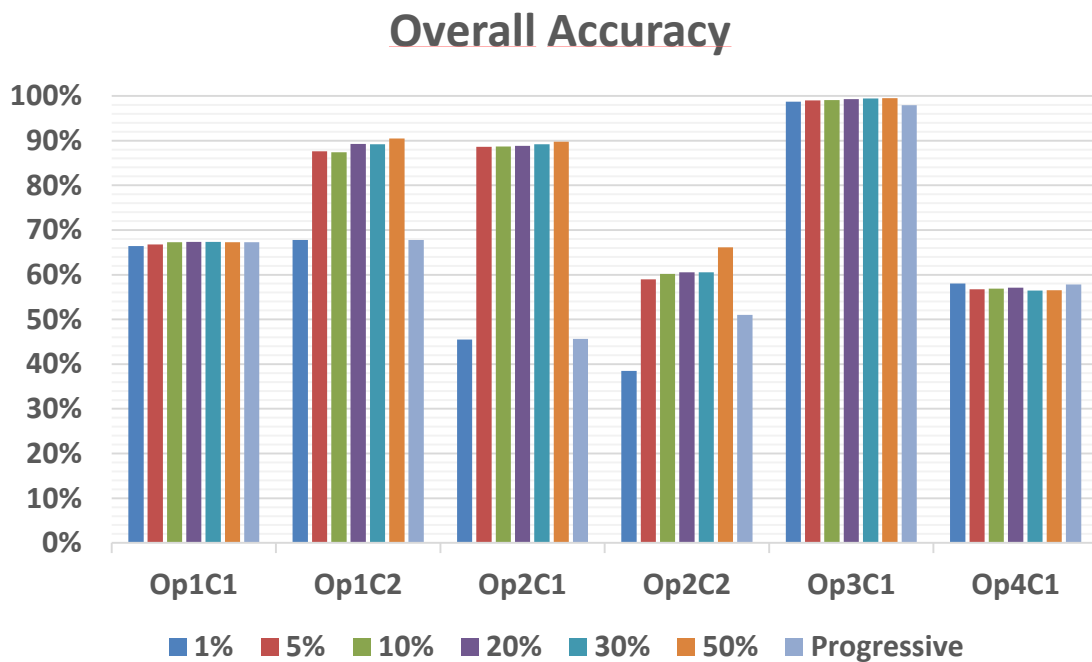


Figure 5.15: Semi-supervised algorithm based on SVM selecting different number of samples in each iteration.

As is shown in the Figure 5.15, the accuracy improves slightly when the number of samples selected in each iteration increases and the results are evenly matched in the range of 5-50. This is because as the number of samples selected per iteration is incremented, fewer iterations are necessary to finish the semi-supervised algorithm and

thus it is less likely to occur errors in one iteration, therefore the algorithm is able to improve the results in a few iterations.

5.2.6. Thematic maps generated by semi-supervised approach using Unmixing-SVM techniques

In this section the thematic maps generated in this work are shown. These maps are a type of map specially designed to show a particular class connected with a specific area in the image. The semi-supervised algorithm based in the combination of SVM and spectral unmixing with FCLSU is used to generate the maps since this process is considered the best option in this work to apply semi-supervised approach. Regarding the number of samples selected per iteration, it is set to 20% of samples of each class since this value offers accurate results.

The images shown below are the same images that the surgeon would see during surgery on a real case. It is important to note that the results of these images are purely subjective since there are no ground truths in this experiment, therefore will be an expert surgeon who will assesses the results in future works. Furthermore, the images obtained might do not match with the accuracy results obtained previously, this means that very poor results might generate a very clear image and vice versa since the previous experiments were performed using only a small set of labelled samples and these maps are generated using the entire images. Moreover, our benchmarks are the areas placed inside the rubber ring markers, whose tissues have been analysed by pathology for tissue diagnosis.

The colours assigned to each class are shown in the following table:

Classes	Colour
Normal tissue	Green
Tumour tissue	Red
Blood vessels	Blue
Background	Black

Table 5.2: Colours assigned by class.

The thematic maps obtained are shown below:

1. Op8C1:

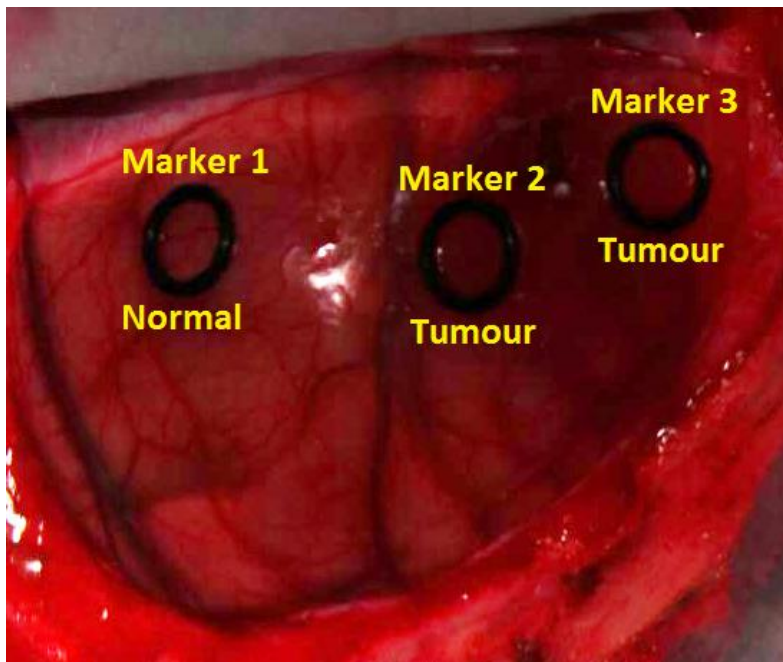


Figure 5.16: RGB image of Op8C1.

Figure 5.16 shows Op8C1 surgery in which we can see three different markers, namely marker 1 corresponding to normal tissues and markers 2 and 3 corresponding to tumour tissues.

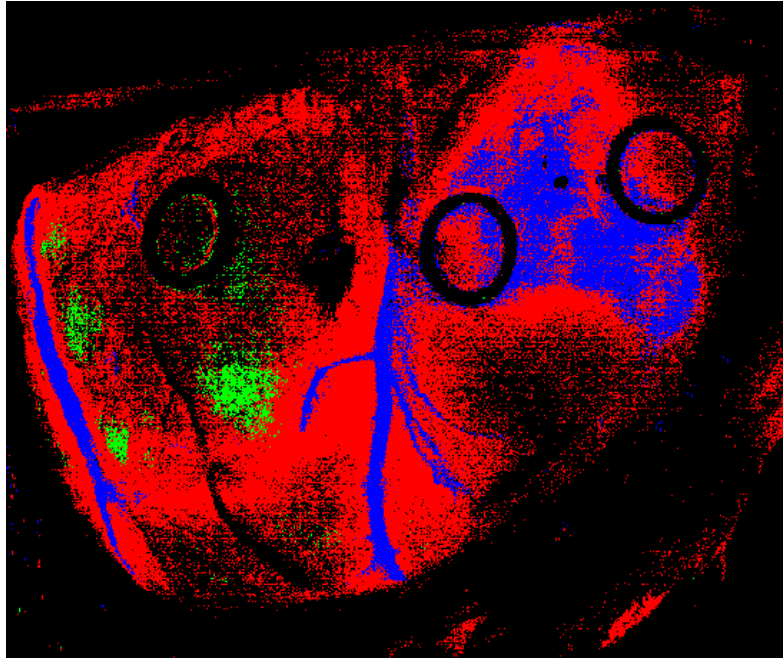


Figure 5.17: Thematic map of Op8C1 using CS3.

In Figure 5.17 we can see the results obtained using CS3 approach. These results show an image characterized by the presence of pixels belonging to background class in the whole brain area. Furthermore, it can be seen that the areas inside the markers are bad classified, especially the normal tissues inside marker 1. Moreover, while majority of brain area is classified as tumour, the presence of blood vessels appears well defined.

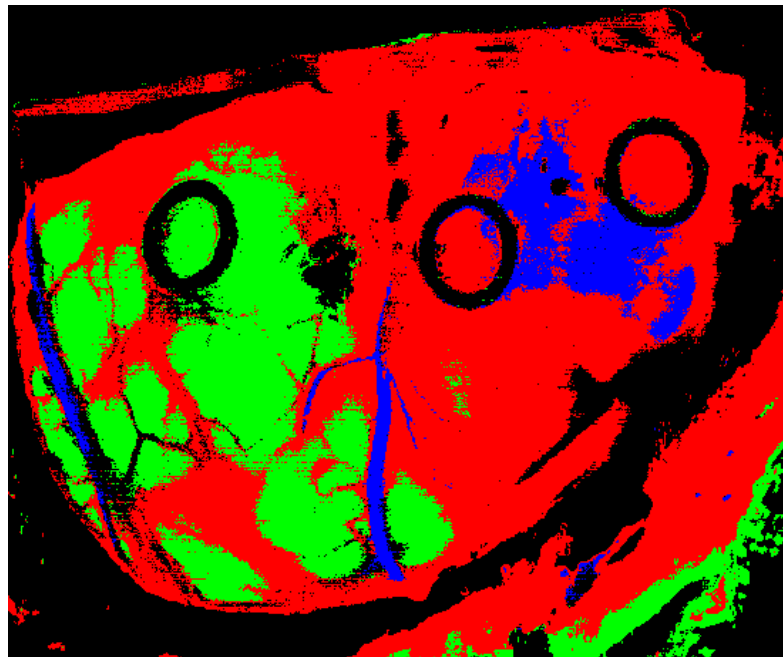


Figure 5.18: Thematic map of Op8C1 using semi-supervised algorithm.

Figure 5.18 shows how semi-supervised algorithm works well offering a cleaner image after its application, in which the healthy area increases remarkably and all markers are good classified with their respective classes. However, some definition is lost in the blood vessels class. In addition, it is interesting to note that there is a blood vessels area in the middle of tumour. This is due to its spectral signatures are very similar because tumours are characterized by being covered by a lot of blood, therefore these classes are often confused with each other and this situation is usually repeated. Perhaps for this reason, the remaining areas of the image away from the tumour area and classified as tumour could be areas with high concentrations of blood.

2. Op8C2:

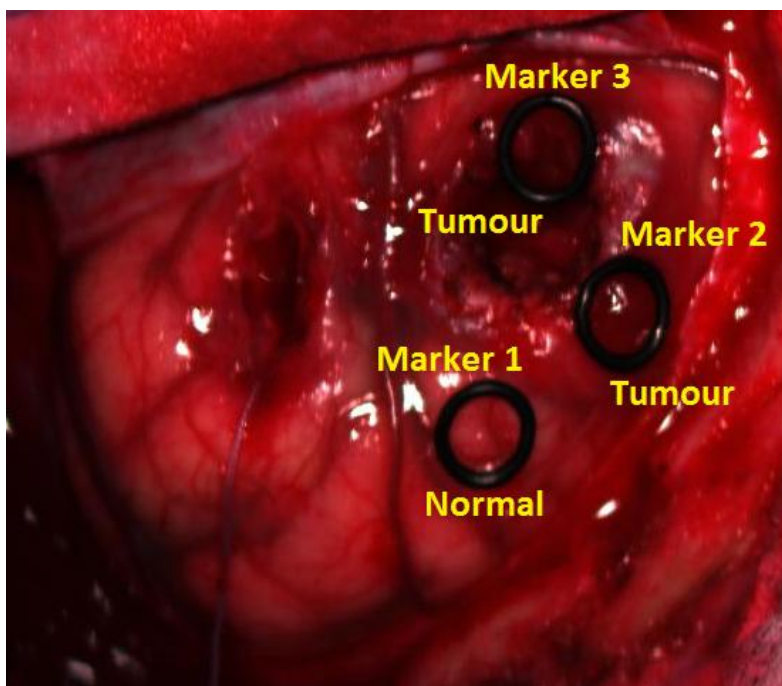


Figure 5.19: RGB image of Op8C2.

In Figure 5.19 it can be seen the Op8C2 surgery in which can be distinguished three different markers, namely marker 1 corresponding to normal tissues and markers 2 and 3 corresponding to tumour tissues.



Figure 5.20: thematic map of Op8C2 using CS3.

The results obtained after applying CS3 approach are shown in Figure 5.20. In this image we can see how the brain area is mainly classified as tumour. Moreover, marker 1 is bad classified while markers 2 and 3 are good classified as tumour.

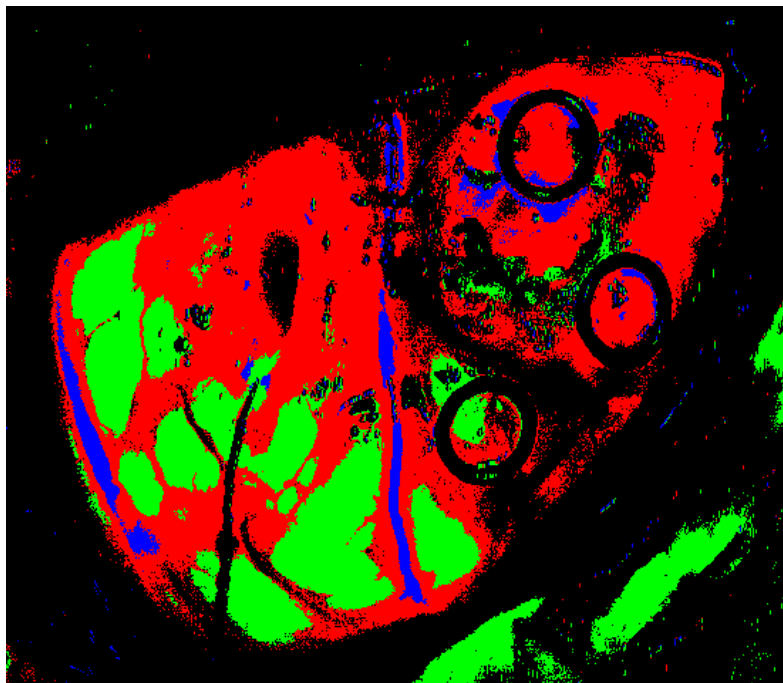


Figure 5.21: thematic map of Op8C2 using semi-supervised algorithm.

Regarding the results shown in Figure 5.21, we can see that after applying the semi-supervised algorithm normal tissues and blood vessels areas are better defined, but

overall no significant improvements are appreciated. Only for marker 1, which should be classified as normal tissues, an improvement is seen in the sense that normal tissues area is increased inside it.

3. Op12C1:

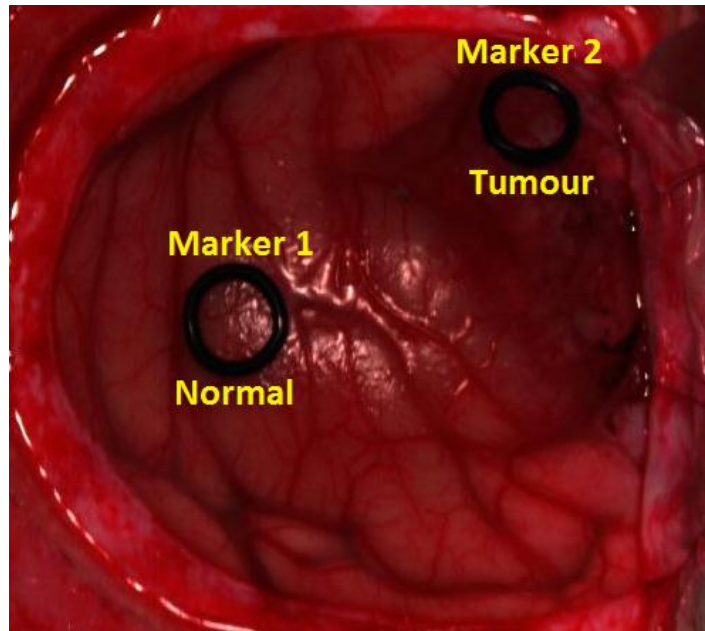


Figure 5.22: RGB image of Op12C1.

Figure 5.22 shows Op12C1 surgery in which we can see two different markers, namely marker 1 corresponding to normal tissues and marker 2 corresponding to tumour tissues.

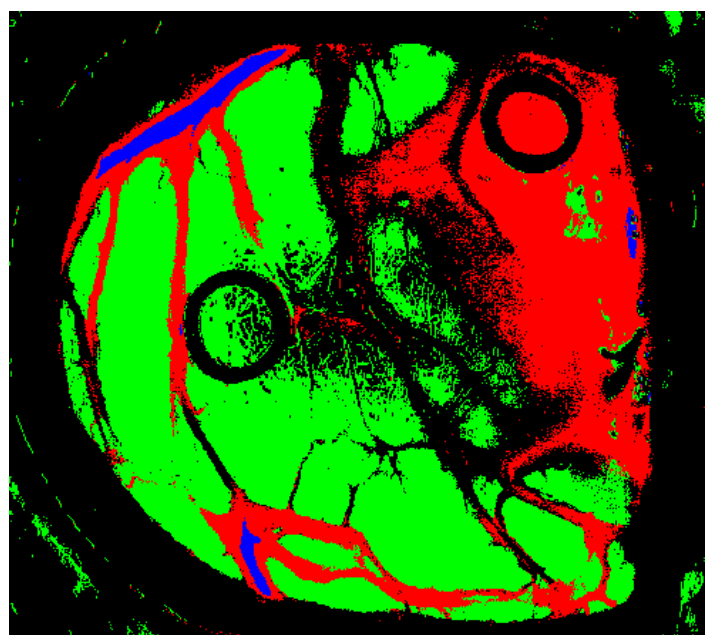


Figure 5.23: thematic map of Op12C1 using CS3.

In Figure 5.23 we can see the results obtained using CS3 approach. These results show an image with high presence of pixels belonging to background class in the central brain area. In addition, the blood vessels class is bad defined and it is confused with tumour class. However, normal and tumour areas appear well defined and the areas inside de markers are well classified.

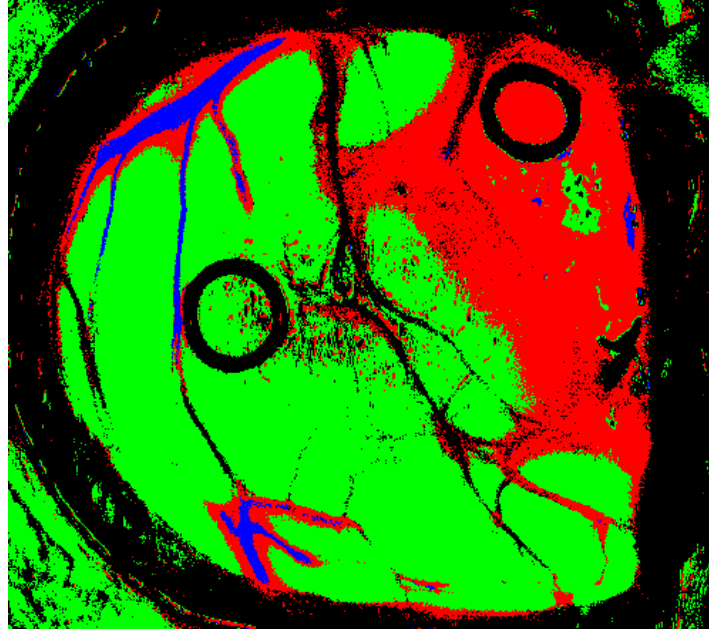


Figure 5.24: thematic map of Op12C1 using semi-supervised algorithm.

As we can see in the Figure 5.24, in this thematic map once again normal and tumour areas seem very accurate and the areas inside de markers are well classified. However, semi-supervised algorithm generates a clearer thematic map than CS3 and blood vessels class is better defined.

4. Op12C2:

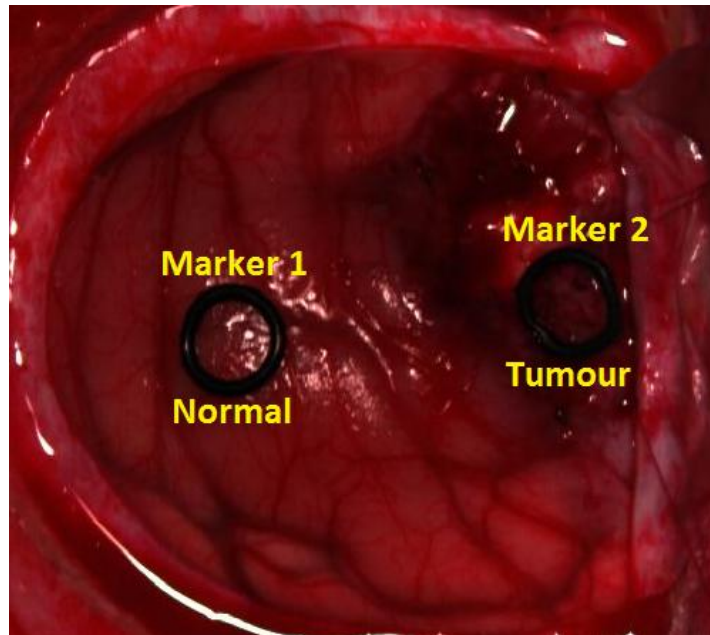


Figure 5.25: RGB image of Op12C2.

In Figure 5.25 it can be seen the Op12C2 surgery in which can be distinguished two different markers, namely marker 1 corresponding to normal tissues and marker 2 corresponding to tumour tissues.

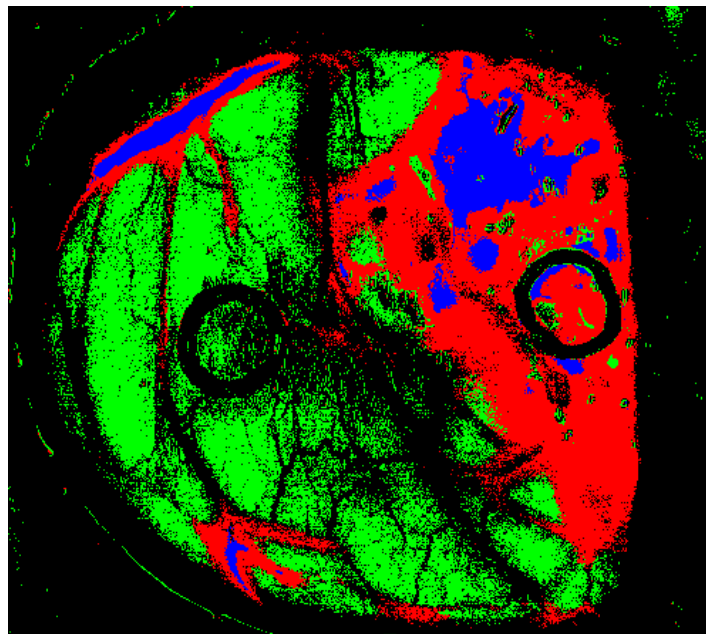


Figure 5.26: thematic map of Op12C2 using CS3.

The results obtained after applying CS3 approach are shown in Figure 5.26. In this case, applying CS3 shows high presence of pixels belonging to background class in the central brain area again. In addition, while marker 2 is well classified as tumour class,

marker 1 is mostly misclassified as background. Moreover, normal and tumour areas appear well defined.

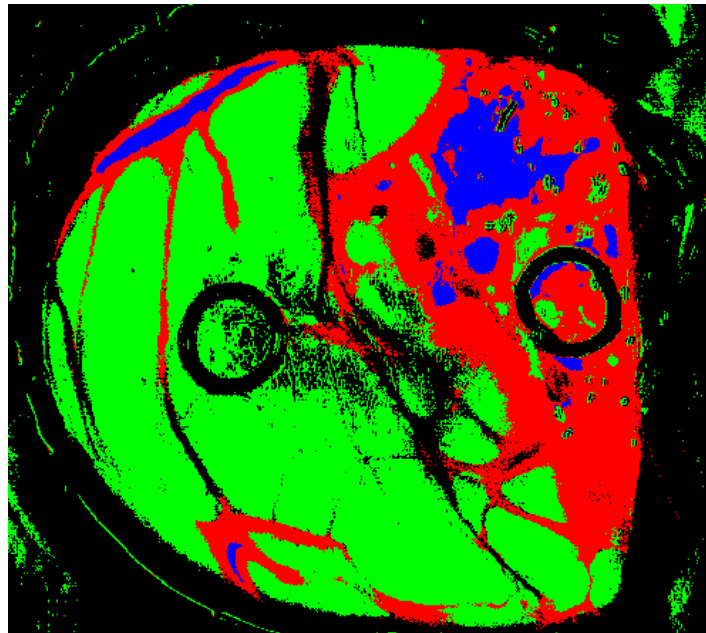


Figure 5.27: thematic map of Op12C2 using semi-supervised algorithm.

The results shown in Figure 5.27 are very similar to those obtained using CS3 and once again normal and tumour areas are well defined in both thematic maps. The main difference is that after applying the semi-supervised algorithm the image is clearer than the previous one since the first thematic map has a lot of background class pixels throughout the central area of the image. Note that there is a blood vessels area in the tumour area which is formed by blood accumulated in the cavity produced by the resection of part of the tumour.

5. Op15C1:

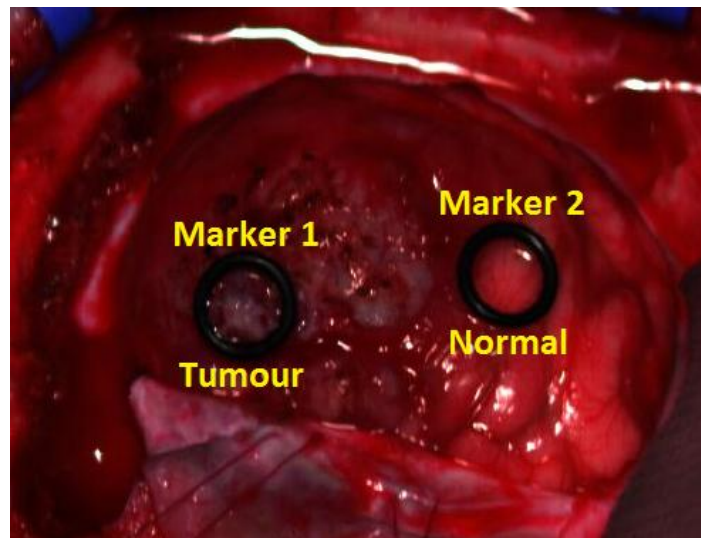


Figure 5.28: RGB image of Op15C1.

Figure 5.28 shows Op15C1 surgery in which we can see two different markers, namely marker 1 corresponding to tumour tissues and marker 2 corresponding to normal tissues.

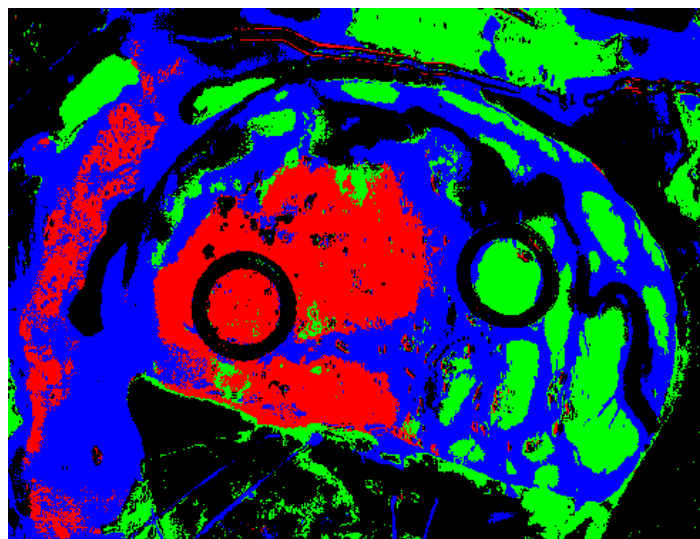


Figure 5.29: thematic map of Op15C1 using CS3.

Figure 5.29 shows the results obtained by CS3 approach, in which we can see a tumour area clearly defined while the remaining classes are poorly classified. However, it is worth highlighting that both markers are well classified.

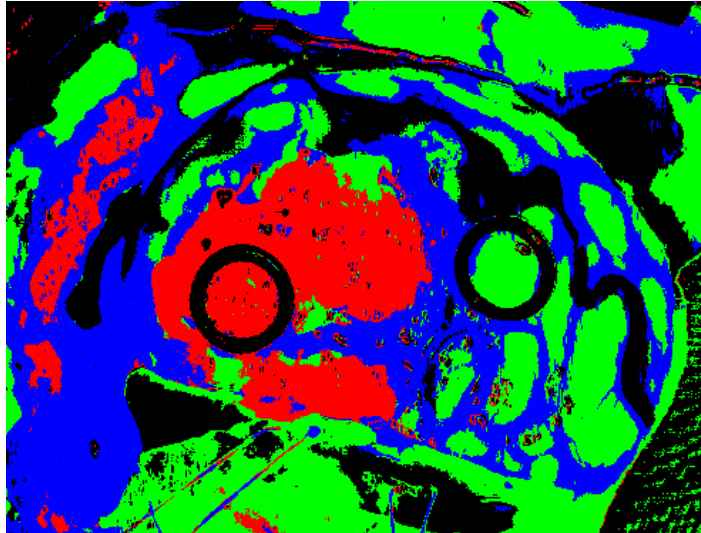


Figure 5.30: thematic map of Op15C1 using semi-supervised algorithm.

The thematic map generated by semi-supervised algorithm is shown in Figure 5.30 and we can see that the results obtained are very similar and significant differences are not appreciated with respect to apply CS3. Note that once again the classes inside the markers are well classified.

6. Op20C1:

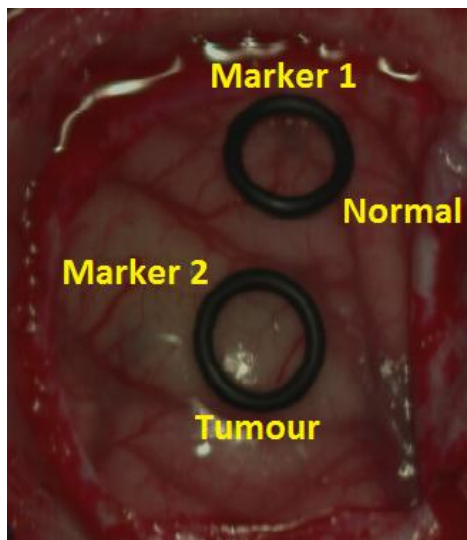


Figure 5.31: RGB image of Op20C1.

In Figure 5.31 it can be seen the Op20C1 surgery in which can be distinguished two different markers, namely marker 1 corresponding to normal tissues and marker 2 corresponding to tumour tissues.

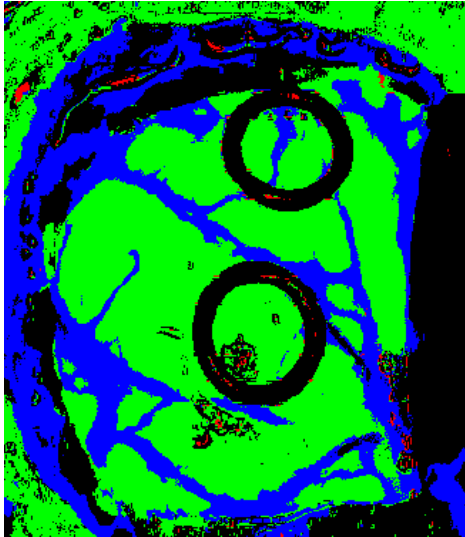


Figure 5.32: thematic map of Op20C1 using CS3.

In Figure 5.32 we can see the results obtained after applying CS3 process. This thematic map shows the normal tissues and blood vessels classes really good defined. However, there is not tumour area classified in the image and this is probably because in this surgery the tumour was covered by normal tissues.

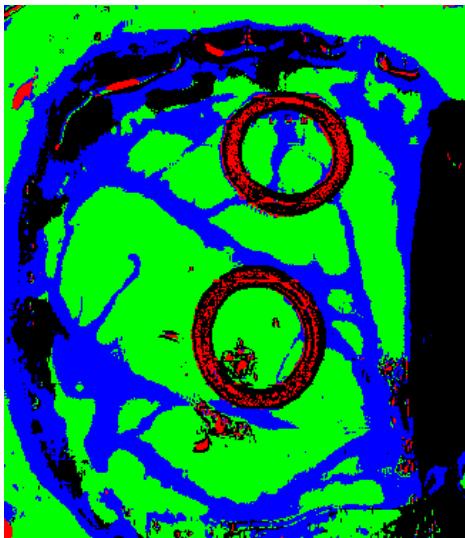


Figure 5.33: thematic map of Op20C1 using semi-supervised algorithm.

Regarding semi-supervised algorithm, the results obtained are shown in Figure 5.33. Once again, there are no appreciable differences in general after applying semi-supervised algorithm and normal tissues and blood vessels classes are still well defined. However, in this case we can see that the markers have been bad classified as tumour tissues because iterative process has selected some markers pixels bad classified as tumour in CS3.

5.3. Global discussion of results

After analysing the experiments performed in the previous sections, we proceed to discuss in general terms the results obtained using semi-supervised approach with the idea of offering an overview about the operation of algorithm analysed. From the results obtained, it may be performed the following general observations, which result in a set of specific recommendations when each of the techniques are used.

Regarding **experiment 5.1.1.**, the results obtained indicate that the application of the SVM classifier is a really effective process to classify accurately tumour tissue, distinguishing it from among remaining classes. In addition, the results for this application using different kernels featuring SVM indicate that using linear kernel or RBF kernel offers similar results and there are no noticeably improvements in the classification success rate obtained by this classifier. Therefore, our specific recommendations when using this classifier, for this type of application, is to use linear kernel in order to increase the computing time significantly. Moreover, in this set of experiments the real problem related to biological human variability is evidenced by the results, in which we can see a huge decrease in the accuracy obtained by CS3 compared to CS1 and CS2.

Regarding **experiment 5.1.2.**, the results obtained show the ability of semi-supervised approach based on SVM to increase the accuracy obtained by CS3 in brain cancer detection, especially classifying tumour and normal tissues. It is shown that semi-supervised algorithm is able to improve the results obtained by supervised approach, therefore it is recommended to apply semi-supervised techniques in our application in order to solve the issues associated with CS3.

Regarding **experiments 5.1.3.**, the results obtained indicate that applying unmixing techniques instead of SVM classifier worsens results obtained with respect to experiment 5.1.2., although unmixing techniques works well in a semi-supervised approach to discriminate tumour tissue and normal tissue. However, the accuracy decreases when all classes are included in the classification process, especially when LSU algorithm is applied to estimate the abundances, in this case the semi-supervised approach leads to a loss of precision. Moreover, if FCLSU technique is used to abundances estimation, the semi-supervised algorithm improves the results obtained in most patients. This means that unmixing techniques using FCLSU might provide some extra information contributing in

the decisions made by semi-supervised process and helping to select the samples in each iteration in combination with SVM classifier.

Regarding **experiment 5.1.4.**, the results obtained in process 1 indicate that this approach worse the overall results compared to experiment 5.1.2., especially using FCLSU, and in most patient semi-supervised approach does not improve the accuracy. In the second process proposed, the accuracy increases using both FCLSU and LSU techniques, particularly with FCLSU. In regard to process 3, the results are better than those obtained by process 2, and once again the use of FCLSU maximizes the accuracy. This reveals that the information provided by unmixing techniques in combination with SVM improve the results obtained previously and that semi-supervised algorithm works better than supervised algorithm for our study. For this reason, it is recommended to use mixed Unmixing-SVM techniques for this application.

On the other hand, it is shown that the semi-supervised algorithm can be used to move CS3 to CS2 instead to CS1 and this approach offers more accurate results, therefore it is an interesting alternative. However, the improvements achieved are only in Op1C2, Op2C1 and Op3C1, while the remaining patients present similar results in all experiments. This is due to the poor ability to classify tumour tissues of these patients in CS3. This problem could be solved increasing the database and including other classifiers in the semi-supervised algorithm to develop a meta-classifier.

Regarding **experiment 5.1.5.**, the results obtained indicate that the semi-supervised algorithm only needs a few iterations to improve the results obtained by CS3, so that it is best to select a larger number of samples in each iteration of the process.

Regarding **experiment 5.1.6.**, the thematic maps obtained indicate the good performance of semi-supervised algorithm, which in most patients is able to provide improvements compared to CS3.

5.4. Summary

In this chapter, we have investigated several strategies to apply semi-supervised classification in hyperspectral imaging for brain cancer detection. For classification scenarios, the best results are obtained using semi-supervised algorithm, being able to obtain more accurate results than supervised techniques. In addition, our experimental

results reveal that the use of mixed Unmixing-SVM techniques it is highly recommended to select the samples in the iterative process in order to maximize the accuracy.

Chapter 6

Conclusions and future research lines

6.1. Conclusions

In this work we have developed a semi-supervised algorithm for the analysis and classification of hyperspectral images. Then, a quantitative and comparative detailed analysis of different techniques from a semi-supervised point of view was conducted. Considered process are based on the combination of different spectral unmixing techniques which have been applied with a highly consolidated classifier in hyperspectral analysis applications (SVM) that is trained using an iterative procedure in the semi-supervised approach. In this regard, the different strategies considered cover a range of highly representative techniques of the state of the art in hyperspectral data analysis, combined with advanced classifiers able to work very accurately with high-dimensional data sets. This work was performed using a dataset formed by real patients which has made possible a detailed study of semi-supervised approach for this type of application using different combinations based on classifiers and spectral unmixing techniques mentioned above, providing an important approximation to the final system developed by HELiCoiD.

On the one hand, it should be noted that the study conducted includes topics of great interest, such as the impact of using dimensionality reduction techniques as well as mixed Unmixing-SVM techniques whose concepts have been seldom studied together, although they exhibit complementary properties that can offer several advantages when they are applied to hyperspectral image analysis. In this regard, it should be noted that in the literature there are few comparative studies of this kind to date, therefore the variety of results achieved and interesting conclusions produced by the analysis of these results may represent a valuable contribution to the existing literature regarding classification of hyperspectral data.

On the other hand, it should be noted that this is a research dissertation within a research Master, therefore the semi-supervised algorithm used in this work was developed exclusively for this study and it is a preliminary version while the final algorithm is still under developing.

6.2. Future research lines

As regards the future research lines derived from the present project, we can make the following considerations. As discussed in the results sections, due to the fact that the semi-supervised algorithm is able to provide improved accuracy, it can delve into the idea of semi-supervised approach, trying to perfecting the strategies proposed in this work in order to find the best possible implementation. In addition, this algorithm was developed exclusively for this project and application, therefore it would be interesting to test other highly representative techniques of the state of the art in semi-supervised classifier. Moreover, as the database is formed only by four patients and it is severely limited, it is necessary to create a database or library sufficiently robust formed by spectral signatures generic enough to use it to train the classifier to classify future patients with good results. During the iterative process, it would also be interesting to train the classifier not only from the patient samples which is being classified, but also with the database or library, so that the training set is formed by samples of the database or library and samples of patient to be classified (move CS3 to CS2).

Furthermore, in order to improve the selection criteria of the samples in each iteration, it would be interesting to add other classifiers with high performance in this type of application. Thus, the selection of the samples would be more accurate thanks to a

combination of several classifiers in the decision making. This strategy is known as meta-classifiers, which are sets of classifiers whose individual predictions are combined in some way (typically by voting) to classify new examples. The meta-classifiers are employed to further improve accuracy in the application of algorithms in a given problem. In addition, it would be advisable further deepening in the number of samples selected by iteration.

On the other hand, it has been shown that the semi-supervised algorithm greatly improves the results when working with only with normal and tumour tissues but lowers performance when all classes are included. For this reason, it might be interesting to test a *one vs. all* strategy consisting of to turn the multiclass classification problem into as many binary classifiers as existing classes. For example, by performing a binary classification to detect whether a given sample is tumour or not and thus try to solve the problem associated with the detection of the tumour class when all classes are used.

Finally, in this application it would be really interesting a fusion of spectral and spatial information in hyperspectral image classification. This is very important because in our problem we have a lot of spatial information which is not being used and could leads a huge improvement in the selection of samples of the iterative process. For instance, a given sample which is surrounded by samples of tumour class probably belongs to the tumour class. This spatial information in combination with spectral information provided by spectral unmixing and classifiers could offer significant improvements in terms of accuracy. Of course the whole system obtained to work with brain tumours could be extended to other tumour types and conditions.

Bibliography

- [1] Gamba P., Plaza A., Benediktsson J. A. and Chanussot. J., "European Perspectives in hyperspectral Data Analysis", *IEEE International Geoscience and Remote Sensing Symposium (IGARSS'07)*, Barcelona, Spain, 2007.
- [2] C. I. Chang. Recent advances in hyperspectral signal and image processing. John Wiley & Sons: New York, 2007.
- [3] J. M. Bioucas-Dias, A. Plaza, N. Dobigeon, M. Parente, Q. Du, P. Gader, and J. Chanussot. Hyperspectral unmixing overview: Geometrical, statistical and sparse regression-based approaches. *IEEE Journal of Selected Topics in Applied Earth Observations and Remote Sensing*, 5(2):354-379, 2012.
- [4] Marta Rojas Muriel. *Caracterización de imágenes hiperespectrales utilizando Support Vector Machines y técnicas de extracción de características*. December 2009.
- [5] Clark, R.N. "Spectroscopy of Rocks and Minerals, and Principles of Spectroscopy". Chapter 1 in *Manual of Remote Sensing*, John Wiley and Sons, New York, 1999a.
- [6] Landgrebe, D., "Hyperspectral Image Data Analysis", *IEEE Signal Processing Magazine*, vol. 19, no. 1, pp. 17-28, 2002.
- [7] Boardman, J.W., Kruse, F.A., Green, R.O., "Mapping target signatures via partial unmixing of AVIRIS data", *Summaries of the VI JPL Airborne Earth Science Workshop*, 1995.
- [8] Hsieh, P.-F., Landgrebe, D., "Classification of High Dimensional Data." Tesis Doctoral, School of Electrical and Computer Engineering, Purdue University, 1998.
- [9] Green, R.O. y col., "Imaging Spectroscopy and the Airborne Visible/Infrared Imaging Spectrometer (AVIRIS)", *Remote Sensing of Environment*, vol. 65, pp. 227-248, 1998.
- [10] Chein-I Chang (31 July 2003). *Hyperspectral Imaging: Techniques for Spectral Detection and Classification*. Springer Science & Business Media. ISBN 978-0-306-47483-5.

- [11] Hans Grahn; Paul Geladi (27 September 2007). *Techniques and Applications of Hyperspectral Image Analysis*. John Wiley & Sons. ISBN 978-0-470-01087-7.
- [12] Guolan Lu and Baowei Fei “Medical Hyperspectral Imaging: a review” (ONLINE FULL TEXT ARTICLE AVAILABLE). *Journal of Biomedical Optics* 19 (1): 10901. January 2014. Bibcode: 2014JBO....19a0901L. doi:10.1117/1.JBO.19.1.010901. PMID 24441941.
- [13] S. Chaudhuri, K. Kotwal. *Hyperspectral Image Fusion*. Springer, 2013.
- [14] C.-I. Chang. *Hyperspectral Data Processing: Algorithm Design and Analysis*. Wiley, 2013.
- [15] D. Glotsos, P. Spyridonos, P. Petalas, D. Cavouras, V.Zolota, P. Dadioti, I. Lekka, G. Nikiforidis, “A hierarchical decision tree classification scheme for brain tumour astrocytoma grading using support vector machines” in Proceedings of the 3rd International Symposium on Image and Signal Processing and Analysis, Vol. 2, pp 1034-1038, 2003.
- [16] *Brain Cancer Health Center, WebMD*. [En línea]. Disponible en: <http://www.webmd.com/cancer/brain-cancer/malignant-gliomas> [visitado el 8 de noviembre de 2014].
- [17] *Multiform glioblastoma. National Brain Tumour Society*. [En línea]. Disponible en: <http://www.braintumor.org/patients-family-friends/about-brain-tumors/tumor-types/glioblastoma-multiforme.html> [visitado el 5 de octubre de 2014].
- [18] Qingli Li, Xiaofu He, Yiting Wang, Hongying Liu, Dongrong Xu and Fangmin Guo. “Review of spectral imaging technology in biomedical engineering: achievements and challenges”. *Journal of Biomedical Optics* 18(10), 100901. October 2013.
- [19] G. Zonios et al., “Diffuse reflectance spectroscopy of human adenomatous colon polyps *in vivo*,” *Appl. Opt.* 38(31), 6628–6637 (1999).
- [20] L. V.Wang and H.-I.Wu, “Introduction,” in *Biomedical Optics*, pp. 1–15, John Wiley & Sons Inc., Hoboken, New Jersey (2009).

- [21] B. Costas, P. Christos, and E. George, "Multi/hyper-spectral imaging," in *Handbook of Biomedical Optics*, pp. 131–164, CRC Press (2011).
- [22] D. G. Ferris et al., "Multimodal hyperspectral imaging for the noninvasive diagnosis of cervical neoplasia," *J. Low. Genit. Tract Dis.* 5(2), 65–72 (2001).
- [23] M. C. Pierce et al., "Accuracy of *in vivo* multimodal optical imaging for detection of oral neoplasia," *Cancer Prev. Res.* 5(6), 801–809 (2012).
- [24] G. Bellisola and C. Sorio, "Infrared spectroscopy and microscopy in cancer research and diagnosis," *Am. J. Cancer Res.* 2(1), 1–21 (2012).
- [25] A. Nouvong et al., "Evaluation of diabetic foot ulcer healing with hyperspectral imaging of oxyhemoglobin and deoxyhemoglobin," *Diabetes Care* 32(11), 2056–2061 (2009).
- [26] R. Salzer et al., "Infrared and Raman imaging of biological and biomimetic samples," *Fresenius J. Anal. Chem.* 366(6–7), 712–726 (2000).
- [27] A. M. Siddiqi et al., "Use of hyperspectral imaging to distinguish normal, precancerous, and cancerous cells," *Cancer Cytopathol.* 114(1), 13–21 (2008).
- [28] P. Y. C. N. Mazzer et al., "Morphologic and morphometric evaluation of experimental acute crush injuries of the sciatic nerve of rats," *J. Neurosci. Methods* 173(2), 249–258 (2008).
- [29] B. D. de Dinechin, R. Ayrignac, P.-E. Beaucamps, P. Couvert, B. Ganne, P. G. de Massas, F. Jacquet, S. Jones, N. M. Chaisemartin, F. Riss, T. Strudel, 2013. A clustered manycore processor architecture for embedded and accelerated applications. *High Performance Extreme Computing Conference (HPEC), IEEE*, pp.1-6.
- [30] Himar Fabelo, Samuel Ortega, Raúl Guerra, Gustavo Callicó, Adam Szolna, Juan F. Piñeiro, Miguel Tejedor, Sebastián López and Roberto Sarmiento, "A Novel Use of Hyperspectral Images for Human Brain Cancer Detection using *in-Vivo* Samples". *Proceedings of the 9th International Joint Conference on Biomedical Engineering Systems and Technologies*, 311-320, 2016, Rome, Italy.

- [31] Shaw, G., Manolakis, D. "Signal processing for hyperspectral image exploitation". *IEEE Signal Processing Magazine*, vol. 19, pp. 12-16, 2002.
- [32] Stein, D.W., Beaven, S.G., Hoff, L.E., Winter, E.M., Schaum, A.P., Stocker, A.D., "Anomaly Detection from Hyperspectral Imagery". *IEEE Signal Processing Magazine*, vol. 19, pp. 58-69, 2002.
- [33] Plaza, P. Gamba, K. Bakos, B. Waske, J. B. Diaz, "HYPERINET_D4.1 – Processing Chain Definition Report", January, 2008 (<http://www.hyperinet.eu>).
- [34] Plaza, P. Gamba, K. Bakos, B. Waske, "HYPERINET_D4.2 – Processing Chain Implementation Report", January, 2009 (<http://www.hyperinet.eu>).
- [35] Chang, C.-I., Ren, H., "An Experiment-Based Quantitative and Comparative Analysis of Target Detection and Image Classification Algorithms for Hyperspectral Imagery". *IEEE Transactions on Geoscience and Remote Sensing*, vol. 38, no. 2, pp. 1044- 1063, 2000.
- [36] Chen, J. M., "Spatial Scaling of a Remotely Sensed Surface Parameter by Contexture". *Remote Sensing of Environment*, vol. 69, pp. 30-42, 1999.
- [37] Stehman, S. V., "Selecting and Interpreting Measures of Thematic Classification Accuracy". *Remote Sensing of Environment*, vol. 62, pp. 77-89, 1997.
- [38] Chiang, S.-S., Chang, C.-I., Ginsberg, I.W., "Unsupervised target detection in hyperspectral images using projection pursuit". *IEEE Transactions on Geoscience and Remote Sensing*, vol. 39, pp. 1380-1391, 2001.
- [39] Manolakis, D., Shaw, G., "Detection algorithms for hyperspectral imaging applications". *IEEE Signal Processing Magazine*, vol. 19, pp. 29-43, 2002.
- [40] Chapelle, Olivier; Schölkopf, Bernhard; Zien, Alexander (2006). *Semi-supervised learning*. Cambridge, Mass.: MIT Press. ISBN 978-0-262-03358-9.
- [41] Theiler, J., Gisler, G., "A contiguity-enhanced k-means clustering algorithm for unsupervised multispectral image segmentation", in: *Proc. SPIE*, vol. 3159, pp. 108-118, 1997.

- [42] Richards, J. A., *Remote Sensing Digital Image Analysis: An Introduction*. Springer-Verlag, Berlin, 1993.
- [43] Sweet, J., Granaham, J., Sharp, M., "An Objective Standard for Hyperspectral Image Quality", in: *Proc. IX -ASA/JPL Airborne Earth Science Workshop*, Pasadena, CA, 2000.
- [44] Plaza, A. Mueller, T. Skauli, Z. Malenovsky, J. Bioucas, S. Hofer, J. Chanussot, Carrere, I. Baarstad, J. Nieke, T. Hyvarinen, P. Gamba, J. A. Benediktsson, M. E. chaepman and B. Zagajewski. "HYPER-I-NET: European Research Network on Hyperspectral Imaging", *IEEE International Geoscience and Remote Sensing Symposium (IGARSS'07)*, Barcelona, Spain, 2007.
- [45] Rellier, G., Descombes, X., Zerubia, J., "Local registration and deformation of a road cartographic database on a SPOT satellite image". *Pattern Recognition*, vol. 35, pp. 2213-2221, 2002.
- [46] Madhok, V., Landgrebe, D., *Spectral-Spatial Analysis of Remote Sensing Data: An Image Model and A Procedural Design*. PhD thesis, School of Electrical Engineering and Computer Science, Purdue University, 1998.
- [47] Tadjudin, S., Landgrebe, D., *Classification of High Dimensional Data with Limited Training Samples*. PhD thesis, School of Electrical Engineering and Computer Science, Purdue University, 1998.
- [48] Naesset, E., "Predicting forest stand characteristics with airborne scanning laser using a practical two-stage procedure and field data". *Remote Sensing of Environment*, vol. 80, pp. 88-99, 2002.
- [49] Vaughan, R.G., Calvin, W.M., Taranik, J., "Analysis of Sub-Pixel Mixing in High Altitude AVIRIS Data Over Virginia City, Nevada, Using Systematic Field-Based Observations", in: *Proc. XI -ASA/JPL Airborne Earth Science Workshop*, Pasadena, CA, 2001.
- [50] Congalton, R.G., "Considerations and Techniques for Assessing the Accuracy of Remotely Sensed Data", in: *Proc. International Geoscience and Remote Sensing Symposium IGARSS*, vol. 3, pp. 1847-1850, 1989.

- [51] Stehman, S.V., "Practical Implications of Design-Based Sampling Inference for Thematic Map Accuracy Assessment". *Remote Sensing of Environment*, vol. 72, pp. 35-45, 2000.
- [52] Steele, B.M., Winne, J.C., Redmond, R.L., "Estimation and Mapping of Misclassification Probabilities for Thematic Land Cover Maps", *Remote Sensing of Environment*, vol. 66, pp. 192-202, 1998.
- [53] Jäger, G., Benz, U., "Measures of classification accuracy based on fuzzy similarity". *IEEE Transactions on Geoscience and Remote Sensing*, vol. 38, no. 2, pp. 1462-1467, 2000.
- [54] Miguel Ángel Tejedor Hernández. *Identificación de tumores cerebrales mediante el estudio de la forma y la composición de los tejidos usando imágenes hiperespectrales*. Septiembre 2015.
- [55] Rafael C. Gonzalez; Richard E. Woods (2008). *Digital Image Processing*. Prentice Hall. pp. 1–3. ISBN 978-0-13-168728-8.
- [56] J. Bioucas-Dias and J. Nascimento, "Hyperspectral Subspace Identification," *Geoscience and Remote Sensing, IEEE Transactions on*, vol. 46, no. 8, pp. 2435-2445, Aug. 2008.
- [57] J. M. Nascimento and J. M. Bioucas-Dias, 2015. Hyperspectral noise estimation. https://github.com/jhausser/ParTI/blob/master/mvsa_demo/estNoise.m, last accessed: November 2015.
- [58] Gabriel Martín Hernández. *Desarrollo de algoritmos para identificación de componentes puros en imágenes hiperespectrales*. June 2010.
- [59] Damien Letexier and Salah Bourennane. *Estimation of N-mode ranks of hyperspectral images for tensor denoising*. August 2009.
- [60] Sourabh Pargal. "Hyperspectral Subspace Identification and End member Extraction by Integration of Spatial-Spectral Information", Indian Institute Of Remote Sensing, April 2011.

- [61] M. Farzam and S. Beheshti, "The Noiseless code-length concept in subspace estimation for low SNR hyperspectral signals," in *Communications, Computers and Signal Processing, 2009. PacRim 2009. IEEE Pacific Rim Conference on*, pp. 425-430, 2009.
- [62] Roweis, S. T.; Saul, L. K. (2000). "Nonlinear Dimensionality Reduction by Locally Linear Embedding". *Science* 290 (5500): 2323–2326.
- [63] Qian, S.-E y col., "Vector quantization using spectral index-based multiple subcodebooks for hyperspectral data compression". *IEEE Transactions on Geoscience and Remote Sensing*, vol. 38, pp. 1183 –1190, 2000.
- [64] Plaza A., Chang, C.-I, *High Performance Computing in Remote Sensing*, CRC Press, 2007.
- [65] Matlab help, Smooth filter. Matlab version 7.10.0.499 (R2010a). The Mathworks, Inc. February 5, 2010.
- [66] Steven W. Smith. *The Scientist and Engineer's Guide to Digital Signal Processing*. Ph.D.
- [67] Eduardo Roldán Arroita. *Estudio y análisis de filtros aplicados a señales vibratorias de ejes ferroviarios para la detección de fallos*. September 2012.
- [68] D. Tuia, F. Ratle, F. Pacifici, M. F. Kanevski and W. J. Emery, Active Learning Methods for Remote Sensing Image Classification, in *IEEE Transactions on Geoscience and Remote Sensing*, vol. 47, no. 7, pp. 2218-2232, July 2009.
- [69] S. Kabwama, C. Sosa, S. Ortega, H. Fabelo, A. Szolna, J. F. Piñeiro, D. Bulters, A. J. O'Shanahan, S. Bisshop, G. M. Callicó, "Intra-operative Hyperspectral Imaging for Brain Tumour Detection and Delineation".
- [70] Samet, H. (2006) *Foundations of Multidimensional and Metric Data Structures*. Morgan Kaufmann.
- [71] C. Ding, , X. He , H. Zha , H.D. Simon, Adaptive Dimension Reduction for Clustering High Dimensional Data, *Proceedings of International Conference on Data Mining*, 2002.

- [72] Hughes G. F., "On The Mean Accuracy Of Statistical Pattern Recognizers", *IEEE Trans. Infor. Theory*, Vol. IT-14, 1968.
- [73] Fukunaga K., "*Introduction to Statistical Pattern Recognition*" Published by Academic Press, 1990.
- [74] Kaarna A., Zemcik P., Kalviainen H., Parkkinen J., "Compression of multispectral remote sensing images using clustering and spectral reduction", *IEEE Transactions on Geoscience and Remote Sensing*, vol. 38, 2000.
- [75] Chang, C.-I, Du, Q., Sun, T., Althouse, L.G., "A Joint Band Prioritization and Band-Decorrelation Approach to Band Selection for Hyperspectral Image Classification", *IEEE Transactions on Geoscience Remote Sensing*, vol. 37, no.6, pp.2631-2641, 1999b.
- [76] N. Keshava and J. F. Mustard. Spectral unmixing. *IEEE Signal Processing Magazine*, 19(1):44-57, 2002.
- [77] J. A. Richards. Analysis of remotely sensed data: the formative decades and the future. *IEEE Transactions on Geoscience and Remote Sensing*, 43(3):422-432, 2005.
- [78] A. Plaza, J. A. Benediktsson, J. W. Boardman, J. Brazile, L. Bruzzone, G. Camps-Valls, J. Chanussot, M. Fauvel, P. Gamba, A. Gualtieri, M. Marconcini, J. C. Tilton, and G. Trianni. Recent advances in techniques for hyperspectral image processing. *Remote Sensing of Environment*, 113:110-122, 2009.
- [79] J. B. Adams, M. O. Smith, and P. E. Johnson. Spectral mixture modeling: a new analysis of rock and soil types at the viking lander 1 site. *Journal of Geophysical Research*, 91(B8):8098-8112, 1986.
- [80] Inmaculada García Dópido. *New Techniques for Hyperspectral Image Classification*. January 2014.
- [81] N. Keshava and J. Mustard, "Spectral unmixing," *Signal Processing Magazine, IEEE*, vol. 19, no. 1, pp. 44-57, 2002.

- [82] Gabriel Martín Hernández. *Comparativa de nuevos algoritmos de extracción de endmembers en imágenes hiperespectrales utilizando información espacial*. February, 2009.
- [83] C.-I. Chang and Q. Du, "Estimation of number of spectrally distinct signal sources in hyperspectral imagery," *IEEE Transactions on Geoscience and Remote Sensing*, vol. 42, no. 3, pp. 608–619, 2004.
- [84] A. Plaza, P. Martinez, R. Perez, and J. Plaza. A quantitative and comparative analysis of endmember extraction algorithms from hyperspectral data. *IEEE Transactions on Geoscience and Remote Sensing*, 42(3):650-663, 2004.
- [85] D. C. Heinz and C. I. Chang. Fully constrained least squares linear mixture analysis for material quantification in hyperspectral imagery. *IEEE Transactions on Geoscience and Remote Sensing*, 39(3):529-545, 2001.
- [86] Vélez-Reyes M.; et. al. "Iterative Algorithms for Unmixing of Hyperspectral Imagery". *Proceeding of SPIE*, April 2003.
- [87] Keshava N.; Mustard J. F. "Spectral Unmixing". *IEEE Signal Processing Magazine*, 19:44 - 57, January issue 1 2002.
- [88] Benediktsson J.A. and Arnason K., "Classification and feature extraction of aviris data", *IEEE Trans. on Geoscience and Remote Sensing*, vol.33, pp. 1194:1205, 1995.
- [89] Vapnik V. *Statistical learning theory*. Wiley, New York, 1998.
- [90] Gualtieri J. A. and Chettri S., "Support vector machines for classification of hyperspectral data", *Proc. IEEE International Geoscience and Remote Sensing Symposium*, volume 2. IGARSS '00. Proceedings, July 2000.
- [91] Cortes C. and Vapnik V. "Support vector networks". *Machine Learning*, 20:1- 25, 1995.
- [92] Schölkopf B., Smola A. "Advances in kernel methods: Support vector learning". 1999.

- [93] Boser B. E., Guyon I. M., and Vapnik V. N.. "A training algorithm for optimal margin classifiers", In D. Haussler, editor, 5th Annual ACM Workshop on COLT, pages 144-152, Pittsburgh, PA, 1992. ACM Press.
- [94] Muller K. R., Mika S., Ratsch G., Tsuda K., Schölkopf B., "An introduction to kernel-based learning algorithms". IEEE Transactions on Neural Networks, vol 12, 2001.
- [95] Mercier G. and Lennon M., "Support Vector Machines for Hyperspectral Image Classification with Spectral-Based Kernels", in IGARSS, 2003.
- [96] Foody G. M., "RVM-based multi-class classification of remotely sensed data" International Journal of Remote Sensing, vol 29, pp 1817-1823, 2008.
- [97] Triguero, Isaac; García, Salvador; Herrera, Francisco (2013-11-26). "Self-labeled techniques for semi-supervised learning: taxonomy, software and empirical study". Knowledge and Information Systems 42 (2): 245–284. ISSN 0219-1377.
- [98] Fazakis, Nikos; Karlos, Stamatis; Kotsiantis, Sotiris; Sgarbas, Kyriakos (2015-12-29). "Self-Trained LMT for Semisupervised Learning". Computational Intelligence and Neuroscience 2016: 1–13. doi:10.1155/2016/3057481.

BUDGET

El presupuesto del presente Trabajo Fin de Máster se ha valorado en función de la última lista de Honorarios Orientativos publicada por el Colegio Oficial de Ingenieros de Telecomunicación, denominada *Costes Estimados de Trabajos Profesionales* correspondiente al año 2008. Así, el presupuesto se ha estructurado en siete secciones:

1. Recursos Humanos
2. Recursos Hardware
3. Recursos Software
4. Material Fungible
5. Aplicación de Impuestos
6. Presupuesto total

Hay que indicar que el motivo por el que este presupuesto toma como referencia una lista publicada en 2008 se debe a las modificaciones introducidas en el ordenamiento jurídico y a la actuación de los colegios profesionales en la ley 25/2009 del 22 de diciembre, por la cual se liberalizan los honorarios profesionales y ya no es posible seguir publicando este tipo de listas por parte del COIT.

Recursos humanos

El coste de los recursos humanos está asociado al tiempo empleado por un ingeniero en la realización de este proyecto. El coste se establece aplicando la fórmula propuesta por el COIT para trabajos por tiempo empleado:

$$\text{Honorarios(€)} = (74.88H_n + 96.72H_e)C_t$$

Donde H_n representa el número de horas normales dentro de la jornada laboral, mientras que H_e se considera el número de horas especiales, siendo 260,00 euros el honorario mínimo a cobrar independientemente del número de horas trabajadas. El coeficiente C_t es el factor de corrección que se debe aplicar al número de horas, variando en función del número de horas empleadas según la tabla 8.1:

Horas trabajadas	C_t
0-36	1
36 - 72	0,90
72 - 108	0,80

108 - 144	0,70
144 - 180	0,65
180 - 360	0,60
360 - 540	0,55
540 - 720	0,50
720 - 1080	0,45
+ 1080	0,40

Tabla 8.1: Factor de corrección en función de horas trabajadas.

Teniendo en cuenta una jornada laboral de ocho horas diarias a razón de veinte días laborales cada mes durante 4 meses, el número total de horas empleadas es de 640 horas normales, siendo cero el número de horas especiales trabajadas. Según la tabla 8.1, el factor de corrección que corresponde al número de horas trabajadas es $C_t = 0,50$.

En la tabla 8.2 se muestra el resultado de la aplicación de la ecuación anterior, recogiendo los costes asociados a los recursos humanos libres de impuestos, que ascienden a *veintitrés mil novecientos sesenta y un euros con seis céntimos* (23961,6€).

Concepto	Tiempo trabajado (horas)	Factor de corrección	Importe (€)
Ingeniero	640	0,50	23961,6
Coste Total			23961,6

Tabla 8.2: Coste total de recursos humanos.

Recursos hardware

El coste de los recursos hardware vendrá determinado por la instrumentación de medida y los equipos informáticos empleados en la realización del presente Proyecto Fin de Carrera.

- Cámara Hiperespectral Headwall's Hyperspec NIR.
- Cámara Hiperespectral Headwall's Hyperspec VNIR.
- Ordenador portátil HP Pavilion dv6 Intel Core i7 (2,60 GHz), con 8 GB de RAM y 1 TB de disco duro.

Para el cálculo de los costes de los recursos materiales, hardware y software, se utilizará un sistema de amortización lineal o constante, en el que se supone que el

inmovilizado material se deprecia de forma constante a lo largo de su vida útil. La cuota de amortización anual se calcula usando la siguiente fórmula:

$$Cuota\ anual = \frac{Valor\ de\ adquisición - Valor\ residual}{Años\ de\ vida\ útil}$$

El valor residual es el valor teórico que tendrá el elemento analizado después de su vida útil. El periodo de amortización de estos recursos se ha considerado de 36 meses, y su tiempo de uso ha sido de 4 meses. Los costes asociados a los recursos hardware libres de impuestos se recogen en la tabla 8.3 y ascienden a *seis mil setecientos setenta y dos euros con treinta y seis céntimos* (6772,36€).

Concepto	Coste unitario (€)	Valor residual (€)	Coste mensual (€)	Importe (€)
Cámara hiperespectral NIR	62000,00	32000,00	1000,73	4002,92
Cámara hiperespectral VNIR	40000,00	21000,00	656,25	2625
Ordenador	1300,00	0,00	36,11	144,44
Coste Total				6772,36

Tabla 8.3: Coste total de recursos hardware.

Recursos software

Para los recursos software se utilizan los mismos criterios que en el epígrafe anterior, tomando en este caso un periodo de amortización de 24 meses. Las herramientas software usadas han sido las siguientes:

- Sistema Operativo Microsoft Windows 7 Enterprise Edition 64 bits.
- MATLAB R2015a.

En la tabla 8.4 se recogen los costes asociados a los recursos software libres de impuestos. El coste total asociado a las herramientas software empleadas asciende a *trescientos ochenta y tres euros con treinta con dos céntimos* (383,32€).

Concepto	Coste unitario (€)	Valor residual (€)	Coste mensual (€)	Importe (€)
Windows 7	300,00	0,00	12,50	50
MATLAB R2015a	2000,00	0,00	83,33	333,32
Coste Total				383,32

Tabla 8.4: Coste total de recursos software.

Material fungible

En este apartado se recopilan los costes relacionados con los materiales utilizados en la realización del proyecto, como son: material de papelería, servicio de impresión del IUMA, discos CD-R y los costes de impresión y encuadernación de la memoria.

Los costes asociados al material fungible libres de impuestos son en este Trabajo Fin de Máster de *sesenta y ocho euros con treinta y siete céntimos* (68,37€).

Concepto	Importe (€)
Servicio de impresión	50,05
CD-R	2,50
Memoria	15,82
Coste total	68,37

Tabla 8.5: Coste total de material fungible.

Redacción del proyecto

De acuerdo a los honorarios orientativos del COIT, el importe de la redacción del presente TFM se calcula mediante la siguiente ecuación:

$$R = 0,07P_t C_r + 0,03P_c C_r$$

Donde P_t es el presupuesto de ejecución material de telecomunicaciones, P_c es el presupuesto de obra civil y C_r es el coeficiente de ponderación por tramos en función del coste del presupuesto. Este Trabajo de Fin de Máster no tiene asociada ninguna obra civil, por lo que P_c es nulo. El presupuesto de ejecución material se corresponde con la suma de los cuatro apartados anteriores:

$$P_t = 23961,6 + 6772,36 + 383,32 + 68,37 = 31185,65€$$

Aplicando la ecuación anterior:

$$R = 0,07 \cdot 30807,42 = 2156,52€$$

Por lo tanto, los costes asociados a la redacción del proyecto libres de impuestos ascienden a *dos mil ciento cincuenta y seis euros con cincuenta y dos céntimos* (2156,52€).

Aplicación de impuestos

En los anteriores apartados se ha recogido cada uno de los costes que se han generado para el desarrollo de este Trabajo Fin de Máster. La realización del mismo estará gravada con el Impuesto General Indirecto Canario (IGIC), en un siete por ciento (7%).

Concepto	Importe (€)
Recursos humanos	23961,6
Recursos hardware	6772,36
Recursos software	383,32
Material fungible	68,37
Redacción del TFM	2156,52
Subtotal	33342,17
IGIC (7%)	2333,96
Total	35676,122

Tabla 8.6: Coste total del Trabajo Fin de Máster.

Presupuesto total

En la tabla 8.7 se recogen todos los costes asociados al Trabajo Fin de Máster y el importe total del mismo después de impuestos.

Así pues, D. Miguel Ángel Tejedor Hernández declara que el presupuesto para el Trabajo Fin de Máster *Título* asciende a un total de *treinta y cinco mil seiscientos setenta y seis con ciento veintidós céntimos* (35676,122€).

Las Palmas de Gran Canaria, 1 de septiembre de 2016

Fdo. Miguel Ángel Tejedor Hernández

SPECIFICATIONS

En el pliego de condiciones descrito en este TFM se exponen las condiciones bajo las cuales se ha desarrollado el trabajo. A continuación, se describe el conjunto de los componentes hardware y software empleados durante la realización del trabajo, así como de las muestras biológicas que se han utilizado.

Recursos hardware

- Cámara Headwall's Hyperspec VNIR: Cámara de imágenes hiperespectrales destinada tanto a la industria como a la investigación. Es capaz de medir simultáneamente las componentes ópticas del espectro y la localización espacial de objetos sobre una superficie. En conjunto con una cámara monocromática y una lente adecuada, la Headwall's Hyperspec forma un sistema hiperespectral en el rango VNIR (380nm-1000nm), con una resolución espectral de 2-3nm.
- Cámara Headwall's Hyperspec NIR: Cámara de imágenes hiperespectrales destinada tanto a la industria como a la investigación. Es capaz de medir simultáneamente las componentes ópticas del espectro y la localización espacial de objetos sobre una superficie. En conjunto con una cámara monocromática y una lente adecuada, la Headwall's Hyperspec forma un sistema hiperespectral en el rango VNIR (900nm-1700nm), con una resolución espectral de 4-5nm.
- Ordenador personal HP Pavilion dv6: Ordenador portátil en el que se ha instalado el MATLAB R2015a y se ha realizado todo el procesado de las imágenes. Además, se ha redactado la memoria de este Proyecto Final de Carrera.

Las principales características de este PC son:

- Procesador Intel Core i7-4510U a 2,60 GHz.
 - 8 GB de memoria RAM.
 - 1 TB de disco duro.
-
- Disco duro extraíble Western Digital de 1 TB: Utilizado para guardar las imágenes procesadas.
 - Impresora HP LaserJet 2430 DTN: Utilizada para la impresión del material necesario para el desarrollo del proyecto y de la presente memoria.

Recursos software

- MATLAB R2015a: Herramienta de software matemático que ofrece un entorno de desarrollo integrado con un lenguaje de programación propio que permite. Facilita el análisis y la visualización de datos.

Recursos biológicos

Las muestras biológicas que se han empleado en este TFM se corresponden con imágenes obtenidas directamente durante intervenciones quirúrgicas por el departamento de Neurocirugía del Hospital Universitario de Las Palmas de Gran Canaria Dr. Negrín mediante el uso de las cámaras hiperespectrales descritas en los recursos hardware y destinadas para tal fin. Estas imágenes han sido procesadas y diagnosticadas por el departamento de Anatomía Patológica de este mismo hospital. El empleo de estas muestras en proyectos de investigación está contemplado en los *ethical issues* del proyecto HELICoiD.

Las Palmas de Gran Canaria, 1 de septiembre de 2016

Fdo. Miguel Ángel Tejedor Hernández